NONLINEAR ELECTROPHORESIS IN NETWORKED MICROFLUIDIC CHIPS

By

HUANCHUN CUI

A dissertation submitted in partial fulfillment of
the requirements for the degree of

DOCTOR OF PHILOSOPHY

WASHINGTON STATE UNIVERSITY
School of Chemical Engineering and Bioengineering

DECEMBER 2007

To the Faculty of Washington State University:

The members of the Committee appointed to examine the dissertation of HUANCHUN CUI find it satisfactory and recommend that it be accepted.

_____
Chair

_____

_____

_____

ACKNOWLEDGMENT

I am deeply grateful to my advisor, Dr. Ivory for his guidance, encouragement and patience over the past five years. Without his help, I could never have been ready for a Ph.D. degree.

I am very thankful to our project collaborators, Dr. Dutta and his students, including Keisuke Horiuchi, Nazmul Huda Al Mamun, Jaesool Shim and Talukder Zaki Jubery for their high quality work.

I appreciate Dr. Zollars and Dr. Dong for taking their time to review my dissertation and providing helpful suggestions and thoughtful comments.

I would like to thank Dr. Ivory's research group members who have been consistently offering me all kinds of help. They are Zheng Huang, Brain Thome, Noah Tracy, Ann Marie Hardin, Jeff Burke, Schurie Harrison, Danny Bottenus and Bingwen Liu.

I would like to acknowledge the Department of Chemical Engineering at Washington State University for providing me this great study opportunity. I would like to thank departmental staff: JoAnn McCabe, Diana Thornton, Paul Golter and Senja Estes for their support.

I thank my parents, my wife Li and my daughter Nicole for their love.

NONLINEAR ELECTROPHORESIS IN NETWORKED MICROFLUIDIC CHIPS

Abstract

by Huanchun Cui, Ph.D.
Washington State University
December 2007

Chair: Cornelius F. Ivory

This dissertation reports the implementation of two major nonlinear electrophoretic techniques (isoelectric focusing and isotachophoresis) onto networked microfluidic chips. A number of improvements have been made to address the issues that occurred during the miniaturization of those two techniques.

Ampholyte-based isoelectric focusing was first demonstrated in a single-channel poly(dimethylsiloxane) chip in which experimental conditions had been optimized to mitigate the adverse effects on the separation resolution due to the problems such as electroosmotic flow, peak drift and pH gradient compression. The resolving power of isoelectric focusing was then further improved in networked microfluidic chips by a staging method. This method couples several stages of IEF in series by first focusing proteins in a straight channel using broad-range ampholytes and then refocusing segments of the first channel into secondary channels that branch from the first one at T-junctions.

Isotachophoresis experiments demonstrated that a mixture of three fluorescent proteins

can be concentrated and stacked into adjacent zones of pure protein in a microchannel. Two-dimensional model was developed to illustrate the stacking and separation features of isotachophoresis and to explore its self-sharpening behavior of sample zones dispersed a T-junction. Sample dispersion at the T-junction was reduced by implementation of an electric valve. With an automated control system, the electric valve utilizing a pair of integrated microelectrodes provided an effective way to maintain current streamlines, thus preventing charged species from dispersion into the T-junction.

TABLE OF CONTENTS

LIST OF TABLES

LIST OF FIGURES

Dedication

To my parents, my wife Li and my daughter Nicole

CHAPTER 1

Introduction

The human proteome is estimated to consist of more than 40,000 proteins with a difference of 10 orders of magnitude in expression levels.[1] This greatly challenges the traditional protein separation platforms, among which two-dimensional polyacrylamide gel electrophoresis (2D PAGE) is most widely employed. 2D PAGE is an old, but powerful technique. Proteins are resolved in the first dimension by polyacrylamide gel isoelectric focusing (IEF-PAGE) and, in the second dimension, by sodium dodecyl sulfate polyacrylamide gel electrophoresis (SDS-PAGE). 2D-PAGE is labor-intensive and the whole process, including stain/destain, usually takes two or more days to complete.[2] 2D PAGE provides a maximum peak capacity of about 5000 proteins and has a dynamic range of less than 10,000.[3] Clearly the peak capacity and dynamic range that 2D PAGE could provide fall far short of that needed for resolving very complex protein mixtures from the human proteome.

New protein separation platforms that can provide shorter analysis time, higher peak capacity and a wider dynamic range need to be developed to handle the complexity of the proteome. The rapid development of microfluidic based protein separation techniques during the past decade makes itself one of the most promising candidates to address this challenge. The heart of a microfluidic device is a microchannel network that is fabricated onto a substrate. The advantages that the microfluidic platform offers are very clear: (1) The separation performance can be enhanced by high surface to volume ratios. (2)

Separation throughput can be greatly improved when large numbers of samples are processed in parallel. (3) The ultra small volume of the separation channel reduces consumption of samples.

Numerous protein separation applications on microfluidic lab-chips have been reported using a variety of electrophoresis techniques, such as isoelectric focusing (IEF)[4], isotachophoresis (ITP),[5] zone electrophoresis (ZE),[6] IEF-ZE[7] and ITP-ZE[8]. However before these microfluidic based electrophoretic separation can outperform gel electrophoresis in terms of resolution, reproducibility, and dynamic range, a number of issues need to be addressed.

First, the microfluidic based separation is usually carried out in free solution for fast analysis. However, without the support of a gel matrix, nonspecific adsorption onto channel walls,[9] electrohydrodynamic instability[10] and electroosmotic flow (EOF) will jeopardize separation resolution and efficiency. Especially in case of IEF, instability of the pH gradient, peak drift and compression of the pH gradient will make the results worse.

Second, protein detection is challenging due to the low sample mass loadings in a microfluidic chip. The best way to increase the loading capacity of a microfluidic chip is to preconcentrate the sample. ITP is a simple and effective preconcentration and separation method which can be easily integrated on a chip prior to other on-chip

operations, especially ZE. However, ITP pre-concentration and separation of proteins on chips has so far received relatively little interest.

Third, the dispersion and sample loss at a T-junction is a common issue associated with electrokinetic separation in networked microchannels. The current strategy to address this problem is to implement physical microvalves[11] which utilize actuators to block the microchannels of interest. However, the structure of these microvalves is relatively complicated since they require moving parts to close and open the microchannels. They are limited in use for controlling electrokinetic flow since valve actuation, which usually requires deformation of polymer layer, heating, cooling or a buffer pH change, can jeopardize the resolution of electrokinetic separation.

Certainly, there are other issues that will appear when dealing with miniaturization of specific applications. This work has been primarily focused on finding solutions to those three issues mentioned above.

Chapter 2 shows how to implement IEF on a single-channel poly(dimethylsiloxane) (PDMS) chip. The dynamic coatings of methylcellulose (MC) on the oxidized PDMS surface reduced both EOF and compression of the pH gradient, improving the resolution and reproducibility of IEF. Because these PDMS microchannels are only 2 cm in length, separation times and applied voltages are greatly reduced when compared to capillary IEF and gel IEF.

A staging method that can improve IEF resolving power is introduced in chapter 3. IEF staging is a fairly routine purification strategy at preparative scales[12]. To our knowledge, however, IEF staging has not yet been applied in micro-scale separations. Microchip IEF is staged by first focusing proteins in a straight channel using broad-range ampholytes and then refocusing segments of that first channel in secondary channels that branch out from the first one. The experiments demonstrate that staging IEF significantly increases the resolving power of IEF.

Chapter 4 demonstrates ITP of proteins in a PDMS channel with T-junctions which we consider the key elements for integration of unit operations. The ITP features such as concentration stacking and self-sharpening of protein zones after they had been dispersed at a T-junction are also explored in this chapter by developing a 2D ITP model.

Finally, chapter 5 addresses dispersion and sample losses at a T-junction during electrokinetic separation by developing an automated electric valve. A pair of platinum microelectrodes integrated in the vicinity of the T-junction to act as the electric valve. The dispersion and sample loss is reduced by controlling distortion in the current streamlines along which the sample species are driven.

Reference

(1) Binz, P. A., Muller, M., Hoogland, C., Zimmermann, C., Pasquarello, C., Corthals, G., Sanchez, J. C., Hochstrasser, D. F., Appel, R. D. *Curr. Opin. Biotech.* 2004, 15, 17-23.

(2) Hoving, S.; Voshol, H.; Van Oostrum, J. *Electrophoresis* 2000, 21, 2617-2621.

(3) Gorg, A.; Obermaier, C.; Boguth, G.; Harder, A.; Scheibe, B.; Wildgruber, R.; Weiss, W. *Electrophoresis* 2000,6,1037-53.

(4) Tan, W.; Fan, Z. H.; Qiu, C. X,; Ricoo, A. J.; Gibbons, I. *Electrophoresis* 2002, 23, 3638-3645.

(5) Grass, B., Hergenroder, R., Neyer, A., Siepe, D. *J. Sep. Sci.* 2002, 25, 135-140.

(6) Effenhauser, C. S.; Bruin, G. J. M.; Paulus, A.; Ehrat, M. *Anal. Chem.* 1997, 69, 3451-3457.

(7) Li, Y.; Buch, J. S.; Rosenberger, F.; DeVoe, D. L.; Lee, C. S. *Anal. Chem*. 2004, 76, 742-748.

(8) Kaniansky, D., Zelensky, I., Hybenova, A., Onuska, F. I. *Anal. Chem.* 1994, 66, 4258-4264.

(9) Li, Y.; DeVoe, D. L.; Lee, C. S. *Electrophoresis* 2003, 24, 193-199.

(10) Baygents, J. C.; Baldessari, F. *Physics of Fluids* 1998, *10*, 301-311.

(11) Unger, M. A.; Chou, H. P.; Thorsen, T.; Scherer, A.; Quake, S. R. *Science* 2000, *288*, 113-116.

(12) Bossi, A.; Righetti, P. G. *Electrophoresis* 1995, 16, 1930-1934.

CHAPTER 2

Isoelectric Focusing in a Poly(dimethylsiloxane) Microfluidic Chip

Huanchun Cui,[†] Keisuke Horiuchi,[‡] Prashanta Dutta,[‡] and Cornelius F. Ivory*,[†]

† School of Chemical Engineering and ‡ School of Mechanical and Materials Engineering, Washington State University, Pullman WA 99164

* To whom all correspondence should be addressed. Email: cfivory@wsu.edu

Abstract

This paper reports the application of ampholyte-based isoelectric focusing in poly(dimethylsiloxane) (PDMS) using methylcellulose (MC) to reduce electroosmosis and peak drift. Although the characteristics of PDMS make it possible to fabricate microfluidic chips using soft lithography, unstable electroosmotic flow (EOF) and cathodic drift are significant problems when using this medium. This paper demonstrates that EOF is greatly reduced in PDMS by applying a dynamic coat of MC to the channel walls and that higher concentrations of MC can be used to increase the viscosity of the electrode solutions in order to suppress pH gradient drift and reduce "compression" of the pH gradient. To illustrate the effect of MC on performance, several fluorescent proteins were focused in microchip channels 5 microns deep by 300 microns wide by 2 cm long in 3-10 min using broad-range ampholytes at electric field strengths ranging from 25 to 100 V/cm.

2.1 Introduction

Isoelectric focusing (IEF) is considered one of the most powerful techniques available for separating proteins, but IEF-PAGE usually requires time-consuming manual preparation

and staining procedures.[1] Capillary IEF (cIEF), first performed in narrow tubes by Hjertén[2] and later adapted to fused silica capillaries by Jorgenson et al.,[3,4] provides several advantages over conventional gels including short analysis times, straightforward automation, and online detection. However, cIEF is not used as frequently as IEF-PAGE in bioanalysis because capillary electrophoresis (CE) protocols are not as robust as PAGE. Microchip electrophoresis is a promising alternative to CE since it has the potential to provide rapid protein analysis,[5] straightforward integration with other microfluidic unit operations, whole channel detection,[6] smaller sample sizes and lower fabrication costs.[7] To reach this potential, robust protocols must be developed for microchip IEF.

The first adaptation of cIEF to microfluidic chips was investigated by Hofmann et al.[8] in glass microchannels using conventional photolithography and microfabrication techniques. The photolithography process, which requires access to clean room facilities, is expensive, time consuming and labor intensive. The disadvantages associated with glass microchips have led researchers[9-13] to investigate the use of polymers, which are less expensive and less fragile than glass, as materials for microchip fabrication. The main advantage of polymers is that the processes used to fabricate such devices are based on several molding technologies,[14] e.g., hot embossing, injection molding and casting, which are cheaper and faster than those used on glass.

Poly(dimethylsiloxane) (PDMS), which is one of the popular polymeric substrates for microfluidic chips, was first introduced by Kumar et al.[15] for the creation of

micropatterned objects. As a material for fabrication of microfluidic devices, PDMS is inexpensive and is optically transparent down to ~230 nm,[16] a property which might allow UV detection in place of current fluorescent labeling/staining procedures.

The first demonstration of capillary zone electrophoresis in native PDMS microchannels was performed by Effenhauser et al.[17] for the separation of DNA fragments and peptides. Duffy et al.[18] reported on CE in plasma-oxidized PDMS microchannels for separation of amino acids, protein charge ladders, and DNA fragments in the presence of hydroxypropylcellulose. The earliest published example of IEF performed in gel-filled PDMS microchannels was reported by Chen et al.[19] as the first dimension of a prototype two-dimensional CE system. The IEF separations in their system, however, required complicated sample/gel loading procedures. More recently, Wang et al.[20] demonstrated IEF of four proteins in a PDMS microfluidic device that integrated IEF with capillary zone electrophoresis as a second dimension of separation. In this system, the IEF channels were permanently coated with polyacrylamide and 1% MC was used in the sample/ampholyte mixture in an effort to control electroosmotic flow (EOF). However, the multiple variants of Green Fluorescent Protein (GFP) which appear as a result of microheterogeneity[21] were not seen in their separations.

IEF separations in aqueous ampholyte solutions are best performed either with no EOF, in which case mobilization is carried out using applied salt or pressure differentials, or using stable, uniform EOF for mobilization. Duffy et al.[18] assumed that native PDMS would not exhibit EOF while others[22] claimed that the pH-dependent EOF which exists in

native PDMS channels would make it difficult to use in IEF separations. When performing IEF separations in aqueous solutions in PDMS microchannels, Li et al.[23] observed that adsorption of proteins onto the channel walls significantly reduced both the separation efficiency and resolution obtained in bare PDMS channels so they reduced protein adsorption by noncovalently coating the channel with bovine serum albumin (BSA) prior to initiation of IEF. They further claimed that EOF was eliminated on native PDMS surfaces by adsorption of focused ampholytes onto the channel walls. The most common method used to eliminate EOF and wall-analyte interactions is to permanently coat the channel walls with neutral and hydrophilic polymers. However, the protocols used to make covalent coatings are both complicated and time consuming and the most commonly used permanent coating on a capillary surface, linear polyacrylamide, is unstable at alkaline pH.[24]

To circumvent the need for permanent coatings, we applied a dynamic MC coating to control EOF and wall-analyte interactions. Dynamic coating procedures are simpler than those used for permanent coatings since only two steps are involved.[24] First, to adsorb a temporary layer of polymer onto the walls, the channels are rinsed with the coating solution. Second, the coating agent is added into the separation medium to suppress the desorption of the coating from the walls. Mazzeo et al.[25] have demonstrated the use of MC as a dynamic coating on silica capillary walls for reduction of EOF and protein adsorption; this work has adapted their protocols to PDMS and extended its use to dampen other anomalous flows.

The following experiments demonstrate, for the first time, that dynamic coatings of MC on the oxidized PDMS surface reduce both EOF and compression of the pH gradient, improving the resolution and reproducibility of IEF in PDMS microchannels. Because these PDMS microchannels are only 2 cm in length, separation times and applied voltages are greatly reduced when compared to cIEF.

2.2 Experimental Section

2.2.1 Materials and reagents

Recombinant green fluorescent protein (GFP, MW ~28kDa) was obtained from Upstate Biotechnology (Lake Placid, NY, USA). Allophycocyanin (APC, MW ~104 kDa), r-phycoerythrin (PE, MW ~240 kDa) and fluorescently dyed flow-tracing particles (F-8820) were purchased from Molecular Probes (Eugene, OR, USA). Methylcellulose (viscosity of 2% aqueous solution at 25ºC: 400 centipoises), Pharmalyte pH 3-10 carrier ampholytes, fluorescent IEF markers with pIs of 3.0 and 8.7 and NaOH were obtained from Sigma (St. Louis, MO, USA). H_3PO_4 was obtained from J.T. Baker Inc. (Phillipsburg, NJ, USA).

2.2.2 Fabrication of PDMS microchips

Fabrication of the PDMS device is based on a soft lithography technique which has two main steps: patterning and replica molding. In a first step, a positive pattern of the desired channel structure is formed on a glass or Si-wafer substrate using positive photolithography technique.[26] The thickness of the pattern is controlled by the photoresist spin rate and time. Currently, this is done in a clean room while the replica-

molding technique can be performed outside the clean room. PDMS prepolymer and curing agent (Sylgard 184, Dow Corning Inc., Midland, MI, USA) were uniformly mixed at a ratio of 10:1, respectively, and degassed for 2 hrs at 0.001 Torr. The thickness of the substrates was controlled by the quantity of PDMS prepolymer applied. The liquid elastomer is cast onto a positive pattern formed on a glass substrate and cured in a hot kiln for 6 hrs at 80˚C. At the end of the curing process, the elastic polymeric material is carefully peeled from the glass substrate to become the bottom layer of the microchip. The open channel on this bottom layer is irreversibly sealed with a flat surface of another layer of PDMS substrate containing holes as reservoirs after both surfaces have been oxidized by plasma.[27] An image of a microchip is shown in Figure 2.1. The microchannel is 2 cm in long, 300 μm wide and 5 μm deep and has a built-in positioning scale (Figure 2.1C) that runs from 0 to 20 mm in 1 mm increments which is used to locate protein bands positions.

2.2.3 Test of EOF in PDMS microchips

To measure EOF, the fluorescently labeled flow-tracing particles are mixed into an electrolyte solution (0.1 mM NaOH, pH~10, containing 0.0%~0.8% w/w MC), which is then loaded into the microchip. This chip is mounted on the stage of an inverted epifluorescence microscope (CKX41 Olympus, Japan) equipped with a CCD camera (PIVCAM 13-8, TSI, Inc., MN, USA) with continuous image capture (Insight, Version 3.20, TSI, Inc, MN, USA). Electric potentials up to 400 V are applied across a 2 cm channel using a 30 kV power supply (Unimicro Technologies, Inc., CA, USA). Particle

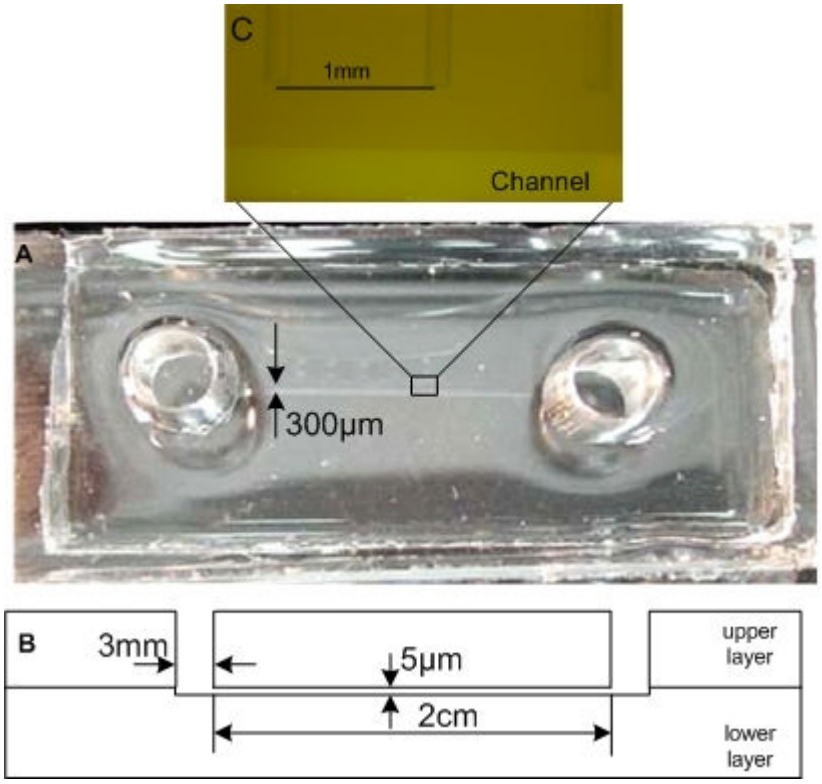

Figure 2.1 Geometry of the PDMS microchip. (A) Photo of PDMS chip with 2-cm-long microchannel. (B) Schematic of side view of microchip. The upper layer contains two holes as reservoirs and lower layer has a channel etched on its surface. (C) A millimeter scale is etched into the surface of lower layer.

tracking[28] is applied to obtain spatially resolved velocity profiles by taking measurements in at least five different runs for each concentration of MC.

2.2.4 IEF in a single PDMS channel

Before running IEF separations, the following conditioning procedure was used to reduce EOF and to discourage protein adsorption on the channel surfaces. First, the channel was flushed for 1 min at 10 psi with 1M NaOH to obtain uniformly deprotonated surface silanol groups. The flush solution was allowed to stay in the channel for 10 min and was then pushed out of the channel using 5 psi compressed nitrogen gas. This was followed by repeating the first flush using 100 mM NaOH. To coat the channel walls, 0.4% w/w MC was introduced into the channel and allowed to remain for 10 min. After this solution was removed using nitrogen, the channel was carefully pressure-filled with a mixture of 4% v/v ampholyte, 0.4% w/w MC and protein. Excessive sample solution in the reservoirs was removed using a micropipet. In an effort to further clean the reservoirs, nanopure water was loaded via micropipet and quickly removed. The anodic and cathodic reservoirs were then filled, respectively, with 50 mM H_3PO_4 in 0.2% w/w MC as anolyte and 50 mM NaOH in 0.2% w/w MC as catholyte. Platinum wire electrodes were then placed in the reservoirs and focusing was carried out at constant electric potentials up to 200V using an XHR 600-1 power supply (Xantrex technology Inc, Vancouver, Canada). Current was monitored using a digital multimeter, 3466A (Hewlett Packard, USA).

The loaded chip was mounted underneath the objective lens of a Leica DMLB fluorescence microscope equipped with a CCD camera (SPOT RT color, Diagnostic

instruments, Inc., Sterling Heights, MI USA) and the channel was checked for the presence of fluorescent proteins. The fluorescent proteins were excited with a mercury lamp (OSRAM HBO® 100 W/2) using filter cubes (DMLB 513804 and DMLB 513808, Leica Microsystems, Inc., IL, USA). The images were collected through 4x and 10x objectives and the positions of the protein bands were obtained according to a channel scale fabricated into the PDMS (Figure 2.1C).

Electropherograms were obtained from the pixel intensities of the microscope still images by using ImageJ (http://rsb.info.nih.gov/ij) to average the intensities across the channel width after subtracting the background signal intensity from the images. In cases where the protein bands were not in the same field of view, spatial electropherograms were obtained by binning each image together based on the built-in scale. Peak resolutions were obtained by using spatial moments to estimate the peak positions and widths from the electropherograms.

These PDMS chips can be reused several dozen times if attention is paid to pressure loading procedures and post-run conditioning, in particular, keeping the loading pressures below 10 psi to avoid separating the mated surfaces of the chip. After each run, the microchannel was rinsed several times with 1 M NaOH and then several times more with nanopure water. Finally, water is removed from the channel using nitrogen gas and the channel is stored at 4 ˚C.

2.3 Results and Discussion

Treatment of native PDMS surfaces with an oxygen plasma converts $-OSi(CH_3)_2-$ groups to Si-OH which temporarily makes those surfaces hydrophilic.[16] Plasma-oxidized PDMS surfaces bond well, facilitating the loading process when higher driving pressures are required to flush liquids through the channel. There is evidence 1) that EOF does not provide perfect plug flow in the separation channel,[29] 2) that the EOF varies along the separation channel due to the pH gradient,[30] 3) and that a plasma-oxidized PDMS surface is unstable when exposed to air,[31] resulting in EOF values that drift over a timescale of days. EOF mobilization is not used in our microchannels since we chose to observe focusing under a fluorescence microscope.

Theoretically, the complete elimination of EOF requires that the charge be identically zero everywhere on the separation surfaces but, in practice, it appears that this ideal surface does not exist for very long.[32] However the following equation,

$$\mu_{eo} = \frac{\varepsilon}{4\pi}\int_0^{\zeta}\frac{1}{\eta}d\psi \tag{2.1}$$

which was derived by Hjertén[2] to describe the electroosmotic mobility, suggests a way to suppress EOF without setting the surface charge to zero. Here ε is the dielectric constant, ζ is the zeta potential, ψ is the electric potential at a distance x from the wall and η is the viscosity in the electrical double layer. Although, eq 2.1 was developed for CE, it is also expected to apply to rectangular channels. It implies that EOF can be damped by coating the surface with a thin layer of hydrophilic, nonionic polymer to increase the viscosity of the fluid within the double layer.[33] Nonionic coatings can also help reduce the surface charge density on the channel wall and lower the net charge within the double layer.[34]

Thus the microchannels were pretreated with MC to form a temporary coating on the channel walls, and to suppress desorption of MC during a run, MC was also added to the sample solution. In this way, the dynamic coating of MC was maintained on the channel walls over the course of the experiment.

Figure 2.2A shows the completed separation of PE and GFP near the center of the channel in 10 min under an electric field of 25 V/cm. It can be clearly seen that GFP was resolved into two bands. Figure 2.2B demonstrates that the same bands have drifted 5 mm closer to the cathode 17 min later. The focused protein bands gradually slowed to a stop after 17 min and remained stationary at this new position ~5 mm from cathode.

Two unexpected phenomena were observed in this experiment. The first is "compression" of the pH gradient in which the focused pH gradient is substantially shorter than the 2-cm length of the channel from anode to cathode. In Figure 2.2 the distance between the PE and GFP bands is ~0.75 mm. However, according to their pIs, ~4.4 for PE and ~6.0 for GFP as obtained by IEF-PAGE, the distance should be ~4.57 mm for a linear pH gradient uniformly distributed across a 2-cm-long channel. This strongly suggests that the gradient extends over a significantly foreshortened region of the channel and, to our knowledge, this phenomena has not been reported in microchips before.

Mosher et al.[35] have predicted compression of ampholyte-based pH gradients the their IEF model and claimed that it is due to electrolyte diffusion into the separation space, in

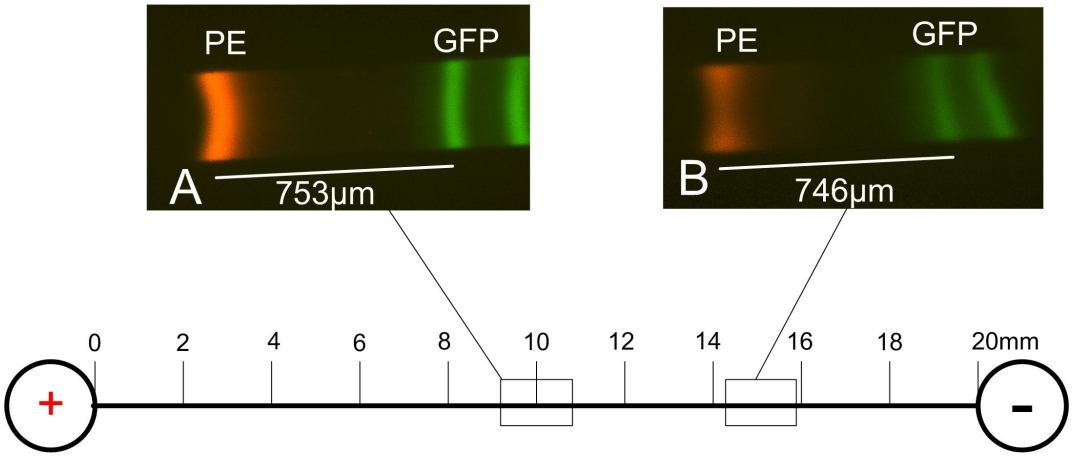

Figure 2.2 IEF separation of PE and GFP. Images A and B were acquired from the same experiment at 10 and 17 min, respectively, after initiation of IEF. Sample solution, 0.4% w/w MC, 4% v/v Pharmalyte 3-10, PE 0.04 µg/µL, GFP 0.04 µg/µL. Cathode solution, 50 mM NaOH containing 0.2% w/w MC, anode solution, 50 mM H_3PO_4 containing 0.2% w/w MC. Voltage, 50 V. The difference in band intensity between (A) and (B) is due to variations in intensity of the mercury lamp.

particular, when running horizontal slab gels with small anolyte/catholyte reservoirs relative to the separation space. However the mechanism in our case may be different from that proposed by Mosher et al[31] since the microchips used in our experiments have large reservoirs relative to the separation channel.

The other phenomenon observed in Figure 2.2 is drift of the protein bands toward the cathode after focusing since they are expected to remain stationary if there is no EOF. To determine if the movement of the focused protein bands toward the cathode resulted from EOF, the effect of MC concentration on EOF was tested. Figure 2.3 demonstrates that the EOF velocity, which is toward the cathode at alkaline pH, was reduced more than 20-fold in presence of 0.1% MC when compared to 0% MC. Further increasing the MC concentration caused incremental reductions in the EOF velocity. Zero EOF velocity (falls off the y-axis in the semi-log plot) was measured at 0.8% MC under an electric field strength of 50 V/cm.

IEF experiments with five species (IEF marker pI 3.0, PE, APC, GFP and IEF marker pI 8.7) were also performed at different concentrations of MC in the pretreatment of the microchannels and in the sample solutions, 0%, 0.4% and 0.8%, while other run conditions remained unchanged. Without MC, pI marker 8.7 and GFP drifted into the cathode reservoir within 5 min after focusing. However, in the presence of 0.4% and 0.8% MC, IEF marker pI 8.7 focused ~5 mm from the cathode reservoir and then slowly drifted to stationary positions ~4 mm from the cathode reservoir. This suggests that the

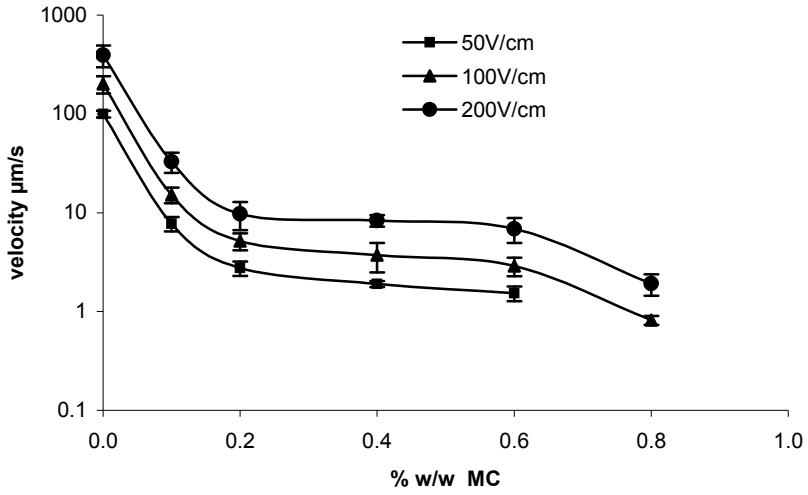

Figure 2.3 Semilog plot showing the effect of MC concentrations on EOF in a PDMS microchannel at different electric field strengths in 0.1 mM NaOH at pH 10. Data points represent the average of five measurements with standard deviations. With the exception of the missing point at 0.8% MC where the EOF velocity was determined to be zero, the electrophoretic mobilities are nearly constant at each fixed MC concentration.

shift of the pH gradient toward cathode after focusing was only partially caused by EOF within the pH gradient.

Since compression of the pH gradient appears to require a flow of anolyte/catholyte into the channel from both of the reservoirs, it should be mitigated by preventing electrolyte from being drawn into the channel. A simple way to achieve this is to increase the viscosity in the electrode solutions by placing high-viscosity polymer solutions in the two reservoirs, like two plugs, to reduce the amount of fluid being drawn into the separations channel from the reservoirs.

This hypothesis was verified by the following experiment in which the concentrations of MC in the electrode reservoir solutions was increased from 0.2% to 2.5%. Figure 2.4 is a comparison of pH gradient lengths under different run conditions. Figure 2.4A shows an electropherogram of focused protein species without MC. In this case, the pH gradient of 3-8.7 had a length of ~1.5 mm. Figure 2.4B shows that focusing with 0.4% MC dynamic coating and 0.2% MC in electrode solutions extended the pH gradient by 70% as compared with 0% MC. Figure 2.4C shows that 0.4% MC dynamic coating and 2.5% MC in the electrode solutions extended the pH gradient ~3-fold when compared with Figure 2.4B. The reader should note, however, that the pH gradient shown in Figure 2.4C is still compressed since the measured distance between pI marker 3.0 and pI marker 8.7, ~7.6 mm, is shorter than the 16.3 mm expected between the PE and GFP bands in an ideal, linear pH gradient formed across a 2-cm-long channel. These results

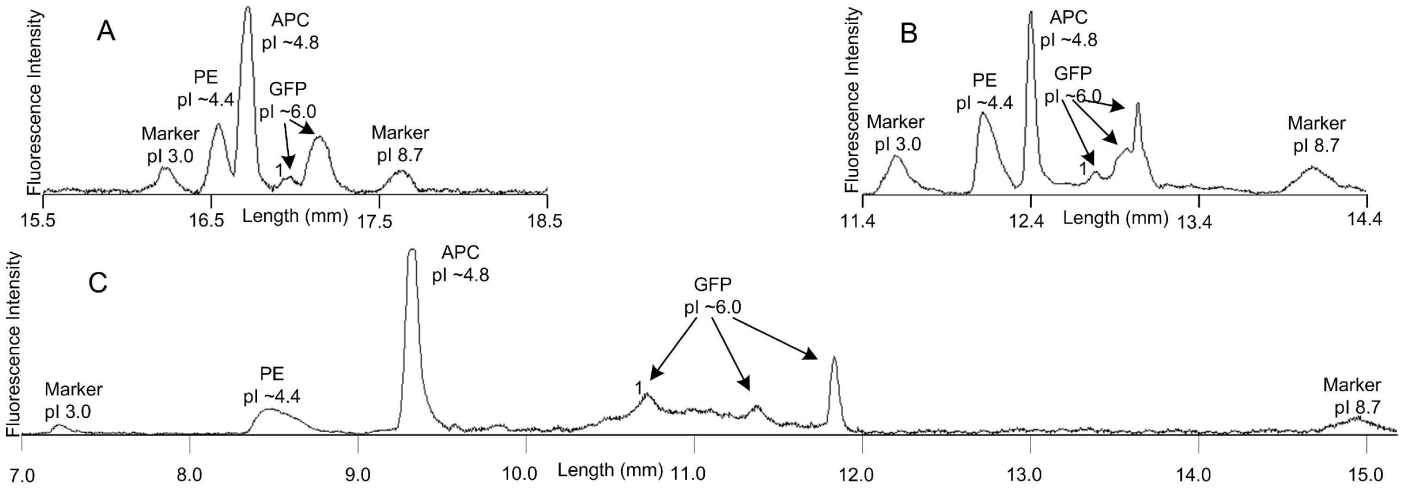

Figure 2.4 Comparison of pH gradient lengths under different run conditions. (A) Without MC in sample solution and electrode solutions. (B) With 0.4% w/w in sample solution and 0.2% w/w MC in electrode solutions. (C) With 0.4% w/w MC in sample solution and 2.5% w/w MC in electrode solutions. All experiments were performed in the same chip at same electric field strength 50 V/cm. Electrophoregrams represent the separations right after focusing was completed. Sample solution, 4% v/v Pharmalyte 3-10, Marker pI 3.0, 0.6 μg/μL, PE 0.014 μg/μL, APC 0.05 μg/μL, GFP 0.034 μg/μL, marker pI 8.7 0.3 μg/μL. Cathode solution, 50 mM NaOH, anode solution, 50 mM H_3PO_4.

Table 2.1 Comparison of pH gradient and resolutions of protein species with different MC concentrations present in sample and electrode solutions

	0% MC in sample and 0% in electrode solutions	0.4% MC in sample solution and 0.2% MC in electrode solutions	0.4% MC sample solution and 2.5% MC electrode solutions
Position of IEF marker pI 3.0 (mm)	15.8±0.7	11.5±0.6	7.1±0.3
Length of pH gradient of 3.0-8.7 (mm)	1.9±0.7	2.3±0.4	7.6±0.5
$R_{PE,APC}$[a]	0.5±0.1	1.03±0.05	1.7±0.4
$R_{APC,GFP1}$[b]	1.3±0.2	1.8±0.1	4.6±0.3

[a]Resolution of PE and APC. [b]Resolution of APC and GFP peak 1. GFP peak 1 is indicated in Figure 2.4. Each data point represents the average of three measurements and the standard error. Experimental conditions are the same as indicated in Figure 2.4. The positions and resolution of peaks were calculated from image intensities using moment analysis.

are also summarized in Table 2.1 where they demonstrate that the use of both MC dynamic coatings in the separation channel and 2.5% MC in the electrode solutions improved IEF resolution and suppressed pH gradient drift at low electric field strengths.

These benefits can be visualized in following experiment (Figure 2.5). When an electric field of 50 V/cm was applied across the channel, two concentration waves formed at opposite ends of the channel (Figures 2.5A and B) and moved towards each other. Time-series photos (Figures 2.5C-H) show that PE and APC passed through the corresponding GFP bands. The final focusing stages of the GFP bands are shown in Figures 2.5I, J and K. Figures 2.5L, M and N demonstrate that, after focusing, the GFP bands remained stationary instead of moving toward the cathode. Four variants of GFP, shown in Figure 2.5N, were visibly resolved into two bright bands and two dim bands. The final positions (Figures 2.5O and P) of the six focused bands were located between 6 mm and 10 mm from the anode and remained stationary.

To reduce focusing time, the electric field was increased to 100V/cm. In this case focusing was completed in 3 min but the protein bands (Figure 2.6c) shifted toward the cathode. At electric field strengths of 25 V/cm and 50 V/cm, focusing was completed within 10 min and 6 min, respectively, but the focused bands remained stationary (Figures 2.6a and b) and became sharper as the electric field was increased (Figure 2.6). The resolution of the two major GFP bands was calculated using spatial moments to determine the peak width and distance between peaks (Figures 2.6A-C). Comparing

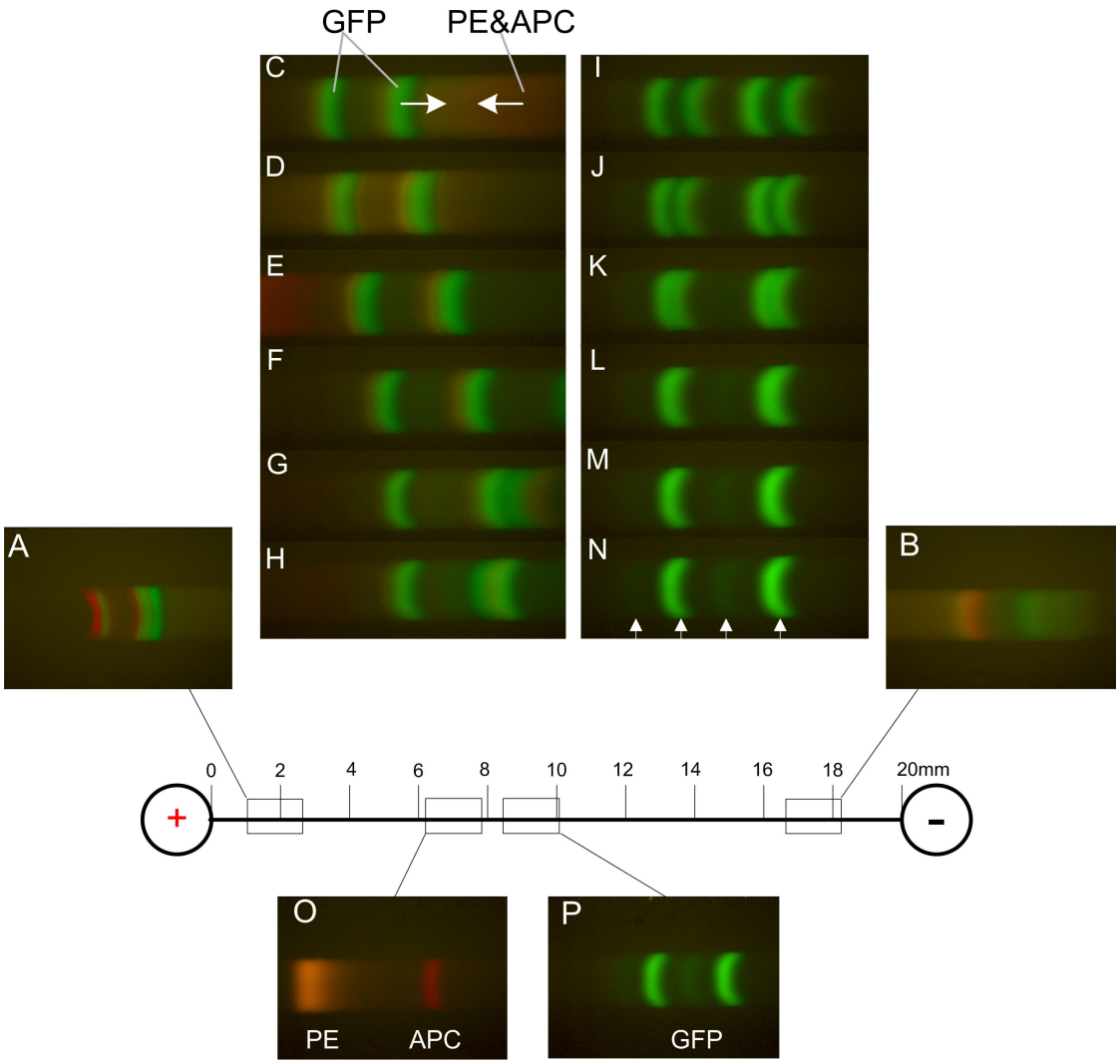

Figure 2.5 IEF separation of PE, APC and GFP with increased viscosity in the electrode solutions. All images were acquired in the same experiment. Sample load solution, 0.4% w/w MC, 4% v/v Pharmalyte 3-10, PE 0.02 µg/µL, PE 0.06 µg/µL, GFP 0.04 µg/µL. Cathode solution, 50 mM NaOH containing 2.5% w/w MC, anode solution, 50 mM H_3PO_4 containing 2.5% w/w MC. Voltage, 50 V/cm. Images A, B, O and P were taken at 40 s, 190 s, 615 s and 645 s, respectively, after the initiation of IEF. Images C-H and I-N were taken continuously with 4-s exposures starting at 310 and 340 s, respectively, after initiation of IEF. The four arrows on image L point to four variants of GFP.

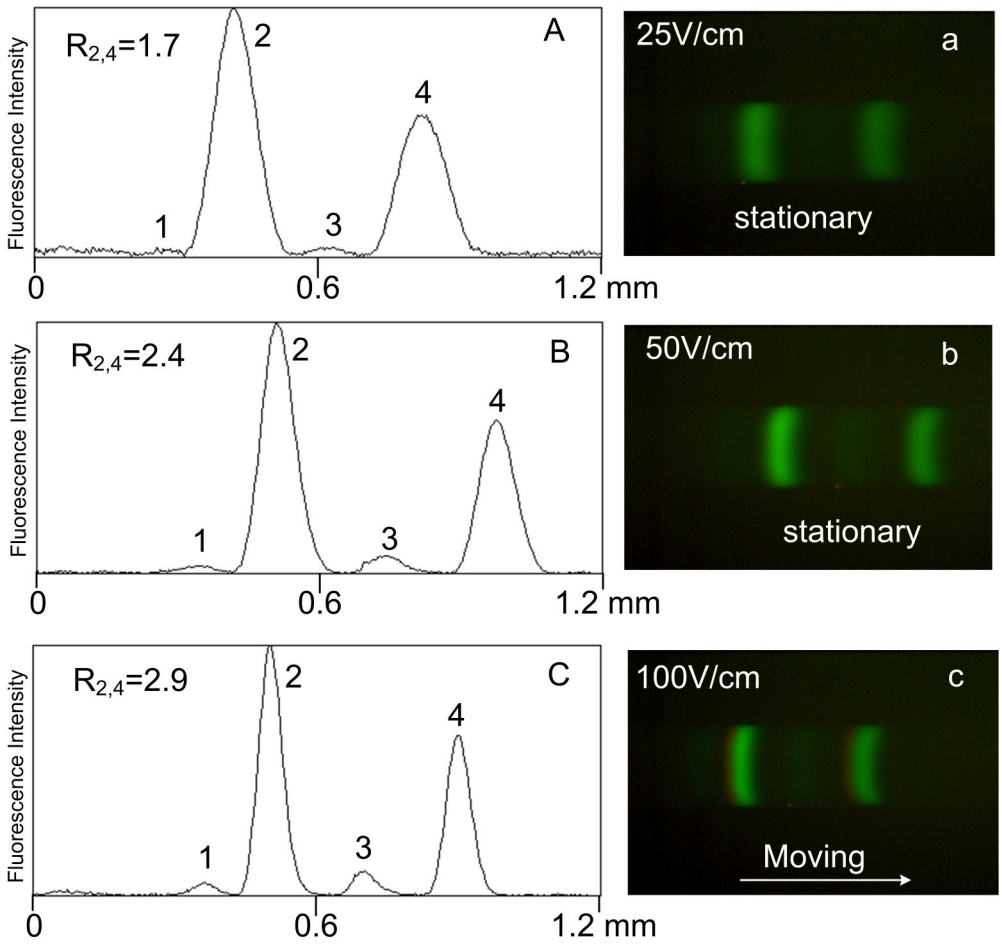

Figure 2.6 Final results of GFP focusing obtained from three separate experiments with identical conditions except the electric field strength, which is shown in the images. Images a-c were taken in 10, 6 and 3 min respectively. Plots A-C are the electropherograms of a-c respectively. $R_{2,4}$ is the resolution of GFP peaks 2 and 4. Sample solution, 0.4% w/w MC, 4% v/v Pharmalyte 3-10, PE 0.02 µg/µL, APC 0.06 µg/µL, GFP 0.04 µg/µL. Cathode solution, 50 mM NaOH containing 2.5% w/w MC. Anode solution, 50 mM H_3PO_4 containing 2.5% w/w MC.

Figures 2.6A and B, the resolution was increased by $\sim\sqrt{2}$ which is consistent with IEF theory.[36] However, when the field strength was doubled again to 100 V/cm, the resolution increased by less than $\sqrt{2}$. This lower-than-expected increase in resolution may be due to a shift in the pH gradient or to the presence of large *transient* temperature gradients (Figure 2.7) induced by the higher electric fields. The resolution achieved here, R~2.4, is ~3 times greater than those found in previous studies[23] in a 1.2-cm-long polycarbonate channel using broad-range ampholytes in free solution under an electric field strength of 1500 V/cm.

An advantage of microchannel-based electrophoretic separation is the reduction in Joule heating, which could otherwise impair the quality of the separation.[37,38] Figure 2.7 is a simulation of the temperature excursion which occurs along the centerline of the separation channel during electrofocusing at 50 V/cm. Since the voltage was held constant in the experiment, the measured current was used to calculate the power per unit volume, $I_T \times \Delta V/(L \times W \times H)$, released within the channel. The ability of the microchip to dissipate Joule heat *rapidly* is largely determined by its thermal diffusivity, $\sim 0.14 \times 10^{-6}$ m^2/s, which is slightly lower than that for water, and about half those of glass and fused silica.

Assuming uniform power dissipation in the channel, using the thermal properties of water in the channel and of PDMS in the body of the chip, we predict that the centerline channel temperature rises ~0.2°C in the first 10 s of the experiment and then tracks the monotonic decline of the current to an overambient of ~0.01°C at 10 min. When the

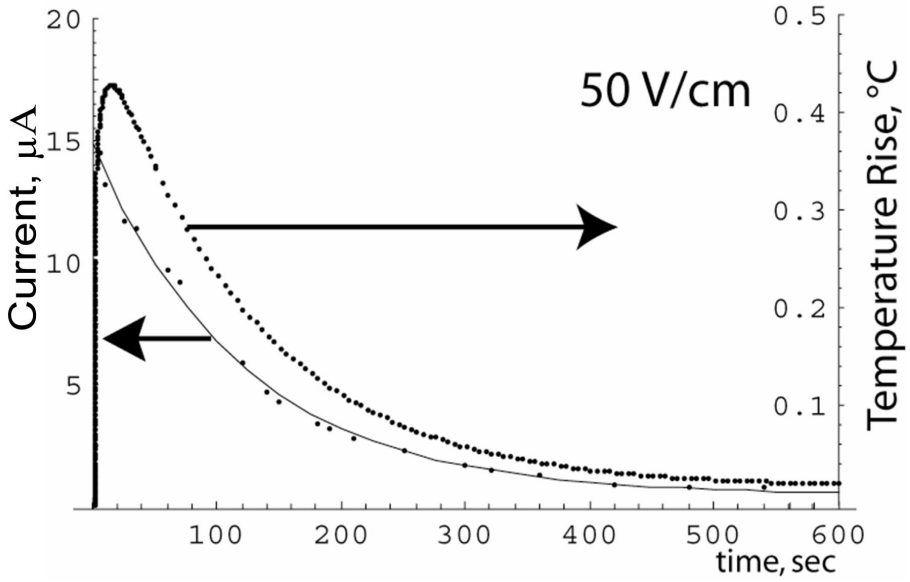

Figure 2.7 Measured current and predicted centerline temperature rise in a PDMS microchip channel. Current across the separation channel was measured during isoelectric focusing in 4% broad-range ampholytes at 50 V/cm. The measured current was fit to an exponential curve, and this was plugged into a scripted finite-element package (FlexPDE from PDESolutions, Antioch CA) to simulate the chip temperatures as a function of time. The maximum temperature rise of 0.43°C occurs near 13 s and the long-term temperature rise at 600 s is ~0.021°C.

voltage is doubled, the maximum temperature rise and long-time temperature rise will nearly quadruple to 0.7 and 0.03°C, respectively, over roughly the same time frame. Doubling the voltage again gives maximum and long-time ΔTs of 1.5 and 0.08°C, over the same time frame yet again since chip cooling rates are largely independent of power input. It is worth noting that, although the steady-state temperature variations above are too small to have much of an impact on resolution,[37,38] the transient excursions are large enough to provoke significant dispersion along the 300 micron edges of the channel.

While the geometry of our PDMS microchip (Figure 2.1), a small channel embedded in a large substrate, is not efficiently designed for cooling, the relatively small channel volume and low applied electric field strength coupled with the thermal diffusivity of PDMS is adequate for IEF separations at these low field strengths. This is consistent with work reported by Effenhauser et al.[17] who successfully performed zone electrophoresis in PDMS microchannels (35 mm in length, 50 μm in width, 20 μm in depth) at electric field strengths of 100-500 V/cm without significant dispersion due to Joule heating.

2.4 Conclusions

Ampholyte-based IEF has been demonstrated for the first time in free solution in oxygen plasma-conditioned PDMS microchip channels using MC to suppress EOF as well as peak drift and pH-gradient compression. MC dynamic coatings provide a convenient way to suppress EOF by one or more orders of magnitude and, when introduced into the anolyte/catholyte reservoirs as a thickening agent, can significantly reduce drift and peak compression, permitting higher resolution across the pH gradient. The fact that viscous

reservoir plugs can substantially reduce these effects strongly suggests that they are driven, at least in part, by convective flows.

The temperature rise in this chip was simulated using a finite element package and showed that, while long-time temperature excursions are too small to cause significant dispersion at lower field strengths, at 100 V/cm and higher fields, the transient temperature excursion may be large enough to negatively impact resolution, especially in the high-aspect ratio channels used here. Since the ultimate resolution in ampholyte-based IEF is path-dependent, high-resolution protocols may require voltage programming similar to that used in IEF-PAGE.

However, the fact that less than 5 nanograms of a protein mixture loaded in the microchannel have been resolved into 6 or more bands in 6 min under an electric field strength of 50 V/cm makes this approach competitive with cIEF in terms of resolving power. Furthermore, the shorter run times and the lower cost of IEF in PDMS microchips make it plausible to integrate IEF with other "on chip" unit operations.

2.5 References

(1) Kilár, F. *Electrokinetic Phenomena: Principles and Applications in Analytical Chemistry and Microchip Technology*; Rathore, A. S., Guttman, A., Eds.; Marcel Dekker: New York, 2004; pp. 43-63.

(2) Hjertén, S. *Chromatogr. Rev.* 1967, 9, 122-219.

(3) Jorgenson, J. W.; Lukacs, K. D. *Anal. Chem.* 1981, 53, 1298-1302.

(4) Jorgenson, J. W.; Lukacs, K. D. *J. Chromatogr*. 1981, 218, 209-216.

(5) Albarghouthi, M. N.; Stein, T. M.; Barron, A. E. *Electrophoresis* 2003, 24, 1166-1175.

(6) Mao, Q.; Pawliszyn, J. *Analyst* 1999, 124, 637-641.

(7) Harrison, D. J.; Fluri, K.; Seiler, K.; Fan, Z.; Effenhauser, C. S.; Manz, A. *Science* 1993, 261, 895-897.

(8) Hofmann, O.; Che, D.; Cruickshank, K. A.; Müller, U. R. *Anal. Chem.* 1999, 71, 678-686.

(9) McMormick, R. M.; Nelson, R. J.; Goretty Alonso-Amigo, M.; Benvegnu, D. J.; Hooper, H. H. *Anal. Chem*. 1997, 69, 2626-2630.

(10) McDonald, J. C.; Duffy, D. C.; Anderson, J. R.; Chiu, D. T.; Wu, H.; Schueller, O. J.; Whitesides, G. M. *Electrophoresis* 2000, 21, 27-40.

(11) Rossier, J. S.; Schwarz, A.; Reymond, F.; Ferrigno, R.; Bianchi, F.; Girault, H.; *Electrophoresis* 1999, 20, 727-731.

(12) Li, Y.; Buch, J. S.; Rosenberger, F.; DeVoe, D. L.; Lee, C. S. *Anal. Chem*. 2004, 76, 742-748.

(13) Liu, R. H.; Yang, J.; Lenigk, R.; Bonanno, J.; Grodzinski, P. *Anal. Chem.* 2004, 76, 1824-1831.

(14) Becker, H.; Gärtner, C.; *Electrophoresis* 2000, 21, 12-26.

(15) Kumar, A.; Whitesides, G. M. *Appl. Phys. Lett*. 1993, 63, 2002-2004.

(16) Sia, S. K.; Whitesides, G. M.; *Electrophoresis* 2003, 24, 3563-3576.

(17) Effenhauser, C. S.; Bruin, G. J. M.; Paulus, A.; Ehrat, M. *Anal. Chem.* 1997, 69, 3451-3457.

(18) Duffy, D. C.; McDonald, J. C.; Schueller, O. J. A.; Whitesides, G. M. *Anal. Chem.* 1998, 70, 4974-4984.

(19) Chen, X.; Wu, H.; Mao, C.; Whitesides, G. M. *Anal. Chem.* 2002, 74, 1772-1778.

(20) Wang, Y.-C.; Choi, M. H.; Han, J. *Anal. Chem.* 2004, 76, 4426-4431.

(21) Tan, W.; Fan, Z. H.; Qiu, C. X.; Ricco, A. J.; Gibbons, I. *Electrophoresis* 2002, 23, 3638-3645.

(22) Ocvirk, G.; Munroe, M.; Tang, T.; Oleschuk, R.; Westra, K.; Harrison, D. J. *Electrophoresis* 2000, 21, 107-115.

(23) Li, Y.; DeVoe, D. L.; Lee, C. S. *Electrophoresis* 2003, 24, 193-199.

(24) Horvath, J.; Dolník, V. *Electrophoresis* 2001, 22, 644-655.

(25) Mazzeo, J. R.; Krull, I. S. *Anal. Chem.* 1991, 63, 2852-2857.

(26) Unger, M. A.; Chou, H. P.; Thorsen, T.; Scherer, A; Quake, S. R. *Science*, 2000, 288, 113-116.

(27) Horiuchi, K.; Dutta, P.; Cui, H.; Ivory, C. F. Proceedings of 2003 Intl. Mechanical Engineering Congress and Exposition (IMECE), Washington DC, USA, Nov. 15-21, 2003.

(28) Santiago, J. G.; Wereley, S. T.; Meinhart, C. D.; Beebe, D. J.; Adrian, R. J. *Exp. Fluids* 1998, 25, 316-319.

(29) Tsuda, T.; Nomura, K.; Nakagawa, G. *J. Chromatogr*. 1982, 248, 241-247.

(30) Herr, A. E.; Molho, J. I.; Santiago, J. G.; Mungal, M. G.; Kenny, T. W. *Anal. Chem.* 2002, 72, 1053-1057.

(31) Ren, X.; Bachman, M.; Sims, C.; Li, G. P.; Allbritton, N. *J. Chromatogr B* 2001, 762, 117-125.

(32) Kim, J.; Chaudhury, M. K.; Owen, M. J.; *IEEE Transactions on Dielectrics and Electric Insulation*, 1999, 6, 695-702.

(33) Hjertén, S. *Capillary Electrophoresis: Theory and Practise*; Grossman, P. D., Colburn, J. C., Eds.; Academic Press: San Diego, 1992; pp 191-214.

(34) Hjertén, S. *J. Chromatogr.* 1985, 347, 191-1998.

(35) Mosher, R. A.; Thormann, W.; Bier, M. *J. Chromatogr.* 1988, 436, 191-204.

(36) Righetti, P. G. *Isoelectric Focusing: Theory, Methodology and Applications*; Elsevier Biomedical Press: New York, 1983; pp 22-31.

(37) Grushka, G.; McCormick, R. M.; Kirkland, J. J. *Anal. Chem.* 1989, 61, 241-246.

(38) Gobie, W. A.; Ivory, C. F. *J. Chromatogr.* 1990, 516(1), 191-210.

CHAPTER 3

Multi-stage Isoelectric Focusing in a Polymeric Microfluidic Chip

Huanchun Cui,[†] Keisuke Horiuchi,[‡] Prashanta Dutta,[‡] and Cornelius F. Ivory*,[†]

† Department of Chemical Engineering, and ‡ School of Mechanical and Materials Engineering, Washington State University, Pullman, Washington 99164

*To whom all correspondence should be addressed. Email: cfivory@wsu.edu

Abstract

This paper reports a protocol that improves the resolving power of isoelectric focusing (IEF) in a polymeric microfluidic chip. This method couples several stages of IEF in series by first focusing proteins in a straight channel using broad-range ampholytes and then refocusing segments of the first channel into secondary channels that branch from the first one at T-junctions. Experiments demonstrate that several fluorescent proteins that had focused within a segment of the straight channel in the first stage were refocused at significantly higher resolution due to the shallower pH gradient and higher electrical field gradient. Two variants of green fluorescent protein (GFP) from the second stage IEF fractionation were further separated in a third stage. Three-stage IEF was completed in less than 25 min at electric field strengths ranging from 50 V/cm to 214 V/cm.

3.1 Introduction

The conventional method of protein separation in proteomics is two-dimensional polyacrylamide gel electrophoresis (2D-PAGE)[1] where, in the first dimension, proteins are resolved by polyacrylamide gel isoelectric focusing (IEF-PAGE) and, in the second

dimension, by sodium dodecyl sulfate- polyacrylamide gel electrophoresis (SDS-PAGE). However, 2D-PAGE is labor-intensive and the whole process, including stain/destain, usually takes two or more days to complete.[2] Microchip electrophoresis is a promising alternative to PAGE gels since it has the potential to provide rapid protein analysis,[3] straightforward integration with other microfluidic unit operations, on-line dection,[4] smaller sample sizes and lower fabrication costs.[5] However, the application of 2D electrophoresis on a microchip is much more challenging than 2D-PAGE due to the difficulty of coupling the two orthogonal separation techniques.

Several research groups have explored integration of zone electrophoresis and IEF on microfluidic chips. Chen et al.[6] described a method for carrying out 2D gel electrophoresis in a microfluidic system where integration of IEF and SDS electrophoresis was made possible by the ability to assemble and disassemble multiple poly(dimethylsiloxane) (PDMS) layers during a run. This system, however, required complicated sample/gel loading procedures and the alignment, bonding, and peeling of six PDMS layers. Herr et al.[7] performed 2D electrophoresis in a plastic microfluidic chip containing an IEF channel which intersected a zone electrophoresis channel. In this system, proteins focused in the IEF channel are mobilized to the intersection by electroosmotic flow (EOF) and then, after IEF field is turned off, zone electrophoresis is applied to them as the second dimension of separation. Each band focused in the IEF channel was processed in this sequence and the IEF bands far from the intersection were refocused repeatedly before they were subjected to zone electrophoresis.

Li et al[8] integrated liquid phase IEF with SDS-PAGE in a microfluidic chip. This chip, which consists of a single IEF channel networked with an array of orthogonal channels, provides a method to perform parallel SDS-PAGE on each of the IEF-focused proteins without rearranging the chip geometry. More recently, Wang et al.[9] developed a microfluidic chip which is able to select a defined p*I* range out of an IEF channel for further zone electrophoresis using two sets of pneumatically actuated PDMS valves.[10] A segment of channel shared by IEF and zone electrophoresis is used to transfer the focused proteins from IEF to zone electrophoresis by opening the valve on zone electrophoresis channel and closing the valve on IEF channel.

All of the examples above represent different schemes for coupling two orthogonal separation techniques in an effort to achieve maximum resolution with minimum loss of sample. However, IEF performance in these examples is low when compared with results reported for ampholyte-based, liquid-phase IEF separation of myoglobins with a resolving power of 0.02 pH units.[11,12] In this paper we developed a method for improving IEF resolving power by implementing an IEF staging technique which first focuses proteins in a broad pH range and then refocuses segments of that broad pH range in narrow pH ranges.

IEF staging is a fairly routine purification strategy at preparative scales. The multicompartment electrolyzer with isoelectric membranes developed by Righetti and coworkers[13-15] for preparing narrow pH cuts from wide pH range carriers ampholytes was prototypical of staged IEF apparatuses. Narrow pH cuts can be further fractionated in the

multicompartment electrolyzer with corresponding isoelectric membranes to produce ultra-narrow pH cuts. The IsoPrime multicompartment electrolyzer (Amersham Biosciences, Piscataway, NJ, USA) and the Rotofor system (Bio-Rad Laboratories, Hercules, CA, USA) are preparative protein purification devices which fractionate proteins in free solution by liquid-phase IEF and can reprocess the fractions that may contain other contaminating proteins as well as the protein of interest. Staged IEF using the IsoPrime multicompartment electrolyzer and the Rotofor system for maximum resolution of protein separations have been reported elsewhere.[16-18] To our knowledge, IEF staging has not yet been applied in micro-scale separations.

In this work, the concept of "staging," in which a single dimension of separation is re-applied to a sample to improve resolution, is introduced for microchip electrofocusing. The term "multi-stage fractionation", in which a single protocol is re-applied to a sample to improve resolution, is used to distinguish this work from "multi-dimensional fractionations", in which two or more orthogonal separation techniques are sequentially applied to a sample. Microchip IEF is staged by first focusing proteins in a straight channel using broad-range ampholytes and then refocusing segments of that first channel in secondary channels that branch out from the first one. The following experiments demonstrate that staging IEF significantly increases the resolving power of IEF.

3.2 Experimental Section

3.2.1 Materials and reagents

Recombinant green fluorescent protein (GFP variants 1 and 2, p*I*=6.0 and 6.31, MW ~28 000) was obtained from Upstate Biotechnology (Lake Placid, NY). Allophycocyanin (APC, p*I*=4.38, MW ~104 000) and r-phycoerythrin (PE, p*I*=4.78, MW ~240 000) were purchased from Molecular Probes (Eugene, OR). p*I*s of PE, APC and two major GFP variants were determined by IEF PAGE with IEF p*I* markers (Sigma, St. Louis, MO). Methylcellulose (MC, viscosity of 2% aqueous solution at 25ºC: 400 centipoises), Pharmalyte pH 8-10.5 ampholine were obtained from Pharmacia Biotech (Uppsala, Sweden). Pharmalyte pH 3-10, 3-4, 4.2-4.9, 4.5-5.4, 6.7-7.7 carrier ampholytes, and NaOH were obtained from Sigma (St. Louis, MO). H_3PO_4 was obtained from J.T. Baker, Inc. (Phillipsburg, NJ). All MC concentrations used in this paper are given in weight/weight units and all ampholyte concentrations are in volume/volume units.

3.2.2 Fabrication of PDMS microchips

Fabrication of PDMS microchips was performed using the procedure reported in our previous work.[19] Briefly, a positive pattern of the desired channel structure is formed on a glass substrate using a positive photolithography technique.[20,21] PDMS prepolymer and curing agent (Sylgard 184, Dow Corning Inc., Midland, MI) were uniformly mixed at a ratio of 10:1, respectively, and degassed for 2 hrs at 0.001 Torr. The liquid elastomer is cast onto a positive pattern formed on the glass substrate and cured in a hot kiln for 6 hrs at 80˚C. At the end of the curing process, the elastic polymeric material is carefully peeled from the glass substrate to become the bottom layer of the microchip. The open

channel on this bottom layer is irreversibly sealed with a flat surface of another layer of PDMS substrate containing holes as reservoirs after both surfaces have been plasma-oxidized.[22] This microchip (Figure 3.1) consists of a straight channel and two secondary channels that branch out from the straight channel (Figure 3.1A). All channels are 300 μm wide and 10 μm deep (Figure 3.1B). Built-in positioning scales (Figure 3.1B) that run along channels in 1-mm increments are used to locate protein band positions.

3.2.3 PDMS microchannel conditioning

Our previous work[19] demonstrates that EOF is greatly reduced in PDMS by applying a dynamic coat of methylcellulose (MC) to the channel walls. To achieve this, the following conditioning procedure was used before running IEF separations. First, all channels were flushed for 1 min at 10 psi with 1M NaOH to obtain uniformly deprotonated surface silanol groups. The flush solution was allowed to stay in the channel for 10 min and was then pushed out of the channel using 5 psi nitrogen gas. To coat the channel walls, 0.4% MC was introduced into the channel and allowed to remain for 10 min. After this solution was removed using nitrogen gas, all channels were carefully pressure-filled with a mixture of 4% ampholyte, 0.4% MC and protein sample (total protein concentration, 0.12~0.2 μg/μL). Excess sample solution was removed from the reservoirs using a micropipet and electrode solutions were loaded into the reservoirs. 2.5% MC was added to the electrode solutions to suppress pH gradient drift as well as to discourage the intrusion of the electrode solutions into the separation channel.

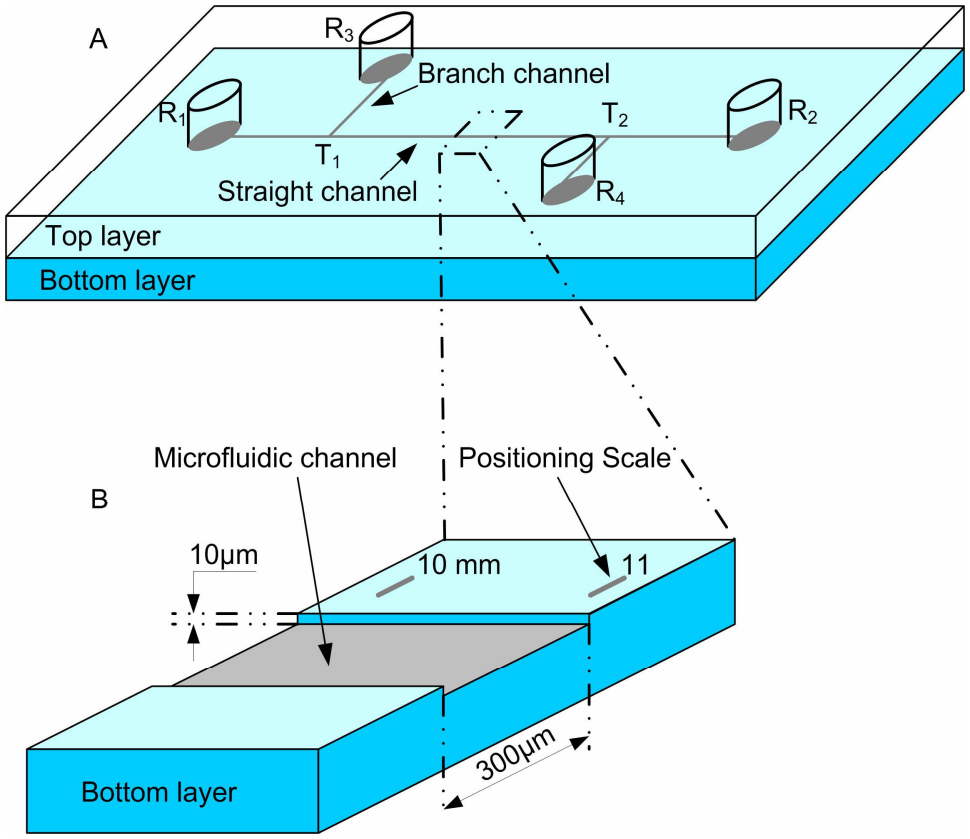

Figure 3.1 (A) Schematic of a PDMS microchip typically used for two-stage IEF. The length of the straight channel and branch channels are 20 mm and 5 mm respectively. The chip for three-stage IEF has two additional branch channels which are not shown in this Figure. R_1-R_4 are reservoirs and T_1-T_2 are T-junctions. (B) Schematic of the microchannel with depth and width of 10 μm and 300 μm, respectively. A millimeter positioning scale is etched into the surface of the bottom layer.

3.2.4 Multi-stage IEF operation

Platinum wire electrodes were placed in the two reservoirs at opposite ends of the straight channel and first-stage focusing was carried out at constant voltage using an XHR 600-1 power supply (Xantrex technology Inc, Vancouver, Canada) while the branch channel reservoirs were left electrically floating. After first-stage focusing had finished, the electrodes were quickly removed from the straight channel reservoirs and placed in the branch reservoirs to perform the second stage of focusing.

An important aspect of multi-stage IEF is the use of anodic and cathodic reservoir solutions to define a narrow pH range in a channel network initially filled with broad-range ampholytes. Initially, all of the networked channels are filled with 4% broad-range ampholytes (pH 3-10), 0.4% MC and protein. Then, to run the first stage of electrofocusing, strong acid (50 mM H_3PO_4**)** and strong base (50 mM NaOH) were used as electrode solutions in the straight channel reservoirs to define a pH range of 3-10. In the second- and third-stages, narrow-range ampholyte solutions were diluted in 2.5% MC solution and then used as reservoir solutions to define narrower pH ranges. For example, commercially available ampholyte solutions with pH ranges of 3-4 and 6.7-7.7 can be used as anodic and cathodic solutions respectively to define a pH range of ~3.5 to ~7.2. Those ampholytes in the separation media that have p*I* values out of this narrower pH range will presumably migrate out of the separation channels and into the reservoirs during second- and third-stage IEF.

3.2.5 Imaging

The loaded chip was mounted underneath the objective lens of a Leica DMLB fluorescence microscope equipped with a CCD camera (SPOT RT color, Diagnostic instruments, Inc., Sterling Heights, MI) and the channel was checked for the presence of fluorescent proteins. The fluorescent proteins were excited with a mercury lamp (OSRAM HBO® 100 W/2) using filter cubes (DMLB 513804 and DMLB 513808, Leica Microsystems, Inc., IL). The images were collected through 4x and 10x objectives and the positions of the protein bands were obtained according to a channel scale fabricated into the PDMS (Figure 3.1B). Electropherograms were constructed from microscope still image pixel intensities using ImageJ (http://rsb.info.nih.gov/ij) to average the intensities across the channel width after subtracting the background signal intensity from the images. In cases where the protein bands were not in the same field of view, spatial electropherograms were obtained by binding images together based on the built-in scale. Peak resolutions were obtained by using spatial moments to estimate the peak positions and widths from the electropherograms.[23]

3.3 Results and Discussion

Optimization of IEF in a single PDMS microchannel was investigated in our previous work.[19] High-viscosity polymer (MC) solutions placed in the reservoirs was used to reduce the intrusion of electrode solutions into the separation channel. Dynamic coatings of MC (0.4% in separation media) were employed on PDMS surfaces to minimize both EOF and wall-protein interactions. At an electric field strength of 50 V/cm, the overall time to reach steady state was increased by about 20% in 0.4% MC separation media when compared to the separation media without MC. It can be seen from eq 3.1[11] below

that the 0.4% MC used in separation media helps to increase resolution, most likely, by decreasing the diffusion coefficient

$$\Delta(pI) = 3\sqrt{\left|\frac{D}{E}\left(\frac{d(pH)}{dx}\Big/\frac{d\mu}{d(pH)}\right)\right|} \tag{3.1}$$

where Δ(p*I*) is the p*I* difference between resolved adjacent proteins, D is the diffusion coefficient of the protein, *d*(pH)/*d*x is the pH gradient, E is the applied electric field strength and *d*μ/*d*(pH) is the derivative of the electrophoretic mobility with respect to the pH at the protein's p*I*.

Eq 3.1 also shows that high resolution is favored by high field strengths. However, both pH gradient drift towards the cathode and bending of protein bands were observed in our previous experiments[19] as the electric field was increased to 100 V/cm in a single 2-cm channel with broad range ampholytes. Under optimal conditions, high resolution can be achieved within 6 min in single microchannel separations using broad-range ampholytes (pH 3-10) at relatively low electric field strengths (50 V/cm).

However, in multi-stage IEF separations, the presence of T-junctions can lead to transient band deformation and temporarily reduced resolution. In the next section, we will first discuss band deformation at T-junctions during IEF, then demonstrate two-stage IEF, three-stage IEF and, finally, present a comparison of integrated multi-stage IEF with single channel IEF.

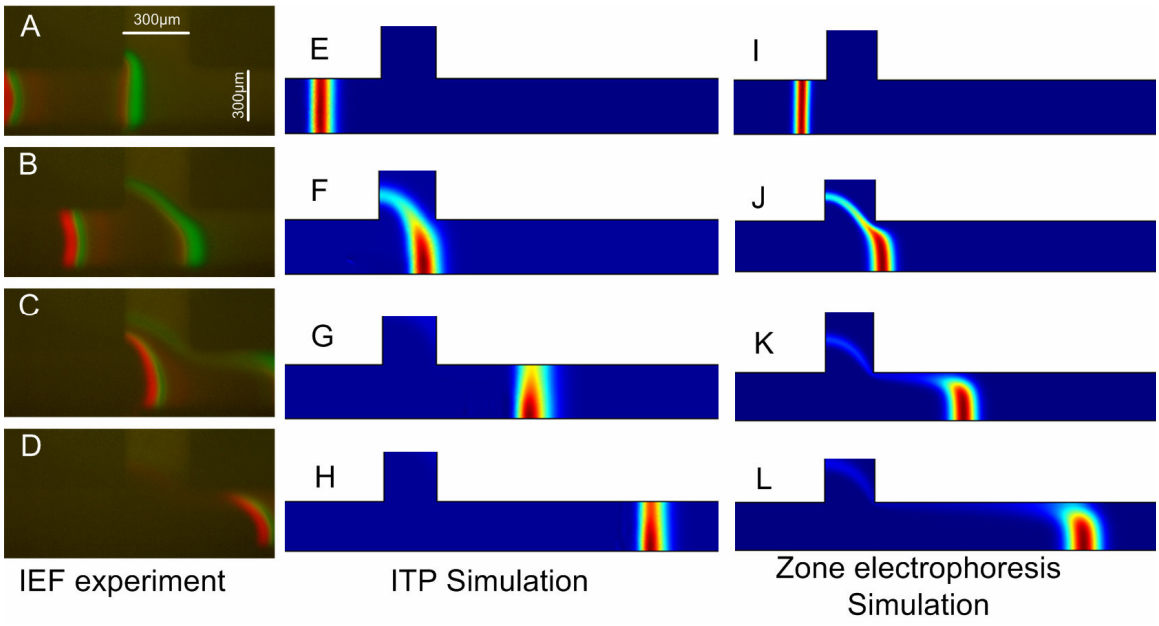

Figure 3.2 Band deformation at a T-junction. Time-series photos A to D were captured at 87, 95, 107 and 123 s, respectively, after the initiation of IEF in the straight channel at junction T_1 as shown in Figure 3.1A. Separation media: 0.4% MC, 4% Pharmalyte 3-10, PE 0.02 μg/μL, APC 0.06 μg/μL, GFP 0.04 μg/μL. Cathode solution, 50 mM NaOH containing 2.5% MC, anode solution, 50 mM H_3PO_4 containing 2.5% MC. Voltage 100 V. Simulation results E-H and I-L are comparison of behavior of zone electrophoresis and ITP both during and after bands pass the T-junction.

3.3.1 Band deformation at a T-junction

In the early part of first-stage focusing, the sharpened front of a moving wave of protein (Figure 3.2A) approaches a T-junction (T_1 in Figure 3.1A). The upper part of the forward edge is stretched up and sharply twisted as it is drawn ~150 μm (roughly half the channel width) into the junction channel while the lower part of the band continues to move to the right, stretching and dispersing as it crosses the T (Figure 3.2B). The rear bands then catch up with the top of the front band and execute the same maneuver, dramatically lowering the resolution of the two bands (Figure 3.2C). Once the bands have left the vicinity of the junction, they eventually refocus at slightly lower resolution as compared with the same protocol without a T-junction (Figure 3.2A). Figure 3.2D shows that a small amount of protein was left in the junction channel because it diffused deep into the junction channel and out of the returning electrical field.

The primary source of dispersion at a T-junction is the deformation of electric field lines as current passes by an open channel. This phenomenon has recently been described by Lin et al.[24] for linear zone electrophoresis but, to our knowledge, it has not been treated for nonlinear electrophoretic techniques like IEF and ITP. One-dimensional IEF and ITP simulations are treated in detail in the works reported by Mosher et al.[25,26] and Baygents et al.[27] and two-dimensional simulations of linear electrophoresis (zone electrophoresis) have been exhaustively investigated,[28-30] but no two-dimensional simulations of nonlinear electrophoresis (IEF and ITP) have yet been reported. Since ampholyte-based IEF simulations require computations of hundreds of components,[31] band dispersion and

bending near the T-junction was instead studied using a model of ITP, which requires only about a half-dozen components to mimic dispersive behavior similar to IEF.

Although the ultimate source of dispersion at a T-junction in both linear and nonlinear electrophoresis is deformation of the field lines, the bands behave differently in linear and nonlinear systems both while and after they pass the T-junction. In particular, nonlinear systems like IEF and ITP, eventually refocus dispersed bands as shown in Figure 3.2E-H while linear systems like zone electrophoresis, lack the ability to resharpen the bands as shown in Figure 3.2I-L. The simulations suggest that multi-dimensional models can be developed by extending the one-dimensional models to be used in chip design to estimate dispersion and refocusing behavior in nonlinear electrophoresis at intersections. We hope to address these issues in greater detail for ITP, IEF, and other nonlinear electrofocusing techniques[32-34] soon.

3.3.2 Two-stage IEF

The microfluidic chip employed to perform two-stage IEF has a 2-cm-long straight channel and two 5-mm-long branched channels (Figure 3.3). Initially, all of the channels were filled with a uniform separation media which is a mixture of protein sample (total mass ~10.8 ng) 4% ampholytes (pH 3-10) and 0.4% MC. The first stage of IEF was performed in the straight channel at an electric field strength of 50 V/cm applied between reservoirs R_1 and R_2 while reservoirs R_3 and R_4 were left electrically floating (Figure 3.3).

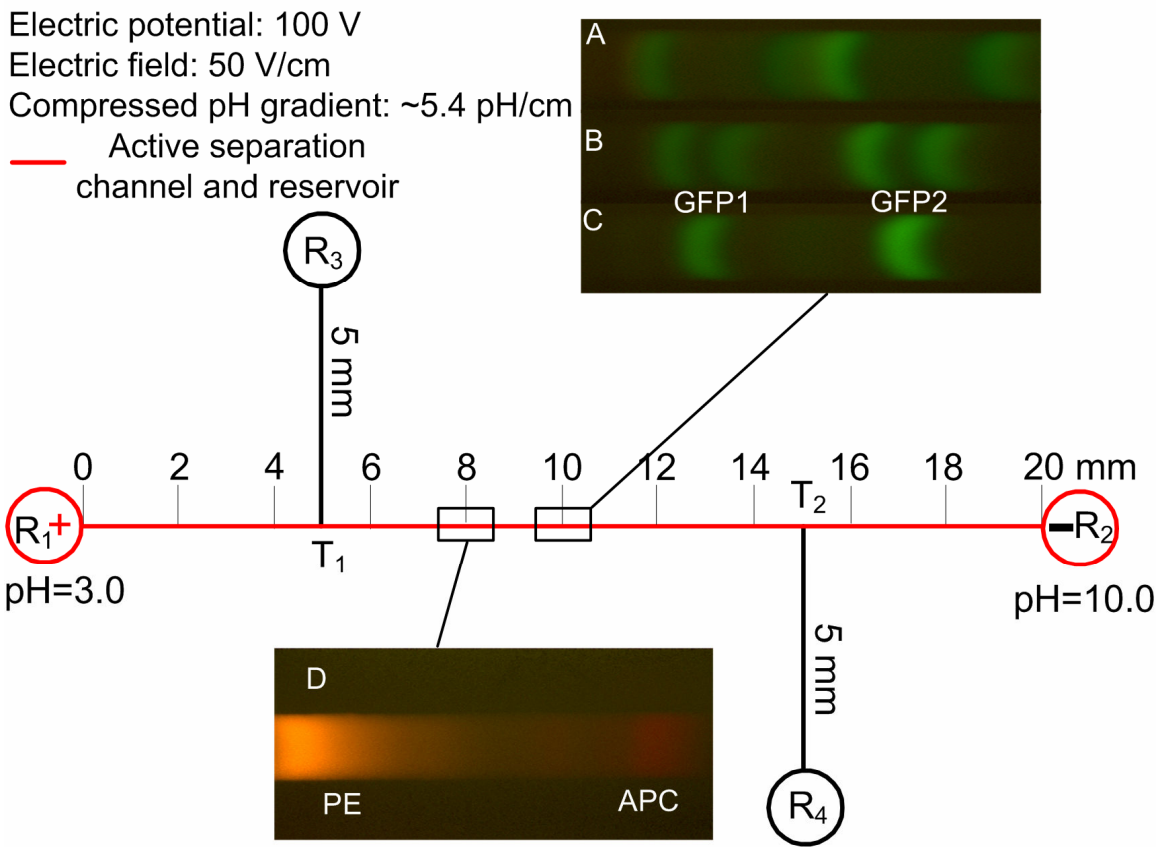

Figure 3.3 First-stage IEF separation in the straight channel. Photos A-C represent the final focusing stages of GFP. Photo D shows final position of PE and APC. Photos A-D at 480, 490, 580 and 610 s respectively. Separation media: 0.4% MC, 4% Pharmalyte 3-10, PE 0.02 µg/µL, APC 0.06 µg/µL, GFP 0.04 µg/µL. Anode solution (R_1): 50 mM H_3PO_4 containing 2.5% MC; Cathode solution (R_2): 50 mM NaOH containing 2.5% MC.

Time-series photos (Figures 3.3A-C) show the final focusing stages of the GFP bands. The final positions of the focused protein bands at this stage, shown in Figures 3.3C and D, were located between 7 mm and 11 mm from the anode and remained stationary. However, due to compression,[19] a 3-10 pH gradient spanned ~13 mm in this 2-cm-long channel yielding a pH gradient of ~5.4 pH/cm rather than the ideal gradient, 3.5 pH/cm. Figure 3.4A shows that the four variants of GFP were resolved into two bright bands and two dim bands. The electropherogram in Figure 3.4A shows two peaks corresponding to the two bright GFP variants. The other two bands were too dim to show up in this electropherogram.

After first-stage focusing had finished, an electric field strength of 100 V/cm was applied between branch channel reservoirs R_3 and R_4 while R_1 and R_2 were left electrically floating. In an effort to refocus the protein bands in segment T_1-T_2, a narrow pH interval of ~3.5 to ~7.2 was established between the branch reservoirs R_3 and R_4 by using pH 3-4 and pH 6.7-7.7 ampholyte solutions as anodic and cathodic solutions respectively. Ampholytes and proteins whose p*I*s were out of this pH interval were assumed to migrate into the anodic or cathodic reservoir shortly after the initiation of second-stage focusing. The resolution of the two bright GFP bands at the end of the first stage (Figure 3.4a) was about 2.33 at an electric field strength of 50 V/cm. Immediately after initiation of the second stage, the GFP bands (Figure 3.4B) became tighter compared to those in Figure 3.4A due to their quick response to a doubling of the electric field strength from 50 V/cm to 100 V/cm. Figure 3.4b shows that the resolution of two bright GFP bands right after the initiation of the second stage at an electric field strength of 100 V/cm was ~2.50,

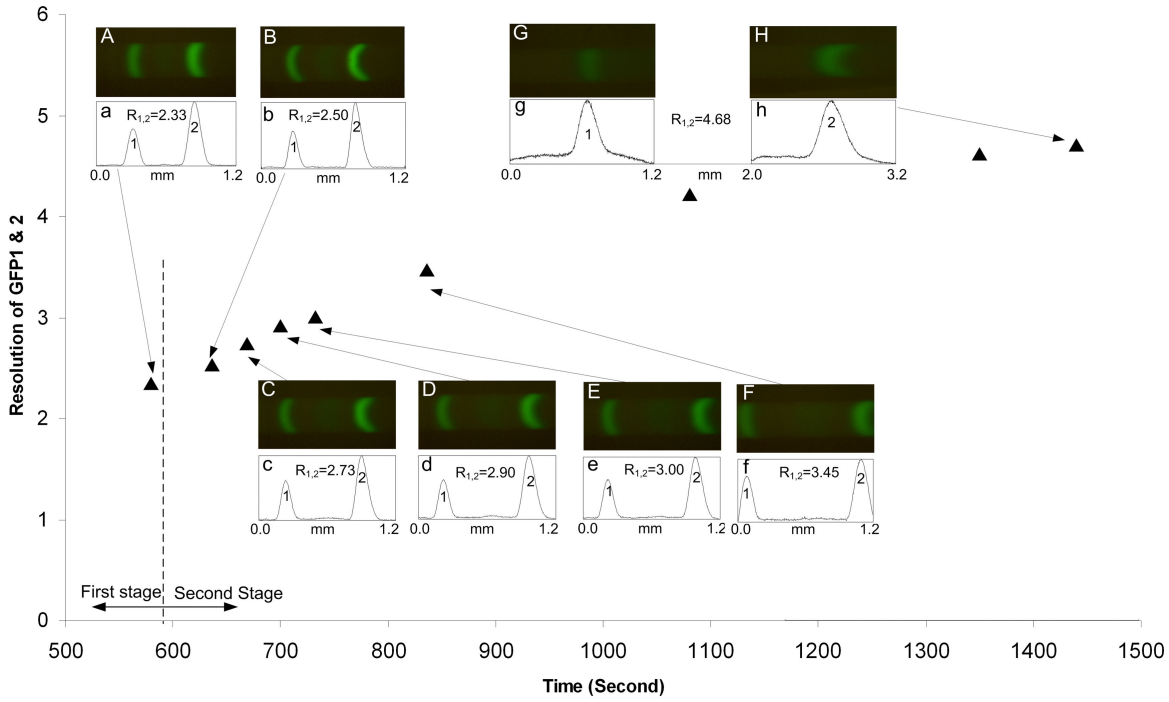

Figure 3.4 Refocusing of GFP in a second stage after the first stage shown in Figure 3.3. Graphs a-h are the electropherograms of the corresponding photos A-H. Numbers 1 and 2 stand for the two bright variants of GFP. Photo G and H represent GFP variants 1 and 2 respectively since they were too far apart to be captured in a single photo. $R_{1,2}$ is the resolution of GFP variants 1 and 2. Resolutions calculated based on eq 3.1 at the beginning and end of the second stage are indicated by solid squares. Anode solution (R_3): 4% 3-4 ampholytes containing 2.5% MC; Cathode solution (R_4): 4% 6.7-7.7 ampholytes containing 2.5% MC. Voltage 200 V.

which is lower than the 3.30 (Table 3.1), anticipated by eq 3.1. The discrepancy between measured and anticipated resolution was because the GFP bands were further bent, a phenomena which accompanied application of the higher electric field strength and possibly due to temperature gradients,[35,36] or electrohydrodynamic instabilities.[37,38]

It took a relatively long time for ampholytes to migrate to their p*I* positions and establish a shallower a pH gradient so the distance between two bright GFP bands (Figure 3.4A and B) did not increase until ~1 min after of initiation of the second stage. Figure 3.4C-F and c-f shows that the two bright GFP bands separated gradually and broadened as they migrated toward their new positions with the band broadening largely due to the shallower pH gradient established in this stage. According to the p*I*s of these proteins and the positions in which they were focused (Figure 3.5), the pH gradient was estimated to be ~1.8 pH/cm. At the end of the second stage, the distance between these two bands (Figure 3.4G and H) was ~2.0 mm and the resolution was ~4.68, which is roughly 2-fold greater than that at the end of first stage. Table 3.1 shows that the resolution of 4.68 is only 17% less than the theoretical resolution of 5.64 predicted from eq 3.1 using twice the electric field strength and one-third of the pH gradient in the first stage. The resolving power of IEF in this microchip was significantly increased by integration of second stage IEF.

Table 3.1 Comparison of measured and expected resolutions of two GFP variants during two-stage IEF

	End of fist stage	Right after doubling of electric field strength at the beginning of second stage	End of second stage
Electric field strength, V/cm	50	100	100
pH gradient, pH/cm	5.4	5.4	1.85
Resolution of GFP1 & 2	2.33	2.50[a]	4.68[a]
		3.30[b]	5.64[b]

[a]Experimentally measured resolutions during the second stage.[b]Resolutions were calculated based on eq 3.1.

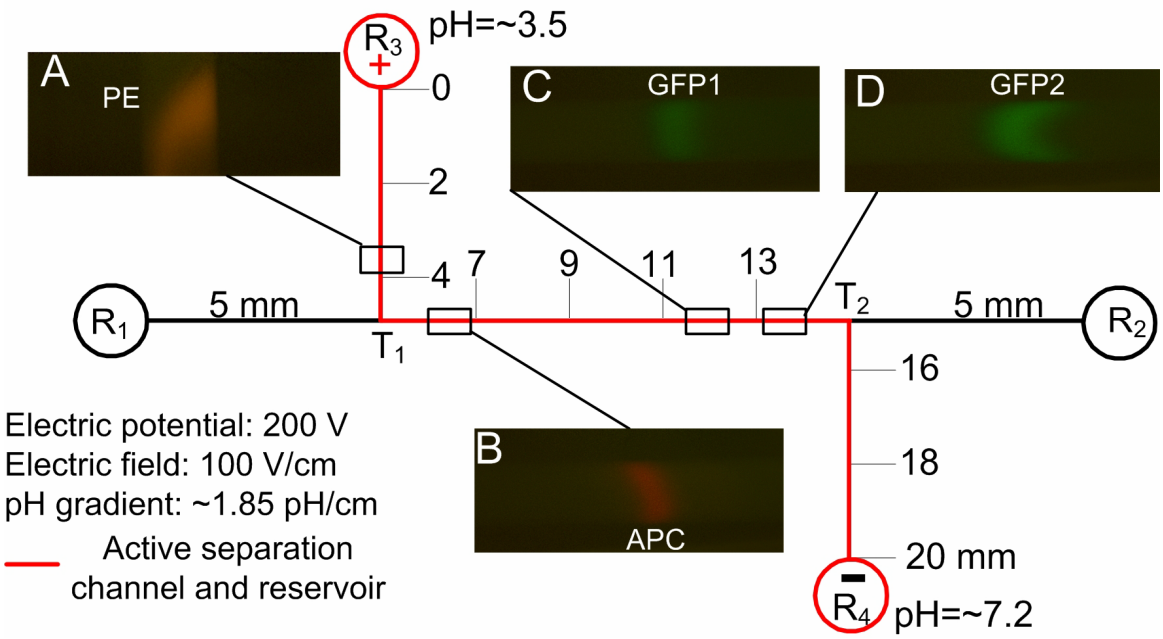

Figure 3.5 Final positions of refocused proteins at the end of second stage IEF. Experimental conditions were shown in Figure 3.4. Photos A-D were taken at 780, 840, 850 and 870 s respectively, after the initiation of the second stage IEF. Resolution of GFP1 and GFP2 is 4.68 which is 2-fold of that at the end of first stage.

3.3.3 Three-stage IEF

The two-stage IEF described above supports the hypothesis that a segment of the pH gradient in the first-stage channel can be successfully refocused into secondary channels. In an effort to further test this concept, we implemented a third stage in the microfluidic chip. The procedure used in the first two stages of this three-stage IEF is virtually identical to that of the two-stage IEF described above. The third stage is designed to further expand a portion of the segment of the pH gradient which was expanded in the second stage.

When an electric field strength of 50 V/cm was applied between R_1 and R_2 (Figure 3.6A), a compressed pH gradient of ~5.7 pH/cm was established in the straight channel. Panels B and C in Figure 3.6 indicate that PE, APC and GFP bands were located in the segment T_3-T_4. It can be clearly seen from Figure 3.6B that PE and APC were completely resolved and that the two GFP variants were grouped tightly. Since Figure 3.6C was obtained by averaging the intensities transversely across the channel while protein bands are tilted, the peaks of PE and APC overlap.

The second stage was used, in part, to further separate PE and APC, and, in part, to migrate them out of the segment, T_3-T_4. In this stage, pH 4.2-4.9 and pH 8-10.5 ampholyte solutions were employed as anodic and cathode solutions, respectively, and a

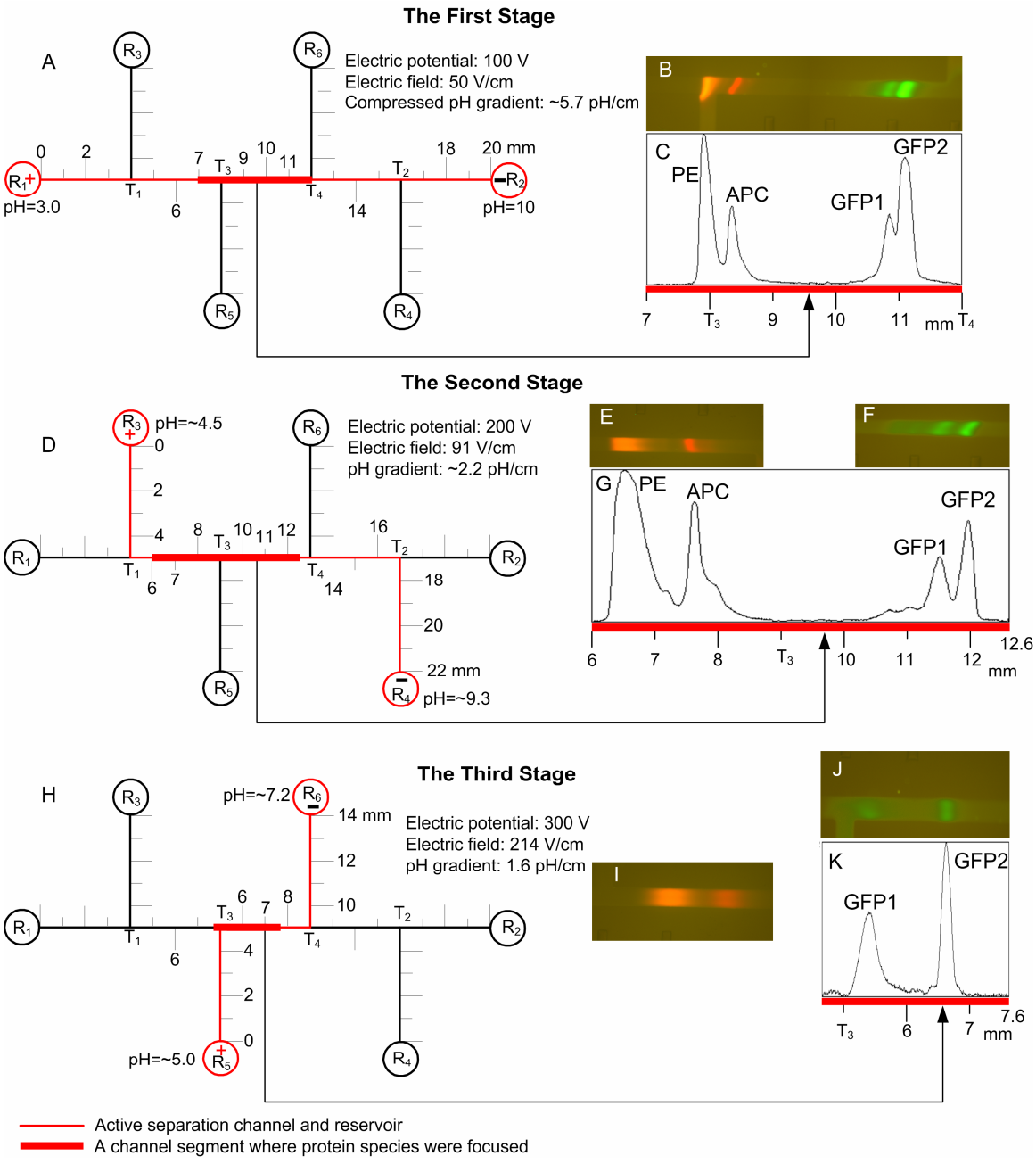

Figure 3.6 Three stage IEF separation. (A, D, H) The layout of IEF at each stage. (B-C, E-F and I-K) Photos and electropherograms of separation results at each stage. Separation media: 0.4% MC, 4% Pharmalyte 3-10, PE 0.04 µg/µL, APC 0.06 µg/µL, GFP 0.08 µg/µL. Electrode solutions: R_1, 50 mM H_3PO_4, R_2, 50 mM NaOH, R_3, 4% 4.2-4.9 ampholytes, R_4, 4% 8-10.5 ampholytes, R_5, 4% 4.5-5.4 ampholytes, R_6, 4% 6.7-7.7 ampholytes. All electrode solution contains 2.5% MC. The applied electric field and pH gradient at each stage is indicated in the figure.

pH gradient of ~2.2 pH/cm was established between R_3 and R_4 (Figure 3.6D) after an electric field strength of 91 V/cm was applied. After PE and APC migrated out of segment T_3-T_4 and before GFP reached T_3, this stage was stopped. Panels E, F and G in Figure 3.6 show the positions of the protein bands at the end of the second stage. The reader should note that, at this moment, IEF has not yet achieved steady state and that all of the protein bands were still moving toward their p*I* positions. Compared with Figure 3.6C, the electropherogram in Figure 3.6G indicates that the protein bands were further resolved and the distance between APC and GFP1 was increased by 25%.

The third stage was designed to further separate the two GFP variants that were kept in segment T_3-T_4 at the end of the second stage. In the third stage, pH 4.5-5.4 and pH 6.7-7.7 ampholyte solutions were employed as anodic and cathodic solutions, respectively. After an electric field strength of 214 V/cm was applied, a shallower pH gradient of ~1.6 pH/cm was established between R_3 and R_4 (Figure 3.6H). Panels 6J and K in Figure 3.6 show that two GFP variants were separated by ~1 mm while the PE and APC bands in Figure 3.6I have broadened, most likely due to diffusion since they were outside of the electric field (Figure 3.6H).

This microfluidic chip (Figure 3.6) could also be used to process two different second-stage IEF separations. In this case, R_3 and R_5 could be used as anodic and cathodic reservoirs to expand the segment T_1-T_3 while the segment T_4-T_2 could be expanded between reservoir R_6 and R_4. These two separations can be performed serially or in parallel when a valve[10,39] is implemented between T_3 and T_4.

3.3.4 Comparison of integrated multi-stage IEF with single channel IEF

An alternative way to improve resolution of microchip IEF is by performing single channel IEF in narrow pH ranges and at higher electric fields. To compare this with the second stage of two-stage IEF and the third stage of three-stage IEF in the same separation media, electrode solutions and electric field were chosen to set up pH ranges of 3.5-7.2 and 5-7.2 in a single channel, respectively. Table 3.2 shows that both cases have similar results in the pH ranges of 3.5-7.2 and 5.0-7.2. When compared to theoretical calculations based on protein p*I*s (Table 3.2), the pH gradient in both cases is shifted about 1.5 mm toward anode. This shift is most likely due to drift of the pH gradient,[40,41] a major drawback inherent in ampholyte-based liquid-phase IEF at high voltages.

Ideally, staging allows the initial fractionation over a broad range, pH 3-10, in the straight channel to be distributed across a multi-channel array of seven secondary stages, each secondary stage covering a pH unit. By contrast, to accomplish the same thing in a single channel IEF chip would require 7 parallel channels to cover pH 3-10 with a unit pH in each channel. The advantages of performing narrow range IEF in a single channel are elimination of dispersion arising from T-junction and all 7 parallel channels can be run at the same time which reduces analysis time. However, if valves[10,39] are implemented in a multi-stage IEF chip, the secondary stages can be run in parallel, instead of serially, and dispersion arising from the T-junctions could be reduced. A major advantage of integrated multi-stage IEF over parallel single-channel IEF is the compact design of the

Table 3.2 Comparison of positions of protein bands obtained form staged IEF, single channel IEF and theoretical calculation based on p*I*s with same pH range and electric field.

		Staged IEF	Single Channel IEF	Calculated based on p*I*
pH range: 3.5~7.2[a], Electric potential: 200V, Channel Length: 20 mm				
Distances of protein bands from anode (mm)	PE (p*I*=4.38)	4.3±0.5[c]	4.7±0.2	4.7
	APC (p*I*=4.78)	6.5±0.4[c]	6.7±0.3	6.9
	GFP1 (p*I*=6.00)	12.0±0.6[c]	12.2±0.3	13.5
	GFP2 (p*I*=6.31)	13.6±0.6[c]	13.9±0.1	15.2
Distance between GFP1& 2 (mm)		1.7±0.3[c]	1.7±0.2	1.7
Resolution of GFP1and 2		3.9±0.7[c]	3.9±0.3	
pH range: 5.0~7.2[b], Electric potential: 300V, Channel Length: 14 mm				
Distances of protein bands from anode (mm)	GFP1 (p*I*=6.00)	5.2±0.7[d]	5.4±0.3	6.4
	GFP2 (p*I*=6.31)	6.6±0.7[d]	6.6±0.3	8.3
Distance between GFP1and 2 (mm)		1.4±0.2[d]	1.2±0.1	1.9
Resolution of GFP1and 2		2.1±0.4[d]	1.9±0.1	

[a]4% ampholytes 3-4 and 6.7-7.7 were used as anolyte and catholyte respectively. [b]4% ampholytes 4.5-5.4 and 6.7-7.7 were used as anolyte and catholyte respectively. [c]Results were obtained from the second stage of two-stage IEF. [d]Results were obtained from third stage of three-stage IEF. Each data point represents the average of three measurements and the standard error.

former, especially when detection, integration of second dimensional separation and integration to mass spectrometers are considered.

Multi-stage IEF provides tertiary stages when the resolving power provided by a secondary stage is not high enough to separate out the protein of interest. However, for single channel IEF, when a narrow pH range is not capable of separating out the target protein, it is difficult to further resolve this pre-focused target protein out of contaminating proteins.

3.4 Conclusions

Multi-stage IEF of an ampholyte/protein/polymer mixture has been demonstrated in a microfluidic chip. Sequentially shallower pH gradients were successfully established in the second and third IEF stages, allowing the target proteins to refocus at 2X higher resolution in the later stages, thus further resolving GFP variants beyond the first stage.

The final positions of the protein species in the later focusing stages are determined by their p*I*s in the newly established pH gradients. The use of narrow pH range amphoytes as anode and cathode solutions to set the pH values of two end points allows ready control of pH range inside the channel. The directions that protein bands are going to mobilize are determined by their current positions and the prospective positions in the newly established pH gradient which is eventually defined by pH values of anode and cathode solutions. Experiments demonstrated that controlled mobilization of the protein species enables selective separation of target protein.

These experiments also showed that band deformation at a T-junction is primarily due to the deformation of electric field lines as current passes through the T-junction. Two-dimensional simulation of nonlinear electrophoresis showed excellent agreement with IEF experiment of band deformation at a T-junction and also provided a clear look of the different behavior from linear electrophoresis during and after protein bands pass a T-junction. When T-junctions are relatively close in three-stage IEF chips, the focused protein bands are skewed due to deformation of the electric field. Such deviations reduce the axial resolution but this distortion may potentially be reduced by the implementation of PDMS valves.[10,39]

Multi-stage IEF provides increased resolution of proteins since the serial application of IEF allows on-chip fractionation in a broad pH range followed by subfractionating a shallower pH gradient without additional reagents. The microchip design flexibility afforded by soft-lithography will allow us to increase resolution beyond the 2X demonstrated here by increasing the number of primary channel segments as well as the number of secondary branches. The implementation of valves should also speed the process by allowing tandem, parallel operation of the stages rather than the serial operation developed here. Eventually, it is expected that the multistage unit operation will be incorporated into a larger network as a single dimension in a separation cascade that leads ultimately to mass spectrometry.

3.5 References

(1) *Proteomics Today: protein assessment and biomarkers using mass spectrometry, 2D electrophoresis, and microarray technology*;

Hamdan, M., Righetti, P. G., Eds.; Wiley-Interscience: Hoboken, N. J., 2005; pp 341-346.

(2) Hoving, S.; Voshol, H.; Van Oostrum, J. *Electrophoresis* 2000, 21, 2617-2621.

(3) Albarghouthi, M. N.; Stein, T. M.; Barron, A. E. *Electrophoresis* 2003, 24, 1166-1175.

(4) Raisi, F.; Belgrader, P.; Borkholder, D. A.; Herr, A. E.; Kintz, G. J.; Pourhamadi, F.; Taylor, M. T.; Northrup, M. A. *Electrophoresis* 2001, 22, 2291-2295.

(5) Harrison, D. J.; Fluri, K.; Seiler, K.; Fan, Z.; Effenhauser, C. S.; Manz, A. *Science* 1993, 261, 895-897.

(6) Chen, X.; Wu, H.; Mao, C.; Whitesides, G. M. *Anal. Chem.* 2002, 74, 1772-1778.

(7) Herr, A. E.; Molho, J. I.; Druvalakis, K. A.; Mikkelsen, J. C.; Utz, P. J.; Santiago, J. G.; Kenny, T. W. *Anal. Chem.* 2003, 75, 1180-1187.

(8) Li, Y.; Buch, J. S.; Rosenberger, F.; DeVoe, D. L.; Lee, C. S. *Anal. Chem*. 2004, 76, 742-748.

(9) Wang, Y.-C.; Choi, M. H.; Han, J. *Anal. Chem.* 2004, 76, 4426-4431.

(10) Unger, M. A.; Chou, H. P.; Thorsen, T.; Scherer, A; Quake, S. R. *Science*, 2000, 288, 113-116.

(11) Righetti, P. G. *Isoelectric Focusing: Theory, Methodology and Applications*; Elsevier Biomedical Press: New York, 1983; pp 22-24.

(12) Vesterberg, O.; Svensson, H. *Acta Chemica Scandinavica*, 1966, 20, 820-834.

(13) Righetti, P. G.; Wenisch, E.; Faupel, M. *J. Chromatogr,* 1989, 475, 293-309.

(14) Righetti, P. G.; Wenisch, E.; Jungbauer, A.; Katinger, H.; Faupel, M. *J. Chromatogr,* 1990, 500, 681-696.

(15) Bossi, A.; Righetti, P. G. *Electrophoresis* 1995, 16, 1930-1934.

(16) Glukhovskiy, P.; Landers, T. A.; Vigh, G. *Electrophoresis* 2000, 21, 762-766.

(17) Zhu, Y.; Lubman, D. M. *Electrophoresis* 2004, 25, 946-958.

(18) Ayala, A.; Parrado, J.; Machado, A. *Appl. Biochem. Biotechnol.* 1998, 69, 11-16.

(19) Cui, H.; Horiuchi, K.; Dutta, P.; Ivory, C. F. *Anal. Chem.* 2005, 77, 1303-1309.

(20) Kumar, A.; Whitesides, G. M. *Appl. Phys. Lett*. 1993, 63, 2002-2004.

(21) Sia, S. K.; Whitesides, G. M. *Electrophoresis* 2003, 24, 3563-3576.

(22) Horiuchi, K.; Dutta, P.; Cui, H.; Ivory, C. F. Proceedings of 2003 Intl. Mechanical Engineering Congress and Exposition (IMECE), Washington DC, USA, Nov. 15-21, 2003.

(23) Hjertén, S. *Capillary Electrophoresis: Theory and Practise*; Grossman, P. D., Colburn, J. C., Eds.; Academic Press: San Diego, 1992; pp 24-43.

(24) Lin, R.; Burke, D. T.; Burns, M. A. *J. Chromatogr A* 2003, 1010, 255-268.

(25) Mosher, R. A.; Dewey, D.; Thormana, W.; Saville, D. A.; Bier, M. *Anal. Chem.* 1989, 61, 362-366.

(26) Mosher, R. A.; Gebauer, P.; Caslavska, J.; Thormann, W. *Anal. Chem.* 1992, 64, 2991-2997.

(27) Sounart, T. L.; Safier, P. A.; Baygents, J. C. *Handbook of Isoelectric Focusing and Proteomics;* Garfin, D., Ahuja, S., Eds.; Academic Press: San Diego, 2005; pp 41-68.

(28) Ermakov, S. V.; Stephen C. J.; Ramsey, J. M. *Anal. Chem.* 1998, 70, 4494-4504.

(29) Griffiths, S. K; Nilson, R. H. *Anal. Chem.* 2000, 72, 5473-5482.

(30) Lin, R.; Burke, D. T.; Burns, M. A. *Anal. Chem.* 2005, 77, 4338-4347.

(31) Thormann, W.; Huang, T.; Pawliszyn, J.; Mosher, R. A. *Electrophoresis* 2004, 25, 324-337.

(32) Koegler, W.; Ivory, C. F. *J. Chromatogr. A* 1996, *229*, 229-236.

(33) Greenlee, R.; Ivory, C. *Biotechnol. Prog.* 1998, *14*, 300-309.

(34) Huang, Z.; Ivory, C. F. *Anal. Chem.* 1999, 71, 1628-1632.

(35) Grushka, G.; McCormick, R. M.; Kirkland, J. J. *Anal. Chem.* 1989, 61, 241-246.

(36) Gobie, W. A.; Ivory, C. F. *J. Chromatogr.* 1990, 516(1), 191-210.

(37) Rhodes, P. H.; Snyder, R. S.; Roberts, G. O. *Journal of Colloid and Interface Science* 1989, *129*, 78-90.

(38) Baygents, J. C.; Baldessari, F. *Physics of Fluids* 1998, *10*, 301-311.

(39) Grover, W. H.; Skelley, A. M.; Liu, C. N.; Lagally, E. T.; Mathies, R. A. *Sensors & Actuators B* 2003, 89, 315-323.

(40) Righetti, P. G.; Macelloni, C. *Biochem Biophys Methods* 1982, 6, 1-15.

(41) Mosher, R. A.; Thormann, W. *Electrophoresis* 2002, 23, 1803-1814.

CHAPTER 4

Isotachophoresis of Proteins in a Networked Microfluidic chip: Experiment and 2-D Simulation

Huanchun Cui,[†] Prashanta Dutta,[‡] and Cornelius F. Ivory*,[†]

† School of Chemical Engineering and ‡ School of Mechanical and Materials Engineering, Washington State University, Pullman WA 99164

* To whom all correspondence should be addressed. Email: cfivory@wsu.edu

Reproduced with permission from "Electrophoresis, 28, 1138-1145, 2007"

Abstract

This paper reports both the experimental application and two-dimensional simulation of isotachophoresis (ITP) of proteins in a networked microfluidic chip. Experiments demonstrate that a mixture of three fluorescent proteins can be concentrated and stacked into adjacent zones of pure protein under a constant voltage of 100 V over a 2 cm long microchannel. Measurements of the isotachophoretic velocity of the moving zones demonstrates that, during ITP under a constant voltage, the zone velocity decreases as more of the channel is occupied by terminating electrolyte. A two-dimensional ITP model based on the Nernst-Planck equations illustrates the stacking and separation features of ITP using simulations of three virtual proteins. The self-sharpening behavior of ITP zones dispersed by a T-junction is clearly demonstrated both by experiment and by simulation. Comparison of two-dimensional simulations of ITP and zone electrophoresis (ZE) confirms that ZE lacks the ability to re-sharpen protein zones after they pass through a T-junction.

4.1 Introduction

Isotachophoresis (ITP) is a well known electrophoretic technique used in the separation of a variety of ionic compounds, ranging from small molecules like metal ions, to large molecules like proteins. ITP is also a powerful sample pre-concentration technique which is useful in the analysis of low abundance species. ITP has been successfully coupled with a number of analytical techniques, such as zone electrophoresis (ZE),[1,2] isoelectric focusing (IEF)[3], liquid chromatography,[4] mass spectrometry,[5] raman spectroscopy[6] and nuclear magnetic resonance spectroscopy.[7,8]

Analytical and preparative ITP of proteins has been extensively explored in gels and capillary tubes since the 1970s.[9] In an effort to replace conventional benchtop electrophoresis systems, microchip-based electrophoresis has received rapidly growing interest during the last decade because it has the potential to provide higher throughput, lower sample consumption and lower fabrication costs. Although integration of ZE and IEF on microchips for protein separation shows a peak capacity comparable to 2-D-PAGE,[10,11] protein detection is challenging due to the low sample mass loadings in a microfluidic chip. The best way to increase the loading capacity of a microfluidic chip is to preconcentrate the sample. Sample preconcentration is very important when analyzing biological samples which may have a large dynamic range of protein concentrations extending from the millimolar down to the femtomolar.[12] ITP is a simple and effective preconcentration and separation method which can be easily integrated on a chip prior to other on-chip operations, especially ZE.

As is the case with two other electrophoretic techniques, ZE and IEF, great progress has been made on the miniaturization of ITP. However, most of the published works on miniaturized ITP were focused on the separation of small organic molecules[13,14] and metal ions[15,16] which were primarily used in the food and beverage industry and for water analysis. ITP pre-concentration and separation of proteins on chips has so far received relatively little interest.

In this work, we demonstrate ITP of proteins in a poly(dimethylsiloxane) (PDMS) channel with T-junctions which we consider the key elements for integration of unit operations, e.g., sample loading. As briefly discussed in our previous work,[17] dispersion of protein zones as they pass by a T-junction during electrophoresis is due to the deformation of electric field lines as current passes by the open channel. However, dispersion behaves differently in linear and nonlinear electrophoresis systems. To explore this difference in detail, a two-dimensional (2-D) model of ITP was developed. One-dimensional (1-D) ITP simulations are treated in detail in the works reported by Mosher et al.[9,18] and 2-D simulations of linear electrophoresis (zone electrophoresis) have been exhaustively investigated[19-21] but, to our knowledge, no 2-D simulations of nonlinear electrophoresis (ITP) have yet been reported aside from those briefly mentioned in our previous work, where ITP of a virtual protein was simulated in the domain of a single T-junction (Figure 2 in reference[17]). In this paper, a 2-D ITP model is simulated using Comsol v3.2 (COMSOL, Burlington, MA), a finite-element based program that is widely available and easy-to-use. 2-D simulations are successfully used

to explore the ITP features such as concentration stacking and self-sharpening of protein zones after they had been dispersed at a T-junction.

4.2 Experimental Section

4.2.1 Chemicals

Recombinant green fluorescent protein (GFP, MW ~28 000) was obtained from Upstate Biotechnology (Lake Placid, NY). Allophycocyanin (APC, MW ~104 000) and r-phycoerythrin (PE, MW ~240 000) were purchased from Molecular Probes (Eugene, OR). GFP, APC and PE are naturally fluorescent. Methylcellulose (MC, viscosity of 2% aqueous solution at 25ºC: 400 centipoises) and epsilon-amino-n-caproic (EACA, MW 131.2) were acquired from Sigma (St. Louis, MO). Hydrochloric acid (HCl, MW 36.5) and tris(hydroxymethyl)aminomethane (Tris, MW 121.14) were purchased from Fisher Scientific (Fair Lawn, NJ).

4.2.2 Electrolytes and protein sample solution preparation.

The leading electrolyte (LE) solution was prepared by adjusting the pH of 10 mM HCl solution to 9.5 with Tris. The terminating electrolyte (TE) solution consists of 60 mM EACA titrated to pH 10.0 with Tris. The proteins PE, GFP and APC were mixed and diluted in the LE solution to the concentrations of 0.03 μg/μL (1.25×10^{-4} mol/m^3), 0.06 μg/μL (2.14×10^{-3} mol/m^3) and 0.06 μg/μL (5.77×10^{-4} mol/m^3), respectively. All solutions contain 2% w/v MC in order to suppress electroosmotic flow (EOF).[22]

4.2.3 Fabrication of PDMS microchips

The procedure used to fabricate PDMS chips was reported in our previous work.[22] Briefly, a positive pattern of the desired channel structure is formed on a glass substrate using a positive photolithography technique. PDMS prepolymer and curing agent (Sylgard 184, Dow Corning Inc., Midland, MI) were uniformly mixed at a ratio of 10:1, respectively, and degassed for 2 hrs at 0.001 Torr. The liquid elastomer is cast onto a positive pattern formed on the glass substrate and cured in a hot kiln for 6 hrs at 80˚C. At the end of the curing process, the elastic polymeric material is carefully peeled from the glass substrate to become the bottom layer of the microchip. The open channel on this bottom layer is irreversibly sealed with a flat surface of another layer of PDMS substrate containing holes as reservoirs after both surfaces have been plasma-oxidized. This microchip (Figure 4.1) consists of a straight channel and two secondary channels that branch out from the straight channel. All channels are 300 μm wide and 10 μm deep.

4.2.4 ITP procedure

Initially, all channels were pressure-filled with the LE from reservoir R_1 (Figure 4.1). After all the reservoirs were cleaned by removing excessive LE, 30 μL of LE and 2% MC solution were loaded into R_1 and R_3, respectively. Protein sample solution was then carefully pressure-filled into the channel from reservoir R_4 at ~5 psi until a drop of liquid appeared at the channel entrance inside reservoir R_2. Reservoir R_2 was cleaned and then loaded with 30 μL of TE. Reservoir R_4 was cleaned and then loaded with 2% MC solution. The reason for loading 2% MC solution into reservoirs R_3 and R_4 instead of leaving them empty is to balance the hydrostatic pressure among all reservoirs. Figure 4.1 indicates the initial solution configuration usually obtained by this loading procedure.

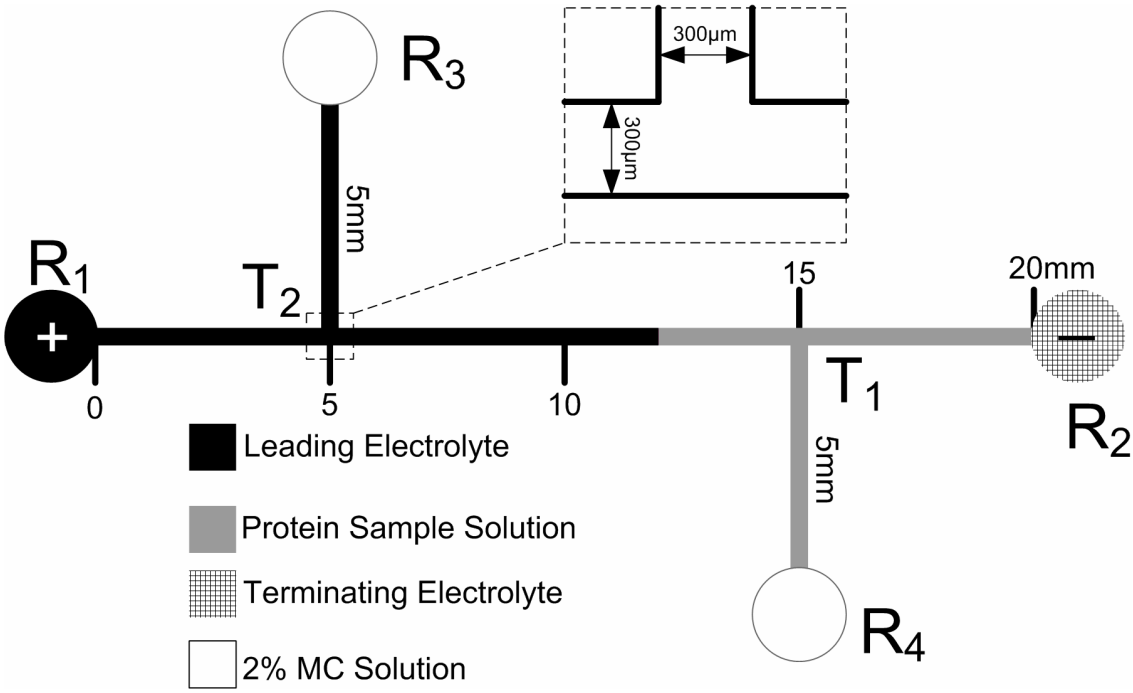

Figure 4.1 Schematic of the initial solution configuration in a microchip used in experiments. Please note that the protein sample solution is superimposed in the leading electrolyte. $R_{1\text{-}4}$ are reservoirs and $T_{1\text{-}2}$ are T-junctions. Constant voltages are applied between R_1 and R_2 while R_3 and R_4 are left electrically floating. The length of the straight channel and branch channels are 20 mm and 5 mm respectively. The microchannel is 10 µm deep and 300 µm wide.

Platinum wire electrodes were immersed into reservoirs R_1 and R_2 while reservoirs R_3 and R_4 were left electrically floating. ITP was carried out at a constant voltage of 100 V using an XHR 600-1 power supply (Xantrex technology Inc, Vancouver, Canada).

4.2.5 Imaging

The loaded chip was mounted underneath the 4x objective lens of a Leica DMLB fluorescence microscope equipped with a CCD camera (SPOT RT color, Diagnostic instruments, Inc., Sterling Heights, MI). The fluorescent proteins were excited with a mercury lamp (OSRAM HBO® 100 W/2) using a filter cube (DMLB 513804, Leica Microsystems, Inc., IL). Electropherograms were obtained from the pixel intensities of the experimental images by using ImageJ (http://rsb.info.nih.gov/ij) to average the intensities across the channel width after subtracting the background signal intensity from the images.

4.2.6 Mathematical model

Under an external electric field, each charged species in a solution migrates by diffusion, electromigration and convection. The flux of each species is given by following equation:

$$J_i = -z_i F \mu_i C_i \nabla \Phi - D_i \nabla C_i + C_i u \qquad (4.1)$$

Here J_i is the flux of species i, C_i is the concentration of species i, F is the Faraday constant, z_i the charge, μ_i the absolute mobility, Φ the electric potential, D_i the

diffusion coefficient, and *u* the bulk flow velocity. The electrophoretic mobility (ω_i) is related to the absolute mobility by the following equation:

$$\omega_i = Fz_i\mu_i \tag{4.2}$$

Each species is governed by the mass conservation law expressed as follows:

$$\frac{\partial C_i}{\partial t} = -\nabla \cdot J_i + R_i \tag{4.3}$$

where R_i is the rate of generation of species *i*.

Electroneutrality is conserved everywhere except inside the electric double layer which extends only a few Debye lengths from the charged surface into the bulk solution. The microfluidic channels employed in our experiments are more than 3 orders of magnitude larger than the Debye length so, to a first approximation, the electroneutrality constraint can be applied everywhere on the scale of the microfluidic channel of interest, i.e.,

$$\sum z_i C_i = 0 \tag{4.4}$$

The current conservation equation is

$$F\frac{\partial \rho}{\partial t} + \nabla \bullet I = 0 \tag{4.5}$$

where ρ is the space charge density and the current is defined as $I = F\sum_i z_i J_i$.

Eq 4.5 can be further simplified to

$$\nabla \bullet I = 0 \tag{4.6}$$

since $\rho = \sum_i z_i C_i = 0$ based on the electroneutrality equation.

4.2.7 Model simplification and setup

Some assumptions are made in the ITP simulation. First, z_i is assumed constant for each species everywhere in the microchip. The reaction term, R_i, in eq 4.3 is zero since the rate of generation of every species is nil. EOF is not included in this model since it was suppressed in the separation media that contains 2% w/v MC. However, if EOF exists, the ITP zones could decelerate or accelerate, achieve stationary steady state, or be flushed out of the separation channel, depending on the direction and strength of EOF.[23] The other forces that induce bulk flows, such as pressure differences among the reservoirs and electrical stresses are neglected and thus the bulk flow velocity, *u*, in eq 4.1 is taken to be zero.

The MC used to suppress the EOF increased the viscosity of the separation media but this is assumed to have no effect on the electrophoretic mobility of each species. The proteins used in the simulations are simply regarded as multiply charged molecules with electrophoretic mobilities between those of the leader and the terminator. Since the electrophoretic mobilities and charges of the proteins used in our experiments are not available in literature, three virtual proteins with multiple charges were used instead and were assigned electrophoretic mobilities between those of the leader and the terminator.

The Nernst-Planck physics built into Comsol v 3.2 was employed to perform ITP simulations. A constant voltage was set on the boundary b_1 (Figure 4.2A) which is the entrance to the anode reservoir R_1 (Figure 4.1) while zero voltage was set on the boundary b_2 to be cathode. The concentration for each species was fixed on boundaries b_1 and b_2. Since boundaries b_3 and b_4 are relatively far way from the main channel where ITP occurs, electric insulation and zero flux of each species were set on these two

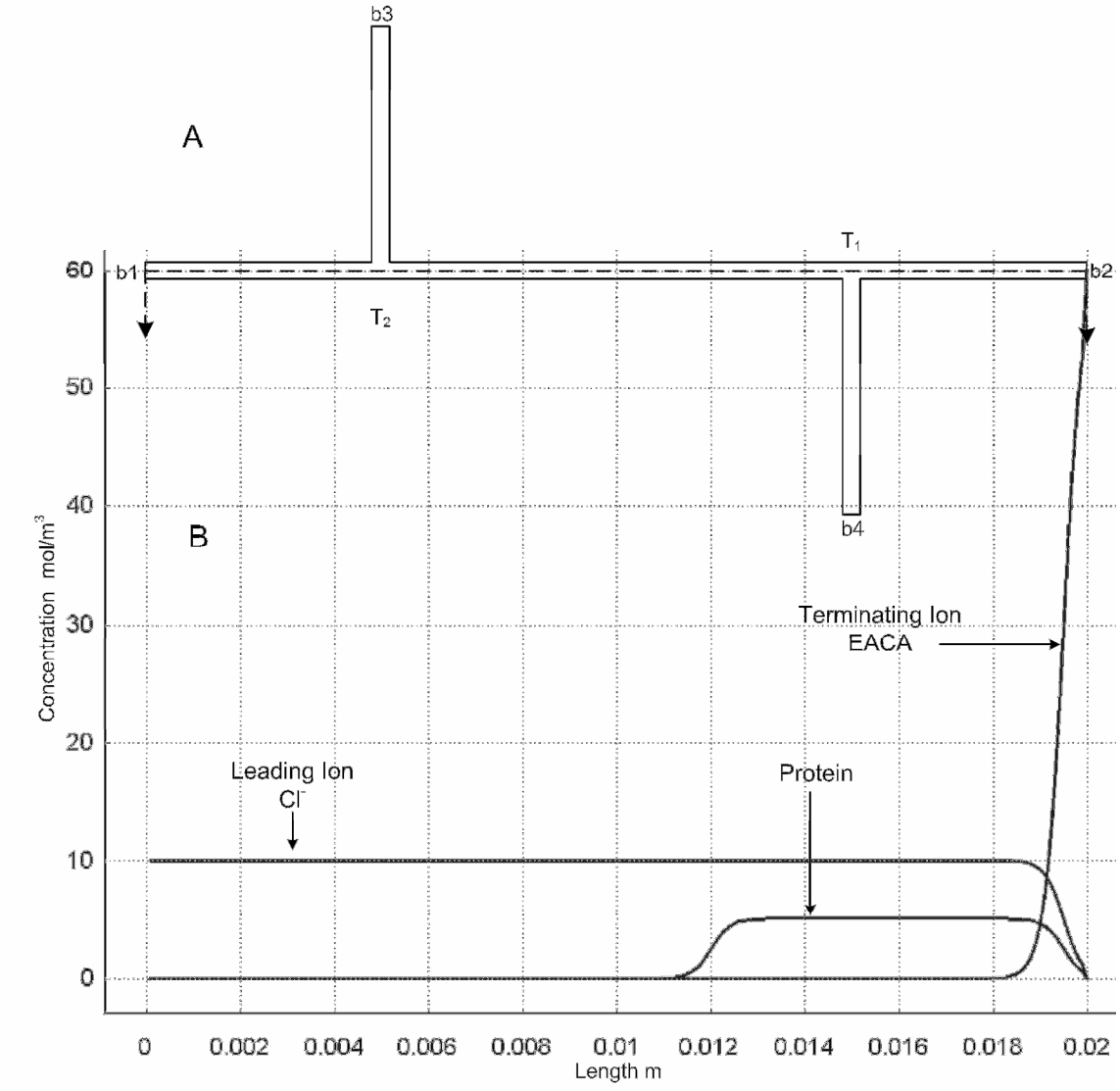

Figure 4.2 Domain and initial concentration profiles setup in COMSOL v3.2. (A) The geometry of simulation domain. (B) The initial concentration plot along the center line of the straight channel. For clarity, the protein concentration depicted in the plot is 10000 times greater than the actual concentrations used in simulations.

boundaries. All channel walls are insulated to electric current and impermeable to species. Based on the initial solution configuration employed in the experiments, initial concentration profiles for LE, protein samples and TE used in simulations are shown in Figure 4.2B. The boundary conditions and initial conditions are summarized in Table 4.1.

4.3 Results and Discussion

4.3.1 Experimental demonstration

The anionic ITP system employed in the experiments comprises the leading ion, chloride (10 mM HCl solution, adjusted to pH 9.5 by addition of Tris), the terminating ion, EACA (60 mM EACA, titrated with Tris to pH 10.0) and a mixture of three fluorescent proteins diluted in LE. Chloride is frequently used as a leader in anionic ITP since its electrophoretic mobility is higher than most other anions. Although EACA is relatively small in terms of molecular weight, it migrates slowly and acts as a terminator because it is partially ionized in pH 10.0 solution. Despite the large molecular weights, three fluorescent proteins are predicted to have electrophoretic mobilities between chloride and EACA due to multiple negative charges in the solution near pH 10.

The loaded protein sample covered nearly half the length of the straight channel while the remainder was filled with LE. As a constant voltage of 100 V was applied between anode and cathode reservoirs (Figure 4.1), a bright yellow edge formed at the entrance of the cathode reservoir and started to move toward the anode. The bright yellow edge gradually separated into three adjacent zones with GFP in the middle as it approached the junction T1 (Figure 4.3A). Experiments with a mixture of only PE and GFP under the

Table 4.1 Boundary and initial conditions setup in simulations (COMSOL v3.2)

	Leading ion Cl^-	Protein sample	Terminating Ion EACA	Counter-ion Tris	Voltage
Boundary[a] (b1)	Concentration $10\ mole/m^3$	Concentration $0\ mole/m^3$	Concentration $0\ mole/m^3$	Electroneutrality[b]	0 Volt
Boundary[a] (b2)	Concentration $0\ mole/m^3$	Concentration $0\ mole/m^3$	Concentration $60\ mole/m^3$	Electroneutrality[b]	100 Volt
Boundary[a] (b3, b4)	Insulation	Insulation	Insulation	Insulation	Insulation
All other boundaries	Insulation	Insulation	Insulation	Insulation	Insulation
Initial condition[c]	$\frac{10\,mole/m^3}{1+\exp(\frac{5(x-0.0195)}{0.001})}$	$\frac{0.0005\,mole/m^3}{1+\exp(\frac{-5(x-0.012)}{0.001})+\exp(\frac{5(x-0.0195)}{0.001})}$	$\frac{60\,mole/m^3}{1+\exp(\frac{-5(x-0.0195)}{0.001})}$	Electroneutrality[b]	N/A

a) Boundaries b1, b2, b3 and b4 are shown in Figure 4.2.
b) Concentration of Tris was calculated based on the electroneutrality equation (eq 4.4)
c) Variable x in the expressions for initial condition stands for x axis which is the centerline indicated in Figure 4.2.

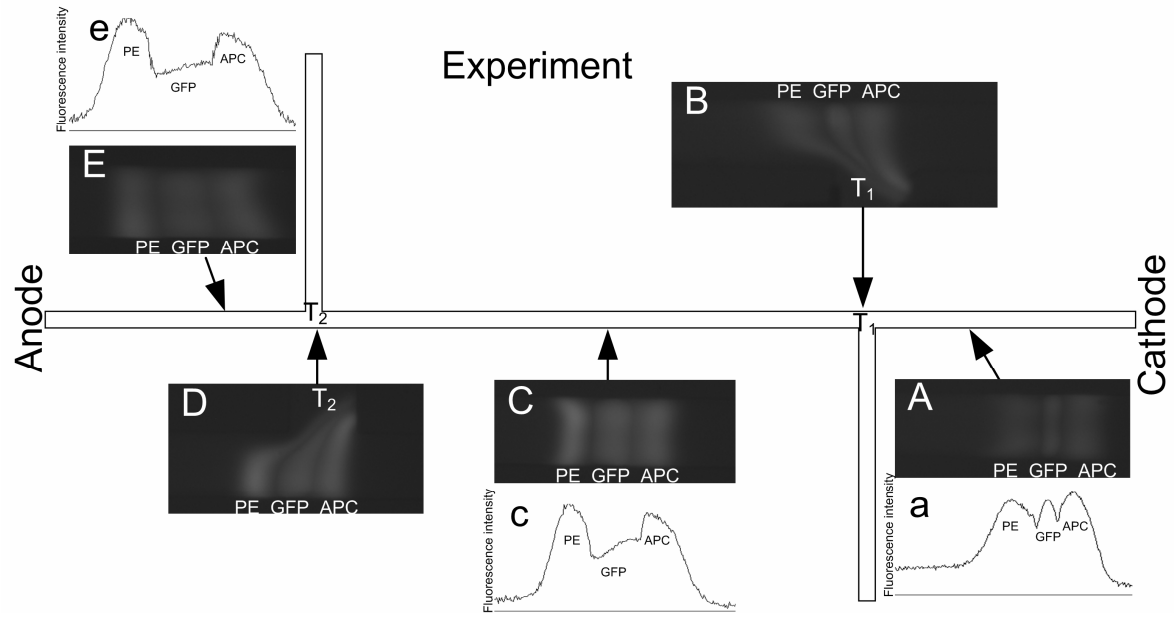

Figure 4.3 ITP stacking and separation of PE, GFP and APC**. (A)** Protein zones are located between T_1 and cathode. (B) Protein zones are passing by T_1. (C) Protein zones are located between T_1 and T_2. (D) Protein zones are passing by T_2. (E) Protein zones are located between anode and T_2. (a), (c) and (e) are the electropherograms of (A), (C) and (E), respectively. Voltage is 100 V. All other experimental conditions are detailed in the experimental section.

same experimental conditions demonstrated that PE migrated isotachophoretically ahead of a green GFP zone. This indicated that three protein zones shown in Figure 4.3 were PE, GFP and APC respectively from left to right. Protein zones deformed when passing junction T1 (Figure 4.3B), but they recovered their normal shape after migrating about 2 mm away from the T-junction. The three well-shaped protein zones shown in Figure 4.3C were about 9 mm from the cathode reservoir. The total length of the three zones (Figure 4.3C) increased by about 50% when compared to that shown in Figure 4.3A mainly because the proteins initially introduced in LE were stacked into the corresponding zones as ITP progressed.

When the protein zones passed junction T2 (Figure 4.3D), deformation again occurred. The protein zones shown in Figure 4.3E were about 1.5 mm from the anode reservoir and the average length of each zone was about 200 μm which indicated that each protein sample was concentrated about 40 fold when compared to the initial sample zone (Figure 4.2B) which was about 8000 μm long, assuming that all of the proteins were present in the protein zones. Figure 4.3E also shows that the GFP zone was plateau-shaped, a common feature of ITP while PE and APC zones were more Gaussian primarily because the initial molar concentrations of PE and APC were much lower than that of GFP and insufficient to produce the plateau-like zones. Figure 4.3a, c and e, the electropherograms of Figure 4.3A, C and E, provide a better view of the shape development of GFP zone from peak to plateau.

In our experiments, ITP was performed with fixed voltages instead of constant current. The electric field in the LE gradually decreased because total passing current decreased because an increasing length of the channel is occupied by the low conductivity TE as ITP progresses. As the result of the decreasing electric field in LE, the phenomenon that leading ion slowed down as ITP progressed should be expected. This phenomenon was witnessed by observing the migration velocity of the leading and the terminating boundaries (Figure 4.4A) since they were required by the ITP principle to migrate at the same velocity as the leading ion. The velocities of the moving boundaries were obtained at three different locations (Figure 4.4A-C) along the channel in a single experiment. Figure 4.4A shows that the local average velocity of the moving boundaries was 20.4 μm/s since the terminating boundary took 49 s to migrate from the 8 mm to the 9 mm position mark. As the protein zones migrated further toward the anode, a deceleration was revealed in Figure 4.4B which indicated that the local average velocity of the moving boundaries was reduced to 17.5μm/s. Further more, Figure 4.4C showed that the leading boundary spent 6 more seconds compared to that shown in Figure 4.4B to travel the same distance (1 mm).

4.3.2 Simulation

In this work, numerical simulations were employed to help determine the underlying mechanisms for dispersion and resharpening. 2D-simulation of ITP is relatively straightforward using the Nernst-Planck physics built into COMSOL v3.2. The ITP model used in the simulation had seven variables of interest, the electric field, the concentrations of LE, three virtual proteins, TE and the counter ion. The Nernst-Planck

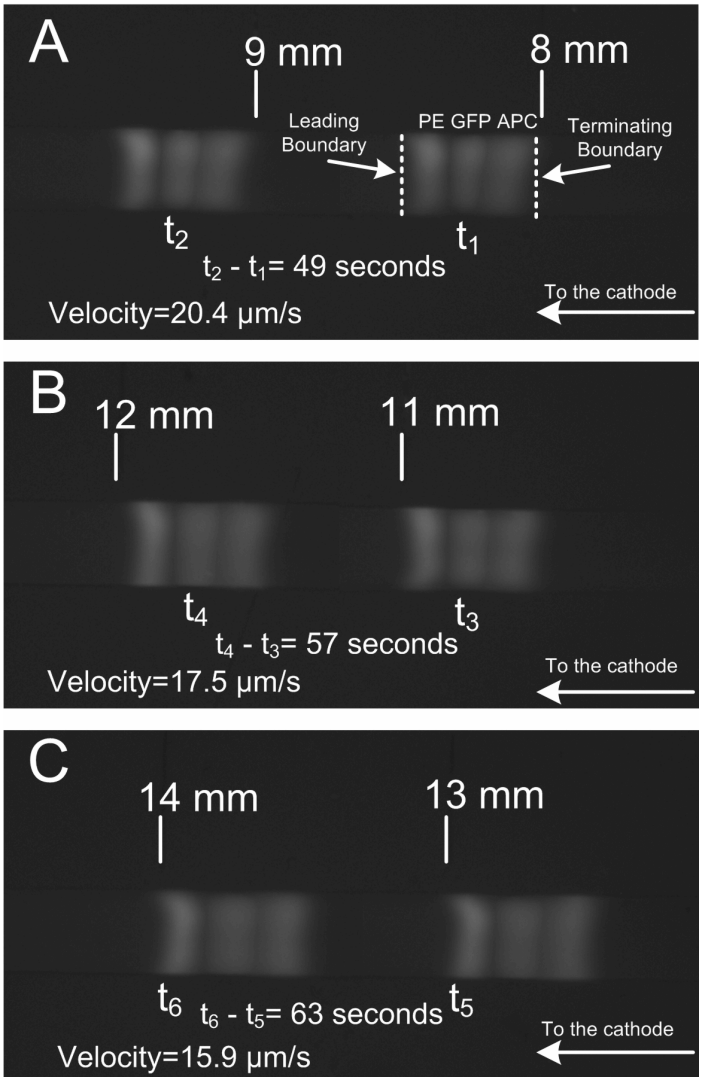

Figure 4.4 Measurement of isotachophoretic velocities in a single experiment at different locations. t_1-t_6 are the times after electric field applied. Protein zones are moving to the left. The velocity indicated in each photo are the local average velocity that is calculated based on the time difference and the distance between two position markers Voltage applied is 100 V. All other conditions are detailed in the experimental section.

physics utilized six equations of mass conservation (eq 4.3) and one electroneutrality constraint (eq 4.4) to solve for seven time-dependent variables.

The initial concentrations are depicted diagrammatically in Figure 4.2. The protein samples were superimposed on the LE buffer and TE was interfaced with both LE and protein samples near the entrance to the cathode. Figure 4.5 depicts simulated concentrations of two virtual proteins at different times. The transport parameters for each species used in the simulations are listed in Table 4.2.

Figure 4.5A shows two small, overlapped peaks corresponding to protein 1 and 2 formed at the right end of the initial sample plug at 12 s. The initial protein samples ahead of these two peaks were also migrating toward the anode, but with speeds lower than the leading boundary and thus were being stacked into the corresponding peaks. At 150 s, two peaks had approximately 50% baseline overlap. The maximum concentration of protein 2 was more than 2 fold higher than that of protein 1 because more protein 2 was stacked into the corresponding peak than protein 1. This situation can be explained by the fact that protein 1 has a higher electrophoretic mobility than protein 2, and thus took a longer time to be caught up by the leading boundary. At 290 s, two peaks still had about 40% baseline overlap which suggests that a steady state had not yet been achieved within the sample zone. The peak heights of two proteins, especially protein 2 at 290 s were reduced when compared to those at 150 s due to the loss of proteins into the junction T_2 when the sample zone passing by it.

Table 4.2 Parameters of Each Species Used in Simulations

	Leading ion Cl^-	Simulation A			Simulation B			Terminating Ion EACA	Counter-ion Tris
		Protein 1	Protein 2	Protein 3	Protein 1	Protein 2	Protein 3		
Concentration mol/m^3 (C_i)	10	5×10^{-4}	5×10^{-4}	5×10^{-4}	5×10^{-4}	5×10^{-4}	5×10^{-4}	60	Electro-neutrality[a]
Absolute mobility[b] $\times10^{-14}\ m^2/Vs$ (μ_i)	82.0	2.19	0.62	1.11	2.59	0.17	1.11	32.5	30.6
Diffusion coefficient[c] $\times10^{-11}\ m^2/s$ (D_i)	202.4	5.41	1.54	2.75	6.4	0.43	2.75	80.2	75.7
Charge (z_i)	-1	-26	-30	-28	-26	-30	-28	-0.15	0.96
Electrophoretic mobility $\times10^{-8}\ m^2/Vs$ (ω_i)	7.91	5.5	1.8	3.0	6.5	0.5	3.0	0.47	2.84

a) Cencentration of Tris was calculated based on the electroneutrality equation (eq 4.4).
b) Absolute mobility was calculated based on eq 4.2.
c) Diffusion coefficient is calculated based on the Einstein expression: $D_i = \mu_i RT$, where R is the gas constant 8.314 $J \cdot K^{-1} \cdot mol^{-1}$ and T is the room temperature 298 K.

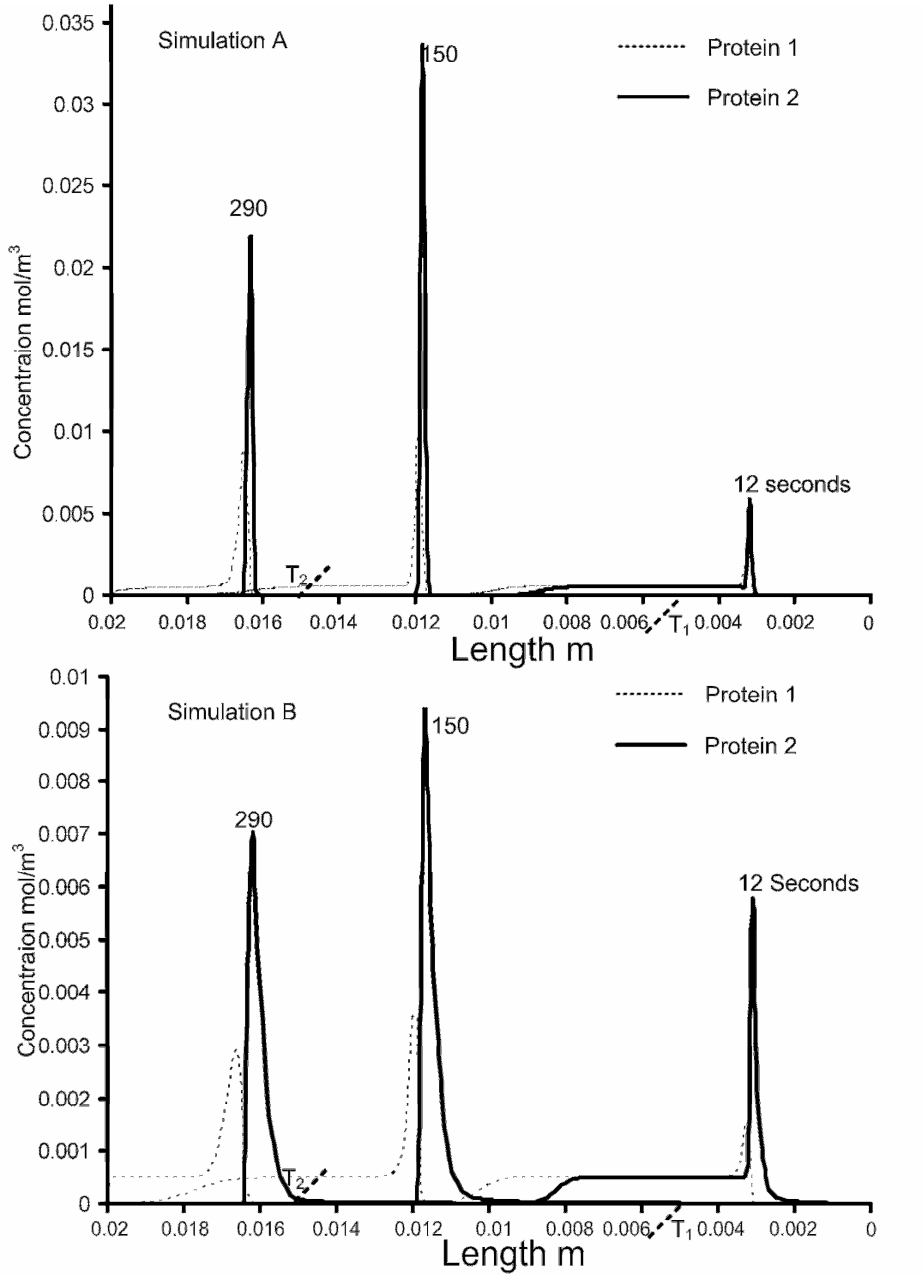

Figure 4.5 Simulation of virtual proteins with different electrophoretic mobilities. For clarity, only two virtual proteins are plotted in this figure. The parameters for each species are listed in Table 4.1. The simulation voltage is 100 V. Three sets of peaks shown in each plot represent the concentration profiles at three times during ITP simulation. Cathode is to the right.

Figure 4.5B shows the same simulation as Figure 4.5A except for the change of the electrophoretic mobilities of two virtual proteins (Table 4.1). The peak baseline overlap was dramatically reduced when compared with that shown in Figure 4.5A due to an increase in the electrophoretic mobility difference between the two proteins.

The simulation above could potentially be used in chip design. For example, the length of the microchannel could be increased to allow all proteins to be stacked into their corresponding zones. It is convenient to explore ITP features, such as concentration stacking and moving boundaries, by means of numerical simulations. However, all the simulations of ITP in the literature including "The Dynamics of Electrophoresis"[9] limited to 1D. The 2D simulation developed in this work provides a better way to explore some ITP features, such as the dispersion and self-sharpening of a protein zone both during and after passing a T-junction which will be discussed in the following paragraph.

4.3.3 The behavior of protein zones both during and after passing a T-junction

In the later part of the ITP experiment, the sharpened leading boundary of a moving zone of proteins (Figure 4.6A) approached a T-junction (T_2 in Figure 4.1). The upper part of the leading boundary was stretched up and sharply twisted as it was drawn about 150 μm (Figure 4.6B, roughly half the channel width) into the junction channel while the lower part continued to move to the right, stretching and dispersing as it crossed the T (Figure 4.6C). The trailing zone boundaries then catch up with the top of the leading boundary and execute the same maneuver (Figure 4.6C). After the protein zones have left the vicinity of the junction, Figure 4.6D shows that the PE zone has re-resharpened, the GFP

zone took on a trapezoid shape and was in the process of resharpening while the upper part of APC zone was still dispersed. As the protein zones migrated farther from the T-junction (Figure 4.6E), they eventually finished resharpening with slightly tilted boundaries. Figure 4.6D and E also show that a very small amount of protein was left in the junction channel because it diffused too deep into the junction channel.

The primary source of dispersion at a T-junction in both linear and nonlinear electrophoresis is deformation of the electric field lines. This dispersion behaves differently in linear and nonlinear systems both while and after they pass the T-junction. In particular, nonlinear systems like ITP eventually resharpen the dispersed zone as shown in Figure 4.6F-J while zones in linear systems like ZE lack the ability to resharpen as illustrated in Figure 4.6K-O.

To clearly explain the self-resharpening ability of ITP, it is necessary to mention the kohlrausch regulating function (KRF) which is well defined elsewhere.[9,24,25] The KRF describes the local concentration of each charged species based on the initial concentration distribution along the electrophoretic axis and the value of KRF is not changed by the applied current.[9] Dilute species, e. g. proteins in ITP experiments, are concentrated into narrow zones in order to maintain the higher concentration which is required by KRF. After application of the electric field, mixed sample species separates based on their electrophoretic mobilities into a series of contiguous zones, demarcated by sharp moving boundaries.[26] The self-resharpening ability of ITP is primarily provided by

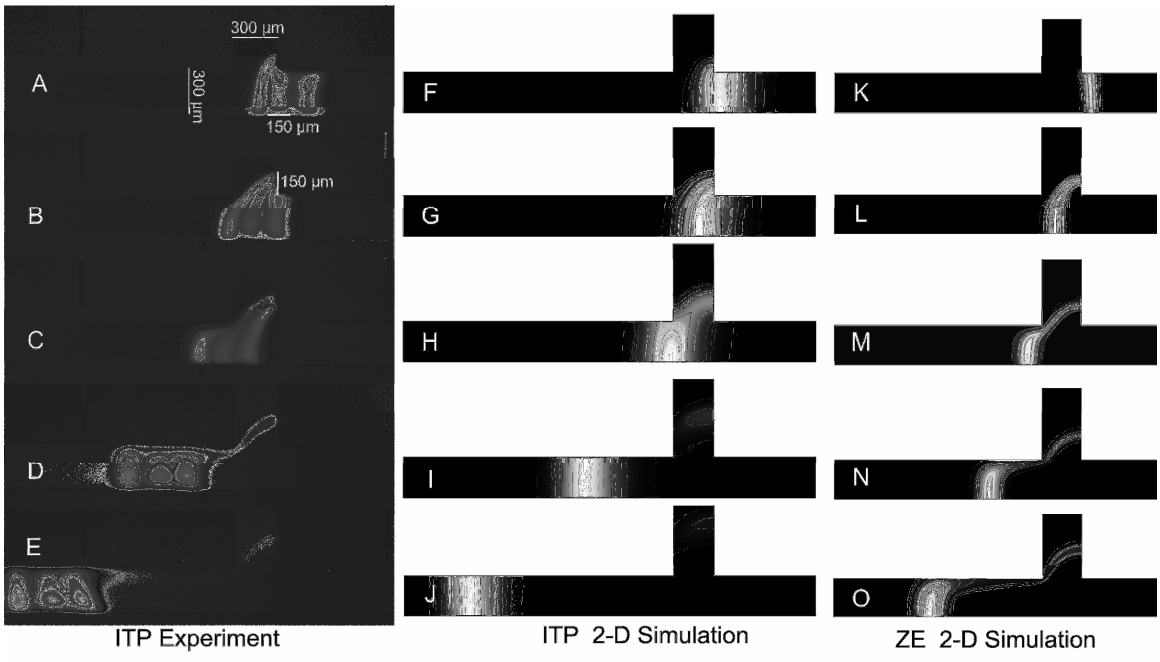

Figure 4.6 Time-series illustrations comparing band dispersion and resharpening by ITP and ZE at the T_2-junction of the PDMS microchip illustrated in Figure 4.1. The time-series photos A-E shows how an ITP train of three model proteins (PE, GFP and APC) first disperses and then resharpens as it migrates straight through a T-junction. Figures F-J are part of an ITP simulation using three "virtual" proteins to illustrate how the ITP model mimics the essential mechanisms of dispersion and resharpening. Figures K-O, which is included only for the purposes of comparison with the ITP experiment and simulation, shows that the morphology of dispersion at a junction is similar in ITP and ZE but that, in the latter case, the band cannot resharpen. Experimental conditions: R1 Anode=100 V; R2 Cathode=0 V; initial concentrations of LE, TE and three fluorescent proteins are given in the Experimental Section. Simulation results F to J and K to O are a comparison of ITP and ZE both during and after the bands pass the T-junction. ITP simulation is based on simulation B presented in Figure 4.5. The ZE simulation has the same computing domain (see Figure 4.2), species parameters and simulation voltage as for ITP but different initial concentration profiles and boundary conditions.

the nonlinear factor which is the step change of conductivities across the moving boundary. The step change of conductivities produces the step change of electric field magnitudes between ITP zones. When a species diffuse out of its own zone, it will experience either higher or lower electric field magnitude which will force it to either accelerate or decelerate back into its own zone.[26] In our case, the upper part of the protein zone was dispersed by the T-junction and retarded into the termination ion zone where the electric field is higher, and thus is accelerated to rejoin the protein zone. Because ZE lacks nonlinear factors, such as conductivity discontinuity, ZE sample zone was not able to resharpen itself and stayed dispersed after passing by the T-junction (Figure 4.6M-O).

4.4 Conclusions

ITP stacking and concentration of mixtures of three fluorescent proteins has been demonstrated in a microfluidic chip with two T-junctions. Protein samples initially introduced into the microfluidic chip were successfully stacked into adjacent zones with an estimated concentration 40 higher than the initial concentration. A gradual reduction of the isotachophoretic velocity during ITP at a constant voltage was due to the decreasing current observed as TE occupied more of the channel.

Simulation provided a convenient tool with which to analyze stacking and moving boundary profiles since these are difficult to obtain from experiments. Two-dimensional simulations of ITP showed excellent agreement with the experimental zone dispersion and resharpenging both during and after passing a T-junction. The resharpening of the protein zones demonstrated here is due to the step change of conductivities across the

terminating boundary. Comparison of 2D simulations of ITP and ZE indicated that linear electrophoresis (ZE) lacks the ability to self-sharpen.

4.5 References

(1) Kaniansky, D., Marak, J. *J. Chromatogr.* 1990, 498, 191-204.

(2) Kaniansky, D., Zelensky, I., Hybenova, A., Onuska, F. I. *Anal. Chem.* 1994, 66, 4258-4264.

(3) Mohan, D., Lee, C. S. *Electrophoresis* 2002, 23, 3160-3167.

(4) Hutta, M., Kaniansky, D., Kovalcikova, E., Marak, J., Chalanyova, M., Madajova, V., Simunicova, E. *J. Chromatogr. A* 1995, 689, 123-133.

(5) Smith, R. D., Fields, S. M., Loo, J. A., Barinaga, C. J., Udseth, H. R., Edmonts, C. G. *Electrophoresis* 1990, 11, 709-717.

(6) Walker, P. A., Kowalchyk, W. K., Morris, M. D. *Anal. Chem.* 1995, 67, 4255-4260.

(7) Korir, A. K., Almeida, V. K., Malkin, D. S., Larive, C. K. *Anal. Chem.* 2005, 77, 5998-6003.

(8) Wolters, A. M., Jayawickrama, D. A., Larive, C. K., Sweedler, J. V. *Anal. Chem.* 2002, 74, 2306-2313.

(9) Mosher, R. A., Saville, D. A., Thormann, W. *The Dynamics of Electrophoresis*; VCH: New York, 1992.

(10) Li, Y., Buch, J. S., Rosenberger, F., DeVoe, D. L., Lee, C. S. *Anal. Chem.* 2004, 76, 742-748.

(11) Herr, A. E., Molho, J. I., Drouvalakis, K. A., Mikkelsen, J. C., Utz, P. J., Santiago, J. G., Kenny, T. W. *Anal. Chem.* 2003, 75, 1180-1187.

(12) Binz, P. A., Muller, M., Hoogland, C., Zimmermann, C., Pasquarello, C., Corthals, G., Sanchez, J. C., Hochstrasser, D. F., Appel, R. D. *Curr. Opin. Biotech.* 2004, 15, 17-23.

(13) Grass, B., Hergenroder, R., Neyer, A., Siepe, D. *J. Sep. Sci.* 2002, 25, 135-140.

(14) Grass, B., Neyer, A., Johnck, M., Siepe, D., Eisenbeiss, F., Weber, G., Hergenroder, R. *Sensors and Actuat. B-Chem.* 2001, 72, 249-258.

(15) Prest, J. E., Baldock, S. J., Fielden, P. R., Goddard, N. J., Kalimeri, K., Brown, B. J. T., Zgraggen, M. *J. Chromatogr. A* 2004, 1047, 289-298.

(16) Prest, J. E.; Baldock, S. J.; Fielden, P. R.; Goddard, N. J.; Brown, B. J. T. *Microchim. Acta* 2005, 151, 223-230.

(17) Cui, H. C., Horiuchi, K., Dutta, P., Ivory, C. F. *Anal. Chem.* 2005, 77, 7878-7886.

(18) Mosher, R. A., Gebauer, P., Caslavska, J., Thormann, W. *Anal. Chem.* 1992, 64, 2991-2997.

(19) Ermakov, S. V., Jacobson, S. C., Ramsey, J. M. *Anal. Chem.* 1998, 70, 4494-4504.

(20) Griffiths, S. K., Nilson, R. H. *Anal. Chem.* 2000, 72, 5473-5482.

(21) Lin, R. S., Burke, D. T., Burns, M. A. *Anal. Chem.* 2005, 77, 4338-4347.

(22) Cui, H. C., Horiuchi, K., Dutta, P., Ivory, C. F. *Anal. Chem.* 2005, 77, 1303-1309.

(23) Thormann, W., Zhang, C. X., Gaslavska, J., Gebauer, P., Mosher, R. A *Anal. Chem.* 1998, 70, 549-562.

(24) Kohlrausch, F. *Ann. Phys. Chem.* 1897, 62, 209-239.

(25) Vreeland, W. N., Williams, S. J., Barron, A. E., Sassi, A. P. *Anal. Chem.* 2003, 75, 3059-3065.

(26) Hanna, M., Simpson, C., Perrett, D. *J. Chromatogr. A* 2000, 894, 117-128.

CHAPTER 5

Automated Electric Valve for Electrokinetic Separation in a Networked Microfluidic Chip

Huanchun Cui,[†] Zheng Huang,[§] Prashanta Dutta,[‡] and Cornelius F. Ivory*,[†]

† School of Chemical Engineering and Bioengineering, ‡ School of Mechanical and Materials Engineering, Washington State University, Pullman, Washington 99164, and § Protasis Corporation, 734 Forest Street, Marlboro, Massachusetts 01752

To whom all correspondence should be addressed. Email: cfivory@wsu.edu

Abstract

This paper describes an automated electric valve system designed to reduce dispersion and sample loss into a side channel when an electrokinetically-mobilized concentration zone passes a T-junction in a networked microfluidic chip. One way to reduce dispersion is to control current streamlines since charged species are driven along them in the absence of electroosmotic flow. Computer simulations demonstrate that dispersion and sample loss can be reduced by applying a constant additional electric field in the side channel to straighten current streamlines in linear electrokinetic flow (zone electrophoresis). This additional electric field was provided by a pair of platinum microelectrodes integrated into the chip in the vicinity of the T-junction. Both simulations and experiments of this electric valve with constant valve voltages were shown to provide unsatisfactory valve performance during nonlinear electrophoresis (isotachophoresis). Based on these results, however, an automated electric valve system was developed with improved valve performance. Experiments conducted with this system showed decreased dispersion and increased reproducibility as protein zones

isotachophoretically passed the T-junction. Simulations of the automated electric valve offer further support that the desired shape of current streamlines was maintained at the T-junction during isotachophoresis. Valve performance was evaluated at different valve currents based on statistical variance due to dispersion. With the automated control system, two integrated microelectrodes provide an effective way to manipulate current streamlines, thus acting as an electric valve for charged species in electrokinetic separations.

5.1 Introduction

Microfluidic systems integrate different analytical operations such as sample preparation, injection, separation and detection into a single microdevice.[1] Valving is one of the most important unit operations required for controlling fluid flow inside microchannels. Since the benefits of microfluidic systems were demonstrated in 1993,[2] a number of microvalves have been developed over the past ten years. Based on the method of actuation, most of these microvalves belong to three major categories: pneumatic,[3, 4] phase change[5, 6] and responsive polymers.[7, 8] A common characteristic of these microvalves is that they all utilize actuators to physically block the microchannels of interest. The structure of these microvalves is relatively complicated since they require moving parts to close and open the microchannels. Most of microvalves mentioned above were designed to control pressure-driven flow during sample introduction, pumping and mixing. However these microvalves are limited in use for controlling electrokinetic flow since valve actuation, which usually requires deformation of polymer

layer, heating, cooling or a buffer pH change, can jeopardize the resolution of electrokinetic separation.

Different flow characteristics require different valve techniques. One way to manipulate electrokinetic driven flow is to control distortion in the current streamlines along which charged species are driven. Ramsey and co-workers[9-14] have developed various valve designs for electrokinetic sample injection and dispensing by manipulating the electric field distribution. Fu and co-workers[15, 16] proposed several unique electrokinetic valve configurations for delivering variable-volume sample plugs by controlling the electric field distribution and magnitude within several adjacent channels. All of the examples above represent different schemes to manipulate the electric field for sample injection in an effort to achieve the sharp sample plug which enables high resolution separation in zone electrophoresis (ZE). To achieve high resolution in separations, it is also necessary to reduce the dispersion that occurs near T-junctions.

Burns and co-workers[17, 18] have successfully developed a method to address this issue by applying shaped electric fields from several pairs of integrated microelectrodes located in the vicinity of an intersection. This method greatly reduced dispersion of DNA bands into side channels while they were being separated by ZE through polyacrylamide gel in the main separation channel. The shaped electric fields were determined primarily based on the electric field applied in the main separation channel. It is relatively easy to find the appropriate shaped electric field for linear electrophoresis, e.g., ZE of DNA since the

electric conductivity is homogenous and the electric field is approximately constant in the main separation channel.

In the case of nonlinear electrophoretic techniques such as isotachophoresis (ITP), it is difficult to find the appropriate electric field for valving since the electrical conductivity is discontinuous and varies as ITP progresses. In this work, we want to address this issue in order to reduce dispersion and sample loss when protein zones pass a T-junction during ITP. This is done using a pair of platinum microelectrodes integrated in the vicinity of the T-junction to act as the electric valve. The positioning of the microelectrodes is similar to that explored by Burns et al.[18]

Determination of the appropriate valve voltages requires knowledge of the local electric field at the T-junction. However, this information is not available during ITP due to transient variations in the local electric field. Instead of manually applying valve voltages, an automated electric valve system has been developed to measure the total current passing through the main separation channel and to automatically inject appropriate valving currents from the microelectrodes based on that measurement. ITP of several fluorescent proteins in free solution was employed to demonstrate and evaluate our valve.

5.2 Experimental Section

5.2.1 Materials and Reagents

Recombinant green fluorescent protein (GFP, MW ~28 000) was obtained from Upstate Biotechnology (Lake Placid, NY). Allophycocyanin (APC, MW ~104 000) and r-phycoerythrin (PE, MW ~240 000) were purchased from Molecular Probes (Eugene, OR). Methylcellulose (MC, viscosity of 2% aqueous solution at 25ºC: 400 centipoises) and epsilon-amino-n-caproic (EACA, MW 131.2) were acquired from Sigma (St. Louis, MO). Hydrochloric acid (HCl, MW 36.5) and tris(hydroxymethyl)aminomethane (Tris, MW 121.14) were purchased from Fisher Scientific (Fair Lawn, NJ).

5.2.2 Electrolytes and Protein Sample Solution Preparation

The leading electrolyte (LE) solution was prepared by adjusting the pH of 10 mM HCl solution to 9.5 with Tris. The terminating electrolyte (TE) solution consists of 60 mM EACA titrated to pH 10.0 with Tris. The proteins PE, GFP and APC were mixed and diluted in the LE solution. All solutions contain 2% w/v MC in order to suppress electroosmotic flow (EOF).

5.2.3 Microfluidic Chip Fabrication

A networked poly-di-methyl-siloxane (PDMS) microfluidic chip with a pair of integrated microelectrodes, as shown in Figure 5.1A, was used in our experiments. The procedure used to fabricate the PDMS chips and the integrated microelectrodes were reported in our previous work.[19, 20] First, a positive pattern of the desired channel structure is formed on a glass substrate using a positive photolithography technique. PDMS prepolymer and curing agent (Sylgard 184, Dow Corning Inc., Midland, MI) are uniformly mixed at a ratio of 10:1, respectively, and degassed for 2 hrs at 0.001 Torr.

The liquid elastomer is cast onto the positive pattern formed on the glass substrate and cured in a hot kiln for 6 hrs at 80˚C. At the end of the curing process, the elastic polymeric material is carefully peeled from the glass substrate to become the bottom layer of the microchip.

Before this bottom layer is sealed with the top layer, which is a flat PDMS substrate with reservoirs, a pair of microelectrodes is fabricated on the bottom surface of the top layer (Figure 5.1B) using the following procedure. The bottom surface of the top layer is spin coated with a highly viscous photoresist, SU-8 2010 (at 1000 rpm for 19 sec) and pre-baked then soft-baked at 65˚C and 95˚C, respectively. The photoresist is then exposed to near-ultraviolet radiation through a mask with a desired pattern of microelectrodes and developed for 60 sec in the SU-8 developer (MicroChem Corp., MA). To produce more rigid pattern structures, the patterned photoresist on the bottom surface of the top layer is hard baked at 115˚C for 150 sec. The exposed part of the bottom surface of the top layer is temporarily activated by an RF plasma in the presence of oxygen gas (Plasma Etcher PE 2000, South Bay Technology Inc., San Clemente, CA) in order to achieve better adhesion between the PDMS surfaces and the metal about to be deposited. The photoresist patterned surface is then sputtered (Edwards Auto 306, BOC Edwards, MA) with a titanium thin film (~30 nm thick) which is followed by a sputtered platinum layer approximately 175 nm thick. The hard-baked photoresist was then stripped off the PDMS surface. The PDMS surface patterned with microelectrodes was then cleaned with acetone, isopropyl alcohol, and DI water. For permanent bonding of the top and

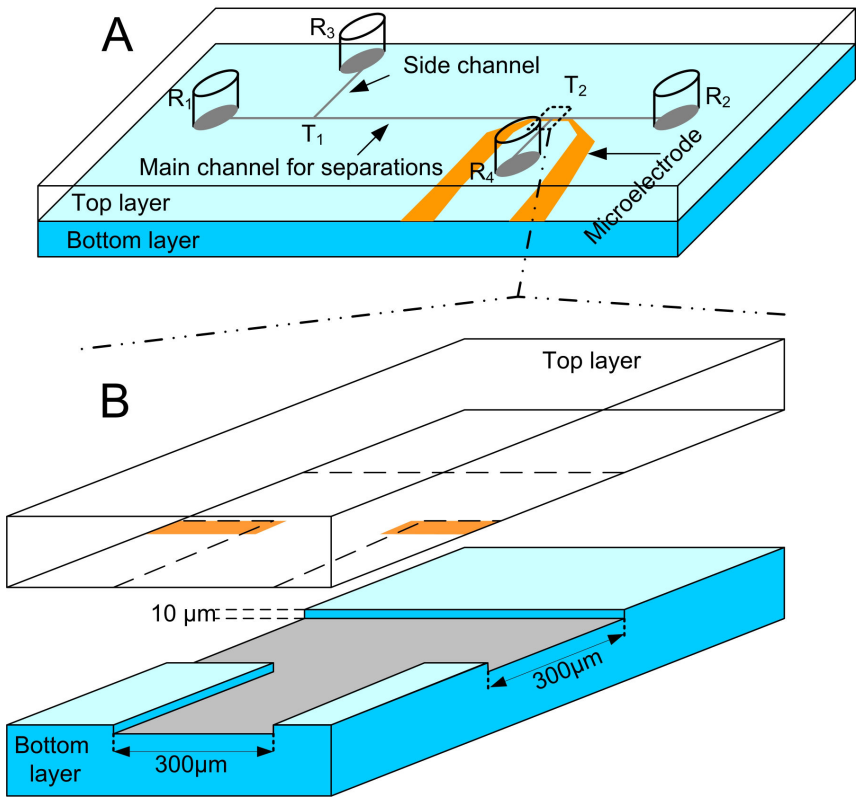

Figure 5.1 (A) Schematic of the PDMS microfluidic chip used in all electric valve experiments presented in this work. The length of the side channels and the main channel are 5 and 20 mm, respectively. R_1-R_4 are reservoirs and T_1-T_2 are T-junctions. A pair of microelectrodes was fabricated at the vicinity of T_2 for electric valve. (B) Schematic of the junction T_2. The depth and width of the microchannel are 10 and 300 μm, respectively. The pair of microelectrodes was deposited on the bottom surface of the top layer.

bottom layers, both layers were cleaned by oxygen RF plasma (PDC-32G, Harrick Scientific Co., NY). This microfluidic chip (Figure 5.1) consists of a main channel andtwo side channels that branch out from the main channel. All channels are 300 μm wide and 10 μm deep.

5.2.4 Automated Control

An electronic circuit (Figure 5.2) designed in-house has the ability to sense the electric current passing through the main channel and then to supply a specific amount of control current to the two microelectrodes. The circuit was drawn in EAGLE (CadSoft Computer, Delray Beach, FL) software and printed onto a prototype circuit board by AP Circuits (Calgary, AB, Canada). The electronic units including operational amplifiers, transistors, isolation amplifiers, DC-DC converters, resistors, capacitors and relays were then soldered onto the circuit board. Five analog inputs, two analog outputs and four digital I/O ports on a data acquisition device (LabJack, Lakewood, CO) were employed to read and send commands to the electronic circuit (Figure 5.2). The data acquisition device was controlled by software programmed in LabVIEW (National Instruments Corporation, Austin, TX). Please note that the electronic circuit was exclusively designed for the purpose of electric valve which has the following functions: current/voltage measurement and inject/drain specific amount of current through microelectrodes. The direct use of this design for other applications is not recommended. However, after slight modifications, it can be used to control voltage/current/conductivity sensors that are integrated in a microfluidic chip. But readers should be very careful about the working range of each electronic unit on the board.

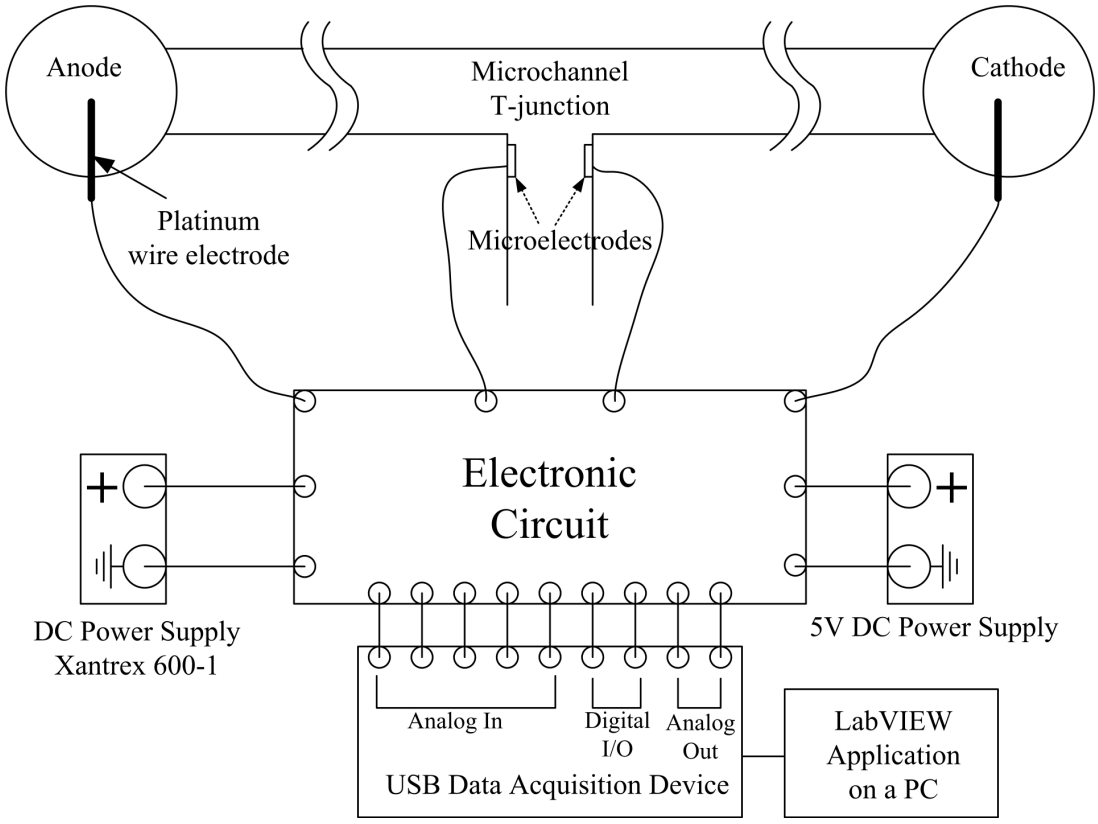

Figure 5.2 Schematic of the automated electric valve system. The electronic circuit and LabVIEW application were designed in-house. 5 "Anolog In", 2 "Digitial I/O" and 2 "Analog Out" connections on the USB data acquisition device are used to control the electronic circuit. The DC power supply, Xantrex 600-1, is used to provide 30 V for separation through the platinum wire electrodes as well as to power the electronic circuit. A 5 V DC power supply is used to power several voltage isolation units integrated into the electronic circuit.

5.2.5 Experimental Procedure

The procedure used to run ITP in a networked microfluidic chip was reported in our previous work.[21] Briefly, all channels were pressure-filled with the LE from reservoir R_1 (Figure 5.1). After all the reservoirs were cleaned by removing excessive LE, 30 μL of LE and a 2% MC solution were loaded into R_1 and R_4, respectively. Protein sample solution was then carefully pressure-filled into the channel from reservoir R_3 at ~5 psi until a drop of liquid appeared at the channel entrance inside reservoir R_2. Reservoir R_2 and R_3 were then cleaned and loaded with 30 μL of TE and 2% MC solution, respectively. Note that the initial buffer distribution varies from experiment to experiment since the volume of protein sample solution loaded by this method is not precisely controlled.

Platinum wire electrodes were immersed in reservoirs R_1 and R_2 while reservoirs R_3 and R_4 were left electrically floating. ITP was carried out at a constant voltage of 30 V supplied by the controller which is powered by an XHR 600-1 power supply (Xantrex technology Inc, Vancouver, Canada) and a 5 V DC power supply (Allied Electronics, Fort Worth, TX). Microelectrodes integrated in the chip were connected by wire to the controller for the electric valve.

5.2.6 Imaging

The loaded chip was mounted underneath the 4x objective lens of a Leica DMLB fluorescence microscope equipped with a CCD camera (SPOT RT color, Diagnostic instruments, Inc., Sterling Heights, MI). The fluorescent proteins were excited with a

mercury lamp (OSRAM HBO® 100 W/2) using a filter cube (DMLB 513804, Leica Microsystems, Inc., IL) and photos were taken by software that controls the CCD camera. The variance of a protein zone is obtained using ImageJ (NIH, Bethesda, MD) with Moment Calculator (http://rsb.info.nih.gov/ij/plugins/moments.html). After subtracting the background signal intensity from an experimental photo, the protein concentration zone is centered inside a rectangular box for moment analysis. The rectangular box is set so that its lateral edges are just outside the edges of the protein zone and they extend for 1 mm along the separation channel with the protein zones roughly centered along this axis.

5.2.7 Simulation

The Nernst-Planck physics built into Femlab (COMSOL, Burlington, MA) was employed to perform two dimensional simulations of linear and nonlinear electrophoresis, ZE and ITP respectively, in a microchannel with a T-junction.

Under an external electric field, each charged species in a solution migrates by diffusion, electromigration and convection. The flux of each species is given by the equation:

$$\mathbf{N}_i = -D_i \nabla C_i - z_i F \mu_i C_i \nabla \mathbf{\Phi} + C_i \mathbf{u} \tag{5.1}$$

Here, $\mathbf{N}_i$ is the flux of species *i*, C_i is the concentration of species *i*, z_i the charge, F the faraday constant, μ_i the ion mobility, $\mathbf{\Phi}$ the electric potential, D_i the diffusion coefficient, and **u** the bulk flow velocity.

Each species is governed by the mass conservation law expressed as following:

$$\frac{\partial C_i}{\partial t} = -\nabla \cdot \mathbf{N}_i \tag{5.2}$$

Some assumptions are made in the simulations. The sources that induce bulk flows such as pressure differences among the reservoirs and EOF due to the methyl-cellulose coated surface charges[19] are neglected, and thus the bulk flow velocity, **u**, in eq 5.1 is assumed to be zero.

A constant electric potential was set between boundaries b_1 and b_2 (Figure 5.3). In the case of the electric valve with constant valving voltages, two additional constant voltages were set on boundaries b_3 and b_4 (Figure 5.3B). In the case of the automatic electric valve, the total current was calculated by integrating the current density along boundary b_2 and a fixed percentage of the total current was assigned in the form of current densities along boundaries b_3 and b_4. All channel walls are impermeable to the current and to migrating species.

5.3 Results and Discussion

5.3.1 Control Current Streamlines Using Integrated Microelectrodes

A simulation result (Figure 5.3A) shows that the uncontrolled current streamlines bend into the side channel as they pass through a T-junction.[22] The bent current streamlines are the primary source of dispersion of a concentration zone of charged species since it is driven along the current streamlines. An obvious way to reduce this type of dispersion is to block the side channel entrance. However this requires actuation of a physical barrier which complicates microfluidic chip fabrication as well as experimental operation.

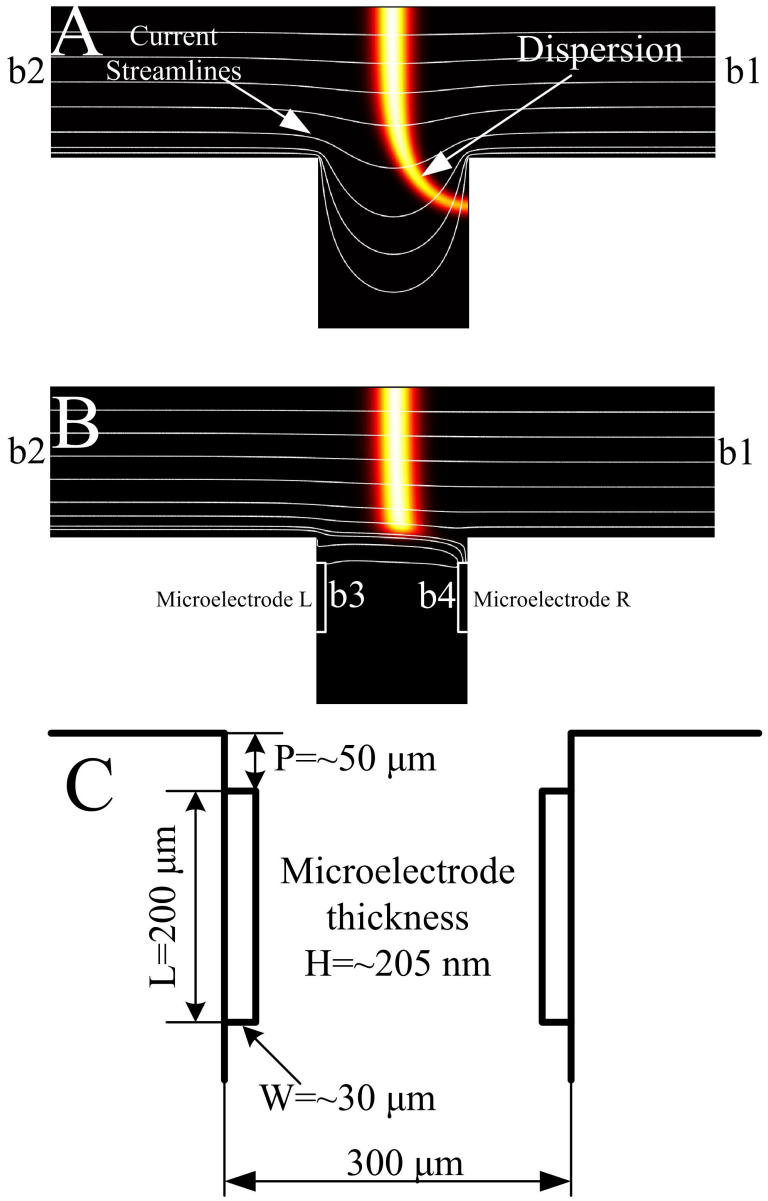

Figure 5.3 (A) Simulated images showing dispersion of a concentration zone and bent current streamlines at a T-junction. (B) Simulation of an electric valve showing greatly reduced dispersion and straightened current streamlines. (C) Schematic of microelectrode positions at the T-junction. P is the distance between the microelectrode and the main channel. L, W and H represent the length, width and thickness of the microelectrode, respectively. The position of the microelectrode differs slightly from chip to chip. The following statement is applied to all the simulation results presented in this paper: The simulated image is only the middle part of whole computing domain which has a 2 mm long main channel and a 0.5 mm long side channel branched out from the middle of the main channel. All concentration zones are negatively charged and migrate to the left (The anode). All channels in the simulated images are 300 μm wide.

Another way to reduce such dispersion is to manipulate the current streamlines by applying additional electric fields in the vicinity of the T-junction. If the current streamlines in the separation channel are straightened by the additional electric field, then dispersion would not be expected to occur since charged species follow the current streamlines.

The concentration zone in Figure 5.3B shows almost no dispersion due to the straightened current streamlines. The two microelectrodes used to control the current streamline act as a virtual valve which not only prevents losses into the side channel but also greatly reduces dispersion of the concentration zone. Since neutral species do not migrate along the current streamlines, this virtual valve exclusively controls the charged species, the targets of electrophoresis.

5.3.2 Microelectrode Design Concerns

The valve voltages applied to the microelectrodes depend on the position and size of the microelectrodes as well as the local electric field around the T-junction. The positioning and sizing of the microelectrodes were experimentally investigated by Burns and coworkers[18] in an effort to obtain minimal mass loss into the side channel. There are concerns about electrode erosion and electrolysis when the current density on a microelectrode is too high. To avoid electrode erosion and electrolysis, the microelectrodes need to be large and thick. To make the microelectrodes larger, they are extended in length (L) instead of width (W) (Figure 5.3C) to make the side channel more accessible. To avoid contact between the microelectrodes and the concentration zone, the

microelectrodes are located 50 μm away from the main channel. With the size and the position shown in Figure 5.3C, no bubble formation due to electrolysis was found in experiments and only some minor electrode erosion was observed after multiple runs.

5.3.3 Electric Valve with Constant Valve Voltages

Once the size and position of each microelectrode is fixed, the valve voltages only depend on the local electric field. Therefore, the valve voltages need not vary in the case of a linear electrokinetic flow since the local electric field remains approximately unchanged due to the homogeneous background buffer ion which dominates the local conductivity. The simulation (Figure 5.4A-C) of an electric valve for linear electrokinetic flow (ZE) with constant valve voltages reveals that the current streamlines remain straight and unchanged before, during and after the concentration zone passes the T-junction. Therefore, using electric valve for linear electrokinetic flow is effective when constant valve voltages are applied.

However, an electric valve with a constant valve voltage is not expected to work effectively for nonlinear electrokinetic flows and our simulation (Figure 5.4D-F) confirms that the shape of the current streamlines changes dramatically as nonlinear electrophoresis (ITP) progresses. In our simulation, constant valve voltages were intentionally chosen in the simulation to have straight current streamlines at the moment when the concentration zone approaches the middle of the T-junction (Figure 5.4E). However, after the concentration zone passed the T-junction, the lower part of it tilted clockwise due to the skewed current streamlines (Figure 5.4F).

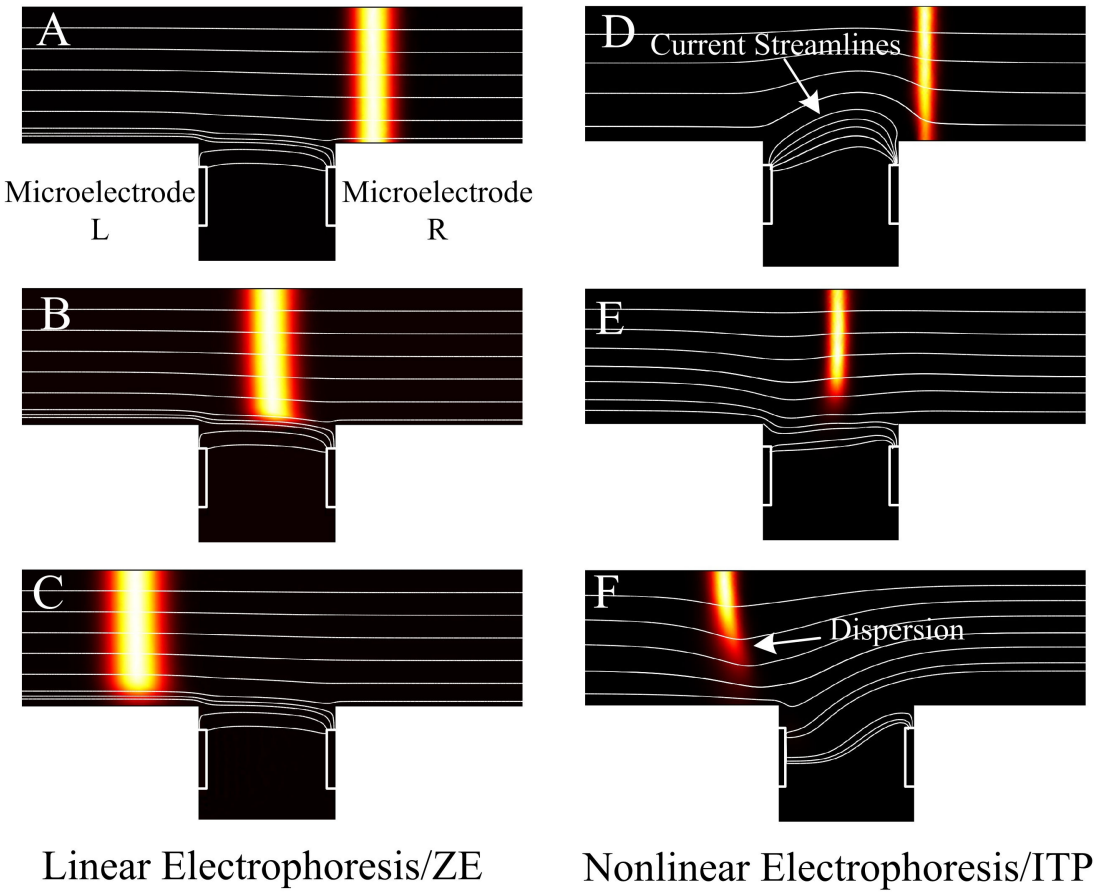

Figure 5.4 Simulation results for an electric valve under both linear electrophoresis and nonlinear electrophoresis using constant electric valve voltages. ZE: 100 V along the main channel, 60 V at microelectrode L, and 45 V at microelectrodes R. Nonlinear electrophoresis/ITP: 100 V along the main channel, 95 V at microelectrode L and 80 V at microelectrode R. See Figure 5.3 for the description of the whole computing domain and simulated images.

It is relatively easy to choose appropriate valve voltages in the modeling since the local electric field around the T-junction can be analyzed in the simulations. However, it is difficult to comprehensively measure and analyze the local electric field during the experiments. Furthermore, variation of the initial buffer and sample distribution from experiment to experiment makes it more difficult to adjust the valve voltages based on the results of previous experiments. The experimental result shown in Figure 5.5 is one of only a few successful runs among tens of experiments performed with constant valve voltages. A series of photos shown in Figure 5.5A-D demonstrates how three adjacent protein zones maneuvered through the T-junction with two fixed valve voltages of 9.5 V and 6.0 V applied to microelectrodes R and L, respectively.

In this case, the protein zones were nicely formed as they approached the T-junction (Figure 5.5A). As they migrated into the T-junction, they skewed slightly and no expansion of their lower part into the T-junction was observed (Figure 5.5B). Figures 5.5C and D show that the protein zones "jumped" across the T-junction with the lower part of it skewing behind the center of mass of the peak before jumping and then skewing ahead. Although no protein loss into the side channel was experimentally observed, the protein zones were dispersed when passing the T-junction and the reproducibility of this result is very low due to the difficulties mentioned above.

5.3.4 Developing an Automated Electric Valve

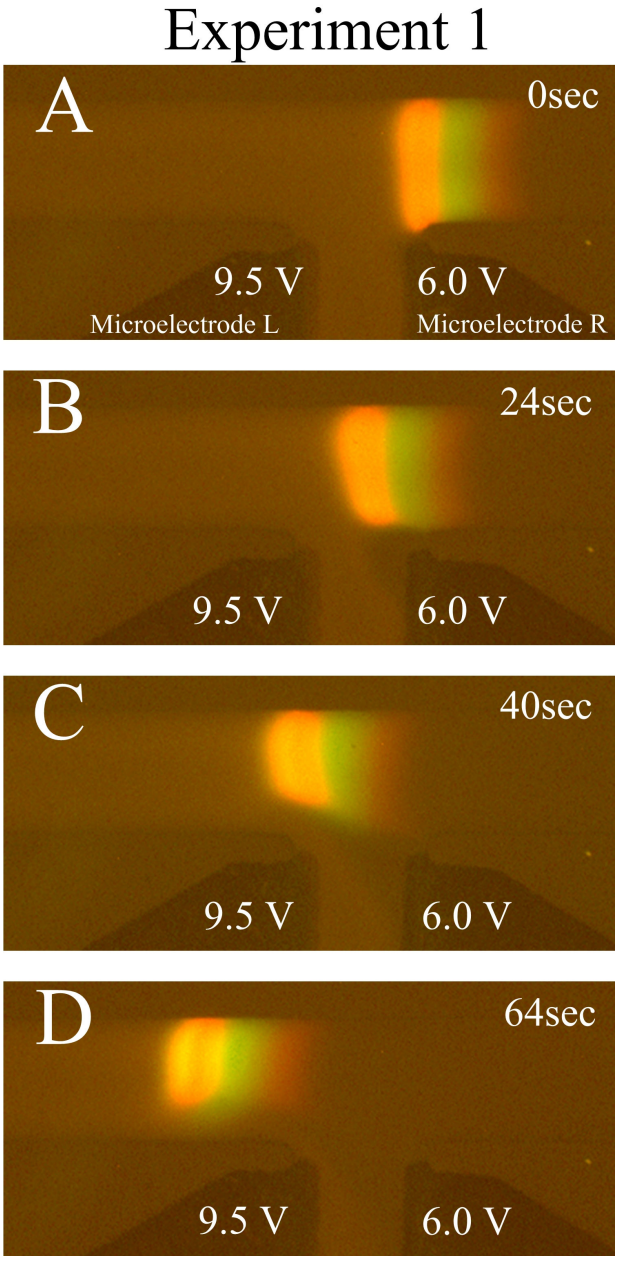

Figure 5.5 Electric valve experiment with constant valve voltages. Time-series photos A-D of ITP near a T-junction were captured at junction T_2 as shown in Figure 5.1A. Valve voltages of 9.5 V and 6.0 V were applied to the left and right microelectrodes, respectively. The initial sample solution consisted of PE (0.04 μg/μL), GFP (0.06 μg/μL), and APC (0.06 μg/μL). The three protein zones from left to right are PE, GFP and APC.

To increase the reproducibility and further reduce dispersion, the valve voltages must change in response to the variation of the local electric field in the T junction. Another microelectrode positioned at the point where the centerline of the side channel crosses the upper wall of the main channel might be used as a voltage sensor to provide the information on the variation of the local electric field. However, integration of such a voltage sensor certainly complicates the design, especially when considering large scale integration of multiple electric valves. Instead of relying on the additional microelectrode to sense the local electric field and then control the valve voltages, an electronic system was developed to control the electric currents carried on the pair of microelectrodes based on the total current passing through the main channel which can be measured outside of the microfluidic chip. The following paragraph details the development of the automated electric valve system.

As ITP progresses, the total current passing through the main channel decreases because an increasing length of the channel is occupied by the low conductivity TE. Ideally, the valve voltages that straighten the current streamlines in a T-junction at any given moment during ITP should exist, but it is difficult to find them because of a lack of knowledge of the local electric field during these experiments. However, knowledge of the total current is available because it can be easily measured. Since any valve voltage applied to an electrode should generate a corresponding valve current, the appropriate valve voltages can be chosen based on the knowledge of the total current if the relationship between valve current and the total current is known. Therefore, the problem turns out to be finding the appropriate valve currents applied to the pair of microelectrodes to make the

total current go straight through the T-junction. If the positions and size of the microelectrodes are fixed, the valve currents only depend on the total current. Although the relationship between the two is elusive, the assumption that the valve currents are a fixed percentage of the total current makes the relationship straightforward. Based on this assumption, an automated electric valve system has been developed which measures the total current every 30 ms and assigns a certain amount of current to the microelectrodes. The ratios of the valve currents on the pair of microelectrodes to total current are crucial to valve performance and need to be experimentally determined. Despite the variation of initial buffer distribution and sample concentration from experiment to experiment, the automated electric valve system is expected to work properly with the determined ratios unless the position and size of the microelectrodes are changed.

5.3.5 Simulation and Experimental Demonstration of Automated Electric Valve

The simulation results shown in Figure 5.6 demonstrate that an automated electric valve, based on the assumption made above, can significantly improve valve performance. In this simulation, 18% of total current flowed from microelectrode L into the channel and 58% of total current flowed from the channel onto microelectrode R. Only slight changes in the shape of the current streamlines (Figure 5.6A, B and C) were observed in this simulation as the ITP concentration zone passed the T-junction so the dispersion which occurred in the lower part of the ITP concentration zone (Figure 5.6C) is negligible and no sign of mass loss into the side channel was witnessed in the simulation. Despite the fact that the current streamlines around the T-junction are not perfectly straight, the

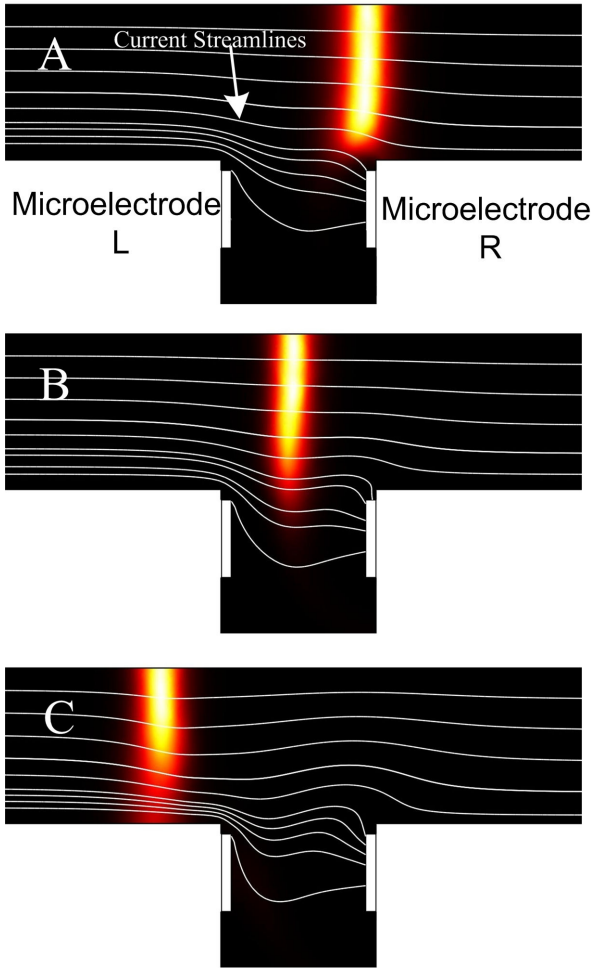

Figure 5.6 Simulation of automated electric valve as an ITP zone passes a T-junction. See Figure 5.3 for the description of the whole computing domain and simulated images. The total current was automatically calculated in the simulation by integrating the current density along the left boundary of the main channel (b2 as shown in Figure 5.3A). 18% of total current flowed from microelectrode L into the channel and 58% of total current flowed from the channel onto microelectrode R. 30 V was applied along the main channel.

strategy that application of fixed percentages of the total current to the pair of microelectrodes is effective enough to provide high quality valving. With the electronic control system, experimental operations became automatic and straightforward and experimental results became reproducible. In order to obtain optimum valve performance, only two parameters (the ratios of two valve currents to the total current) need to be adjusted in the homemade LabVIEW program which controls the electronic circuit.

The following two experiments shown in Figure 5.7 demonstrate the benefits of the automated electric valve system. Experiments 2 and 3 are two independent runs performed in the same microfluidic chip and under same experimental conditions except that they have different initial buffer distributions and sample concentrations. 15~17% of the total current goes from microelectrode L into the channel while 38~40% of the total current goes from the channel onto microelectrode R. The difference in the breadth of the protein zones in Experiments 2 and 3 (Figure 5.7) is due to their different initial sample concentrations. Despite such differences, the protein zones in both experiments followed very similar paths when passing the T-junction. Although there was a small jump in the protein zones near the left corner of the T-junction (Figure 5.7C and G) in both experiments, the intensity of the jump was greatly reduced when compared to the experiment shown in Figure 5.5, in which the valve voltages were constant. To understand why this happened, it is necessary to examine the resulting valve voltages on the pair of microelectrodes which were automatically recorded in the LabVIEW application. For example, the valve voltages in experiment 2 shown in Figure 5.7A-D

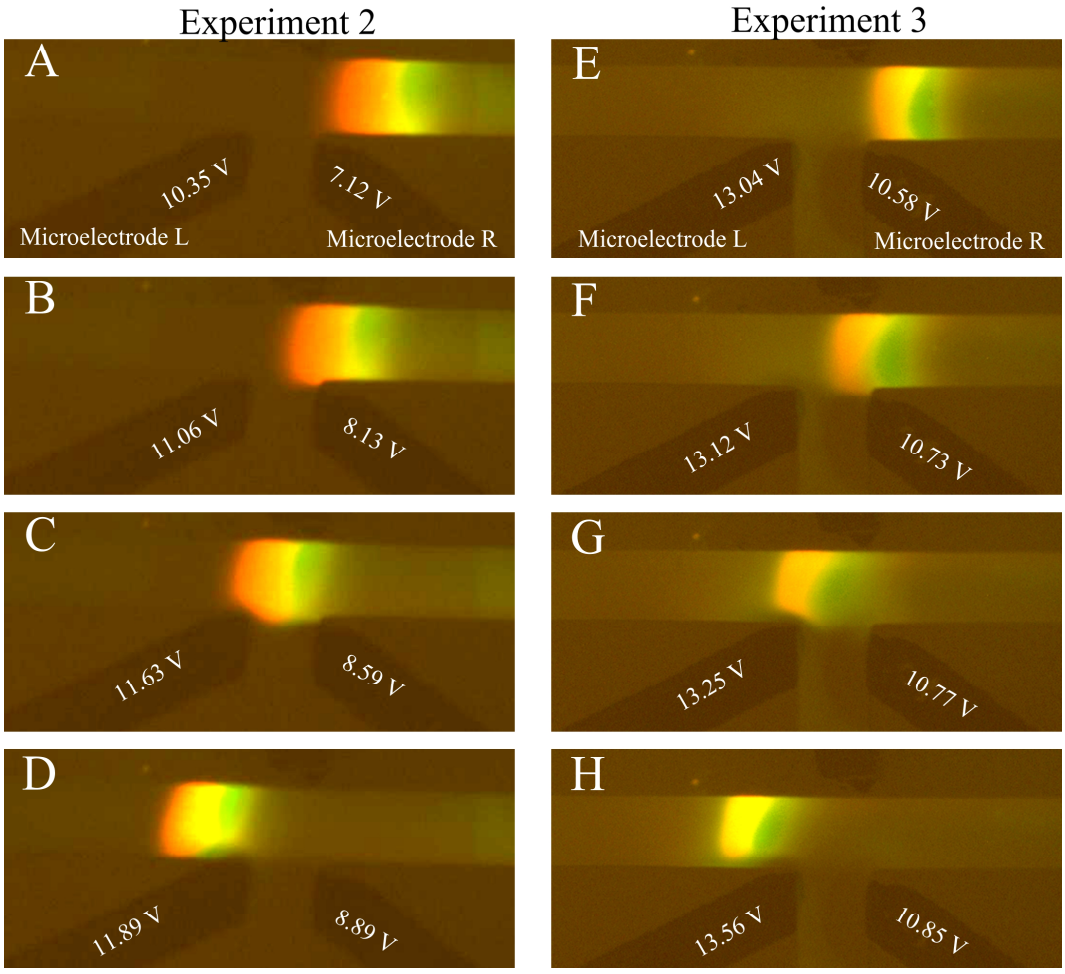

Figure 5.7 Automated electric valve experiments with different initial protein sample concentrations and initial buffer distributions. Both experiments were performed in the same chip. Both experiments had 15~17% of the total current flowed from microelectrode L into the channel and 38~40% of total current flowed from the channel onto microelectrode R. Experiment 2: the initial sample solution consisted of PE (0.06 μg/μL), GFP (0.06 μg/μL). Experiment 3: the initial sample solution consisted of PE (0.03 μg/μL), GFP (0.05 μg/μL). The resulting valve voltages at each moment are indicated on the microelectrodes.

increased gradually from 10.35 V to 11.89 V on microelectrode L and from 7.12 V to 8.89 V on microelectrode R. This increase is the response to the change of the local electric field in an effort to maintain the shape of the current streamlines. The valve voltages on the pair of microelectrodes in experiment 2 (Figure 5.7A-D) are different from those in experiment 3 (Figure 5.7E-H) primarily because of the different initial buffer distributions and initial sample concentrations. It is very unlikely that an operator could apply the appropriate valve voltages without the help of an automatic control system because of the variation in the initial experimental conditions.

Figure 5.8 is a data plot of the valve currents, the total current and the valve voltages recorded in another experiment that was performed in the same chip as that shown in Figure 5.7. The automated electric valve was turned on for about 20 mins. During this period, the protein zones approached and passed the junction T_2 (Figure 5.1A) and continuously migrated toward the anode reservoir until it approached the junction T_1 (Figure 5.1A). Figure 5.8A shows that, as expected, the total current gradually decreased from ~1.0 μA to ~0.4 μA as ITP progressed. The corresponding valve currents also shown in Figure 5.8A are 15~17% of the total current on microelectrode L and 38~40% of total current on microelectrode R. The gap between the two vertical lines (Figure 5.8) indicates the length of time that the protein zones took to pass the T-junction. The resulting valve voltages are shown in Figure 5.8B. The valve voltages reached the peak right after the protein zones passed the T-junction and decreased as they migrated further away from the T-junction. The total current, valve current and the valve voltages stayed constant (not shown in Figure 5.8) after the ITP concentration zones entered the anode

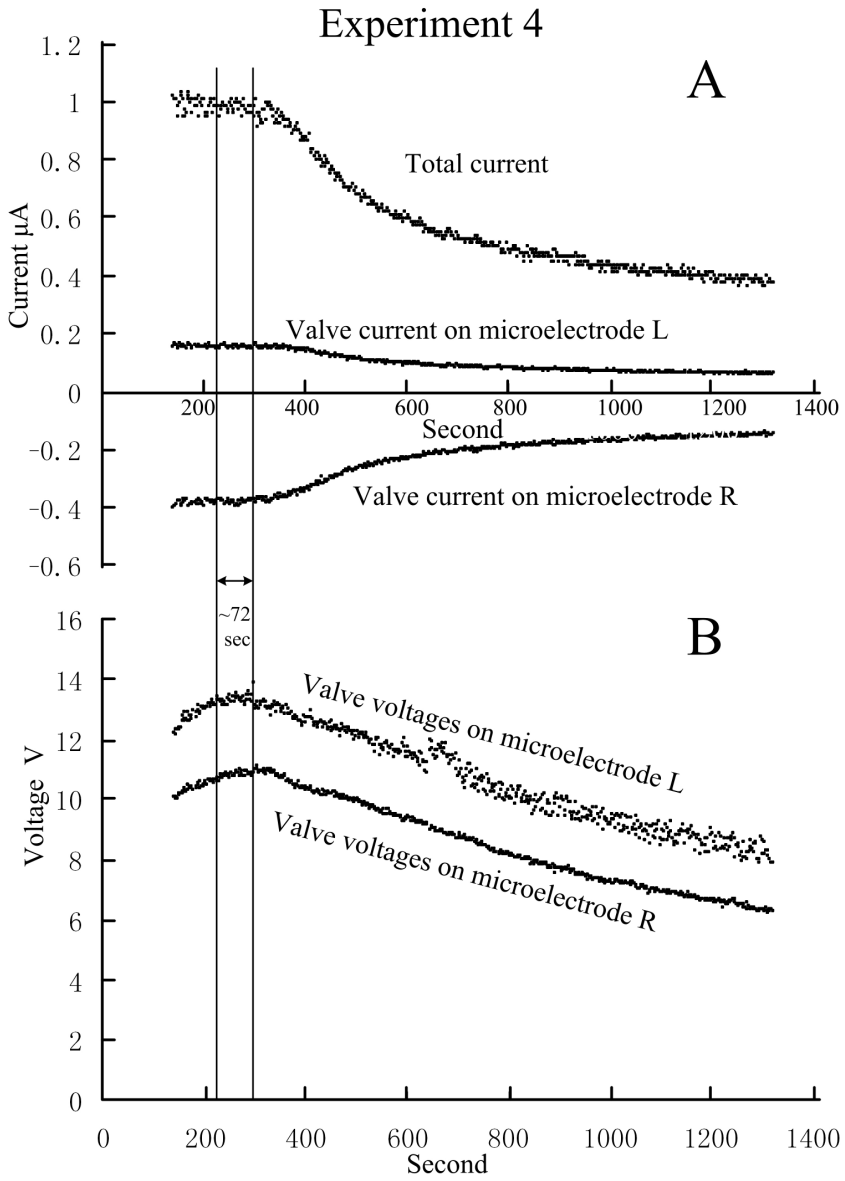

Figure 5.8 Variation of the total current, valve currents and valve voltages with time. The automated electric valve system was turned on before the ITP concentration zone approached junction T_2 as shown in Figure 5.1A and was not turned off until the ITP concentration zone approached the junction T_1 as also shown in Figure 5.1A. 15~17% of the total current flowed from microelectrode L into the channel and 38~40% of total current flowed from the channel onto microelectrode R. Two vertical lines indicate the time period during which the ITP concentration zone was passing the T-junction.

reservoir because the whole channel was occupied by uniform TE buffer and the local electric field around the T-junction no longer changed.

5.3.6 Performance Evaluation of Automated Electric Valve

Valve performance can be evaluated in terms of dispersion and sample loss at a T-junction. Since no obvious sample loss into the side channel was observed in our experiments, the valve performance was evaluated only by the dispersion. The dispersion of a protein zone is quantified by its variance. The method used to obtain the variance of a protein zone is mentioned in experimental section. The initial variance is defined as the variance of the protein zones before entering the junction area. Experiments with different valve currents were employed to evaluate the valve performance. These experiments (Figure 5.9) were performed in the same chip with the same sample concentration. Please note that the chips employed in these experiments have slightly different microelectrode positions from the chips used in those experiments shown in Figure 5.5 and Figure 5.7. This difference in the microelectrode positions was introduced during the fabrication step where the top layer of PDMS substrate containing the pair of microelectrodes was manually aligned to the bottom substrate that contains channels before bonding.

Experiment 5 (Figure 5.9A-D) differs from Experiment 6 (Figure 5.9E-H) by the percentage of the total current that flows from microelectrode L into the channel. Figure 5.9A and E show that the protein zones in both experiments were similar and well formed when approaching the T-junction. As they migrated further into the T-junction, the ITP

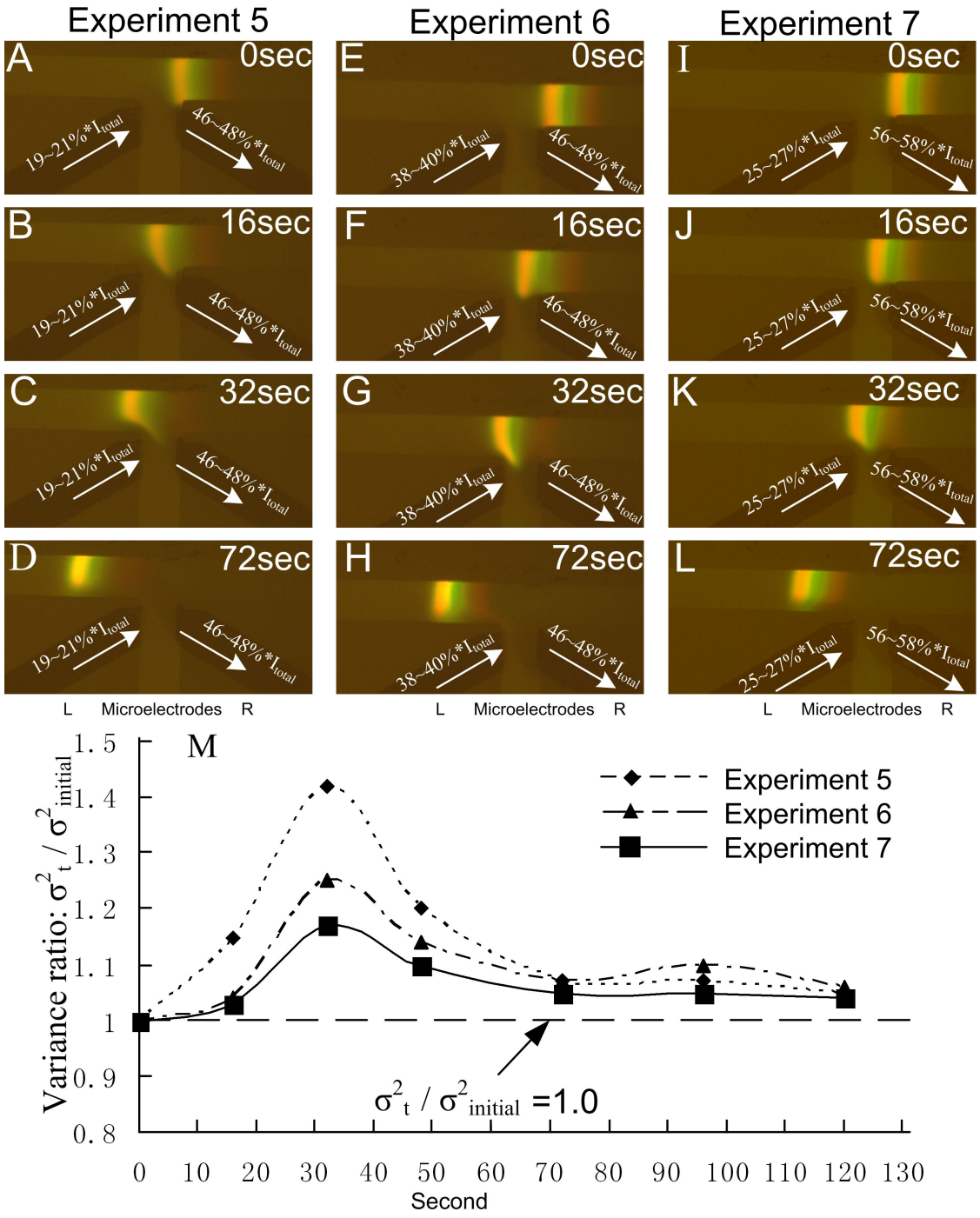

Figure 5.9 Evaluation of valve performance based on the variance ratios of dispersion at different valve currents. The percentages of the total current (e.g. 19~21%*I_{total}) are indicated on the microelectrodes and the arrows indicate the direction of the valve currents. Photos A-L correspond to the variance ratios plotted in M. The corresponding photos of other points plotted in M were not shown. The initial sample concentration in all experiments consisted of PE (0.03 μg/μL), GFP (0.06 μg/μL), and APC (0.06 μg/μL)

concentration zone shown in Figure 5.9B was slightly dispersed while the counterpart in Figure 5.9F maintained its shape. The comparison of dispersion was quantified in Figure 5.9M which revealed that at t=16 sec, the variance ratio ($\sigma_t^2/\sigma_{initial}^2$) in Experiment 5 reached 1.15 while it stayed close to 1.0 in Experiment 6.

To explain why the protein zones behaved differently in Experiments 5 and 6, it is necessary to emphasize the fact that all the proteins were negatively charged and thus they are attracted to the anode. The potential on an anode increases as more applied current flows out from it. The increased potential makes the anode more attractive to the negatively charged proteins. On the other hand, the potential on a cathode decreases as more current flows into it and thus it repels the negative charged proteins more strongly. Since microelectrode L supplied a higher percentage of total current into channel in Experiment 6 than in Experiment 5, it was relatively more anodic in Experiment 6. Therefore, the dispersion that occurred in Experiment 5 (Figure 5.9B) was greatly reduced in Experiment 6 (Figure 5.9F) because the lower part of the protein zones was straightened by the stronger attraction toward microelectrode L. For the same reason, the lower part of the protein zones jumped over the left corner of the T-junction in Experiment 5 (Figure 5.9C) while the counterpart in Experiment 6 (Figure 5.9G) climbed over the left corner. The corresponding variance ratio at this moment (32 sec) increased to 1.42 and 1.25 for Experiments 5 and 6, respectively (Figure 5.9M). After the protein zones passed the T-junction (Figure 5.9D and H), dispersion was greatly reduced due to the well known self-sharpening ability of ITP. This was also demonstrated in Figure 5.9M in terms of the intensity of the variance ratio which dropped quickly in both

experiments after the protein zones passing by the T-junction and stayed very closely to 1.0 as they migrated further away from the T-junction.

Although the valve performance was greatly improved in Experiment 6 when compared to that in Experiment 5, there was still room for improvement. For example, the dispersion which occurs near the left corner of the T-junction in Experiment 6 can potentially be reduced. This dispersion happened because microelectrode L excessively attracted the lower part of the protein zones and pulled it down into the side channel more than 50 μm. Experiment 7 was designed to reduce this type of dispersion by further adjusting the valve currents. To prevent the lower part of the ITP zone from entering the side channel, it has to be pushed up vertically by the joint repelling force from both microelectrodes. To do so, the valve currents used in Experiment 7 decreased on microelectrode L and increased on microelectrode R when compared to those in Experiment 6. Figures 5.9I-L clearly demonstrated that the dispersion was further reduced during the ITP zone passing by the T-junction because the lower part of the ITP concentration was successfully prevented from entering the side channel. Figure 5.9M also confirms that the protein zones were least dispersed in Experiment 7 based on the variance ratio.

5.4 Conclusion

An automatically controlled electric valve system has been demonstrated in a microfluidic chip with T-junctions as a means of reducing dispersion and sample loss into side channels during nonlinear electrophoresis (ITP) of proteins. The dispersion and

sample loss at a T-junction is primarily due to the deformation of current streamlines as current passes through the T-junction. Simulation results clearly demonstrated that the current streamlines bent by a T-junction in linear electrokinetic electrophoresis can be straightened by applying constant valve voltages onto a pair of microelectrodes that were appropriately positioned along the side channel walls. However, both simulation and experimental results confirm that constant valve voltages were not able to produce satisfactory valve performance for isotachophoretic concentration zones passing a T-junction due to the variation of the local electric field as ITP progresses.

To optimize valve performance, the valve voltages must automatically change in response to the variation of the local electric field during ITP. This was accomplished by using an electronic control system that was developed to measure the total current passing through the main channel and to automatically assign a specific amount of valve current to the pair of microelectrodes. The simulation of the automated valve strategy proves that the shape of the current streamlines maintains very well and the valve performance was greatly improved as the concentration zone passes a T-junction. Experiments with an automated electric valve system showed excellent valve performance and dramatically improved reproducibility. Experiments also demonstrated that the behavior of protein zones when passing a T-junction can be manipulated by carefully adjusting the valve currents. Comparison of the variance ratio of protein zones provides an effective way to evaluate the valve performance.

The automated electric valve system provides a robust and simple method for controlling current streamlines and reducing dispersion at T-junctions during nonlinear electrophoresis. This system can be easily expanded to provide automated electric valves for a microfluidic chip with multiple T-junctions. Eventually, it is expected that the automated electric valve units will be incorporated into large scale microfluidic network as virtual valves for electrokinetic flow.

5.5 References

(1) Vilkner, T.; Janasek, D.; Manz, A. *Analytical Chemistry* 2004, *76*, 3373-3385.

(2) Harrison, D. J.; Fluri, K.; Seiler, K.; Fan, Z. H.; Effenhauser, C. S.; Manz, A. *Science* 1993, *261*, 895-897.

(3) Unger, M. A.; Chou, H. P.; Thorsen, T.; Scherer, A.; Quake, S. R. *Science* 2000, *288*, 113-116.

(4) Thorsen, T.; Maerkl, S. J.; Quake, S. R. *Science* 2002, *298*, 580-584.

(5) Pal, R.; Yang, M.; Johnson, B. N.; Burke, D. T.; Burns, M. A. *Analytical Chemistry* 2004, *76*, 3740-3748.

(6) Chen, Z. Y.; Wang, J.; Qian, S. Z.; Bau, H. H. *Lab on a Chip* 2005, *5*, 1277-1285.

(7) Beebe, D. J.; Moore, J. S.; Bauer, J. M.; Yu, Q.; Liu, R. H.; Devadoss, C.; Jo, B. H. *Nature* 2000, *404*, 588-590.

(8) Luo, Q. Z.; Mutlu, S.; Gianchandani, Y. B.; Svec, F.; Frechet, J. M. J. *Electrophoresis* 2003, *24*, 3694-3702.

(9) Ermakov, S. V.; Jacobson, S. C.; Ramsey, J. M. *Analytical Chemistry* 2000, *72*, 3512-3517.

(10) Kutter, J. P.; Jacobson, S. C.; Ramsey, J. M. *Analytical Chemistry* 1997, *69*, 5165-5171.

(11) Jacobson, S. C.; Ermakov, S. V.; Ramsey, J. M. *Analytical Chemistry* 1999, *71*, 3273-3276.

(12) Jacobson, S. C.; Ramsey, J. M. *Analytical Chemistry* 1997, *69*, 3212-3217.

(13) Alarie, J. P.; Jacobson, S. C.; Culbertson, C. T.; Ramsey, J. M. *Electrophoresis* 2000, *21*, 100-106.

(14) Thomas, C. D.; Jacobson, S. C.; Ramsey, J. M. *Analytical Chemistry* 2004, *76*, 6053-6057.

(15) Fu, L. M.; Yang, R. J.; Lee, G. B.; Liu, H. H. *Analytical Chemistry* 2002, *74*, 5084-5091.

(16) Fu, L. M.; Yang, R. J.; Lee, G. B. *Analytical Chemistry* 2003, *75*, 1905-1910.

(17) Lin, R. S.; Burke, D. T.; Burns, M. A. *Journal of Chromatography A* 2003, *1010*, 255-268.

(18) Lin, R. S.; Burke, D. T.; Burns, M. A. *Analytical Chemistry* 2005, *77*, 4338-4347.

(19) Cui, H. C.; Horiuchi, K.; Dutta, P.; Ivory, C. F. *Analytical Chemistry* 2005, *77*, 1303-1309.

(20) Mamun, N. H. A.; Dutta, P. *Journal of Microlithography Microfabrication and Microsystems* 2006, 5, 039701.

(21) Cui, H. C.; Dutta, P.; Ivory, C. F. *Electrophoresis* 2006, in production.

(22) Cui, H. C.; Horiuchi, K.; Dutta, P.; Ivory, C. F. *Analytical Chemistry* 2005, *77*, 7878-7886.

CHAPTER 6

Summary

Conclusions

The work presented in this dissertation involves the miniaturization of isoelectric focusing (IEF) and isotachophoresis (ITP) onto networked microfluidic chips. The main advantages of miniaturization are smaller sample size and faster analysis. The protocols have been optimized and the improvements have been made in order to improve separation resolution and efficacy.

Liquid phase IEF has been demonstrated for the first time in oxygen plasma-conditioned poly(dimethylsiloxane) (PDMS) microchannels using methylcellulose (MC) to suppress electroosmotic flow (EOF) as well as peak drift and pH-gradient compression. MC dynamic coatings provide a convenient way to suppress EOF by one or more orders of magnitude and, when introduced into the anolyte/catholyte reservoirs as a thickening agent, can significantly reduce drift and peak compression, permitting higher resolution across the pH gradient. A few nanograms of a protein mixture loaded in the microchannel have been resolved into 6 or more bands in 6 min under an electric field strength of 50 V/cm.

Staged IEF of has been demonstrated for increased separation resolution. Sequentially shallower pH gradients were successfully established in the second and third IEF stages, allowing the target proteins to refocus at 2X higher resolution in the later stages. The use of narrow pH range amphoytes as anode and cathode solutions to set the pH values of

two end points allows ready control of pH range inside the channel and the protein species, which enable selective separation of target protein.

ITP experiments have demonstrated that protein samples initially introduced into the microfluidic chip were successfully stacked into adjacent zones with an estimated concentration 40 higher than the initial concentration. Two-dimensional simulations of ITP showed excellent agreement with the experimental zone dispersion and resharpening both during and after passing a T-junction. The resharpening of the protein zones is due to the step change of conductivities across the terminating boundary. Comparison of 2D simulations of ITP and ZE indicated that linear electrophoresis (ZE) lacks the ability to self-sharpen.

An automated electric valve system has been demonstrated in a microfluidic chip with T-junctions as a means of reducing dispersion and sample loss into side channels during nonlinear electrophoresis (ITP) of proteins. Simulation results clearly demonstrated that the current streamlines bent by a T-junction in linear electrokinetic electrophoresis can be straightened by applying constant valve voltages onto a pair of microelectrodes that were appropriately positioned along the side channel walls. The valve voltages automatically change in response to the variation of the local electric field during ITP, which was accomplished by this control system. Experiments with this control system showed excellent valve performance and dramatically improved reproducibility.

Future directions

The established single channel IEF and ITP protocols are ready to be integrated with other separation methods for multidimensional separation. For example, microchip zone electrophoresis can be combined with IEF to mimic 2D gel electrophoresis. ITP also can be performed before zone electrophoresis for preconcentration.

Staged IEF process is expected to speed up by the implementation of physical valves (reference 10 and 39 in chapter 3) which allows tandem, parallel operation of the stages rather than the serial operation developed here. Eventually, the multistage unit operation will be incorporated into a larger network as a single dimension in a separation cascade that leads ultimately to mass spectrometry.

The automated electric valve system provides a robust and simple method for controlling current streamlines and reducing dispersion at T-junctions during nonlinear electrophoresis. This system is expected to provide low-dispersion electric valves for a networked microfluidic chip with multiple T-junctions.

APPENDIX

A. Electronic circuit for the automated electric valve control system

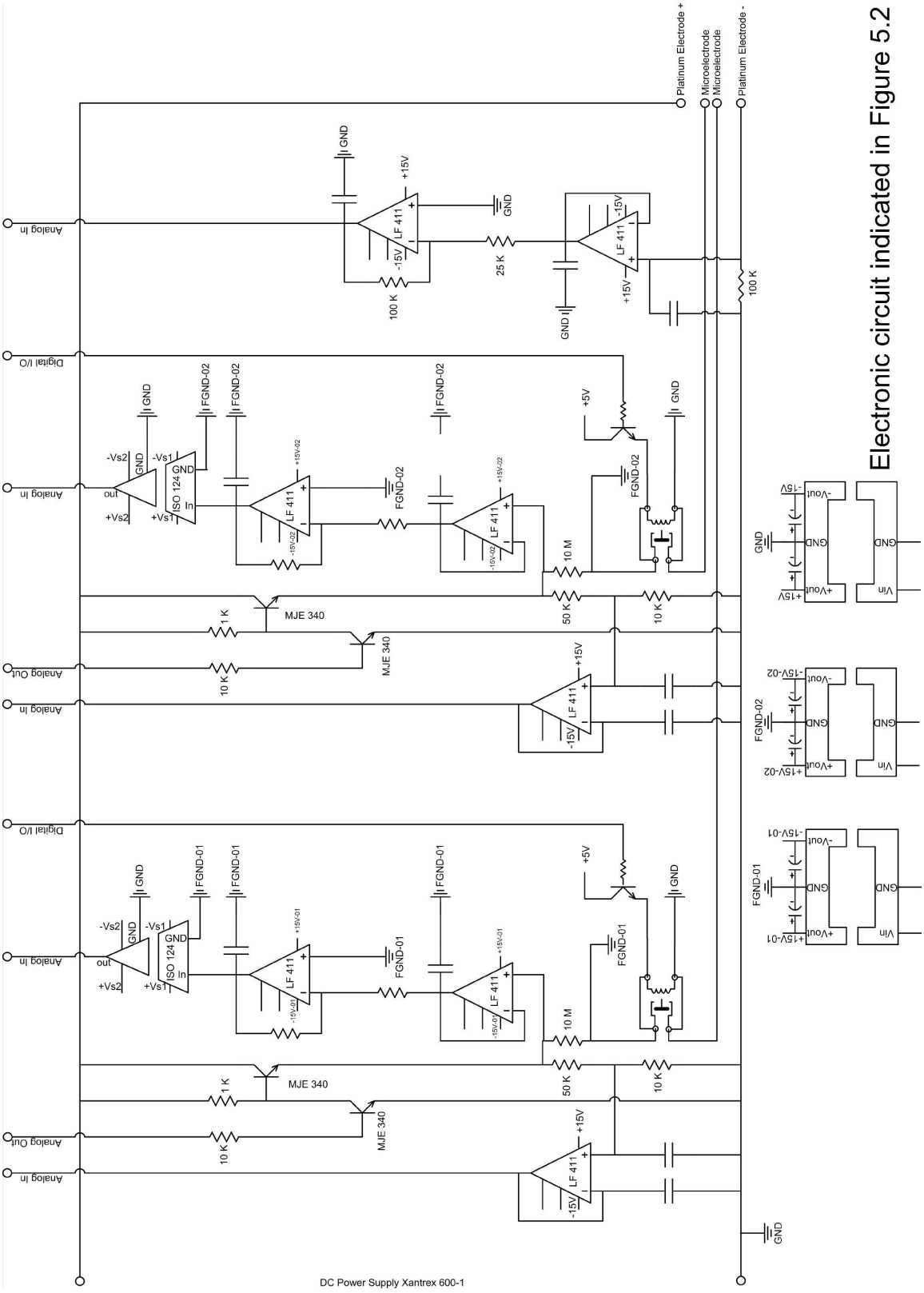

B. The prototype circuit board design of the electronic circuit shown in appendix A

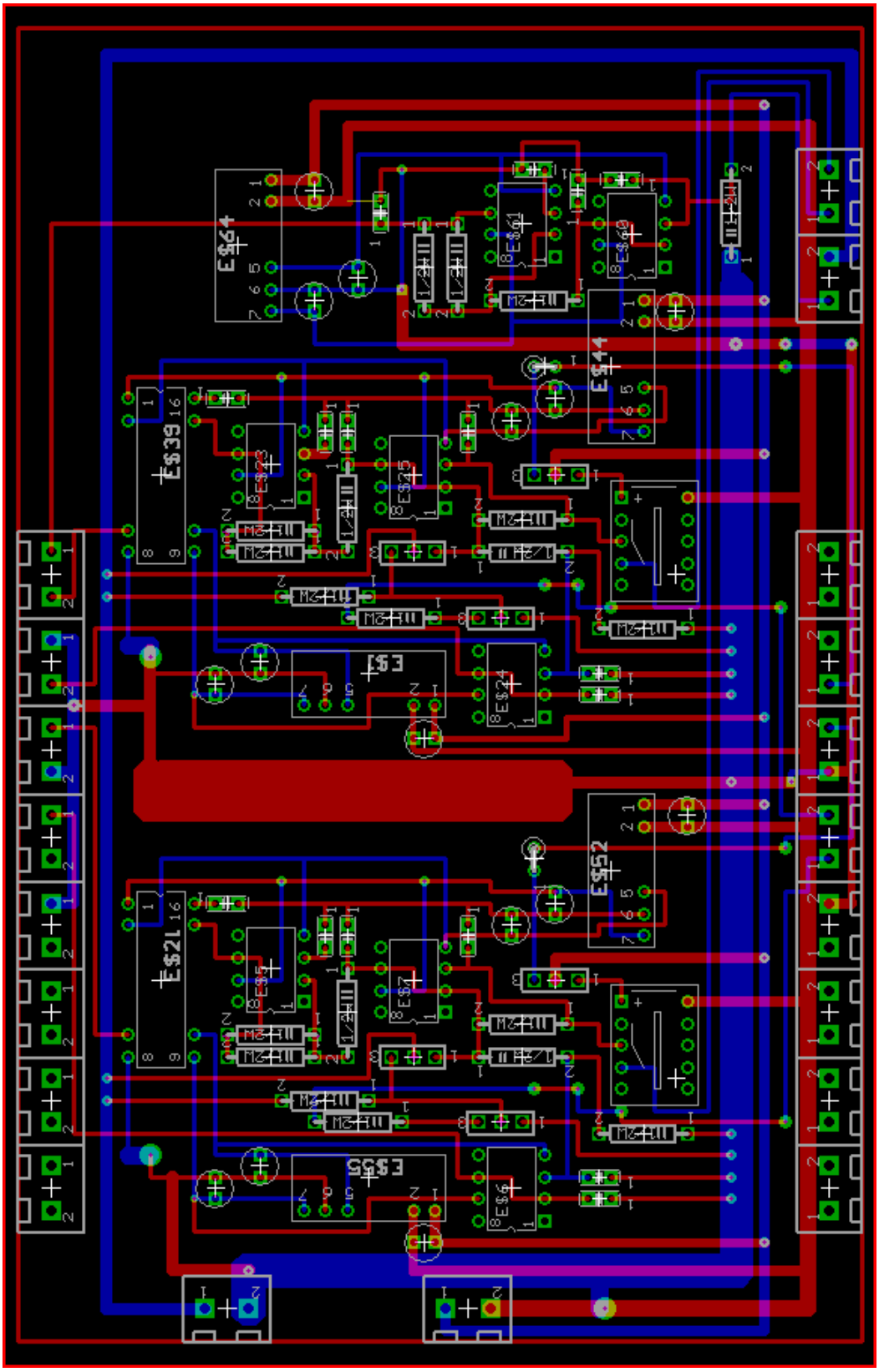

C. User interface of the LabVIEW application for the automated electric valve control system

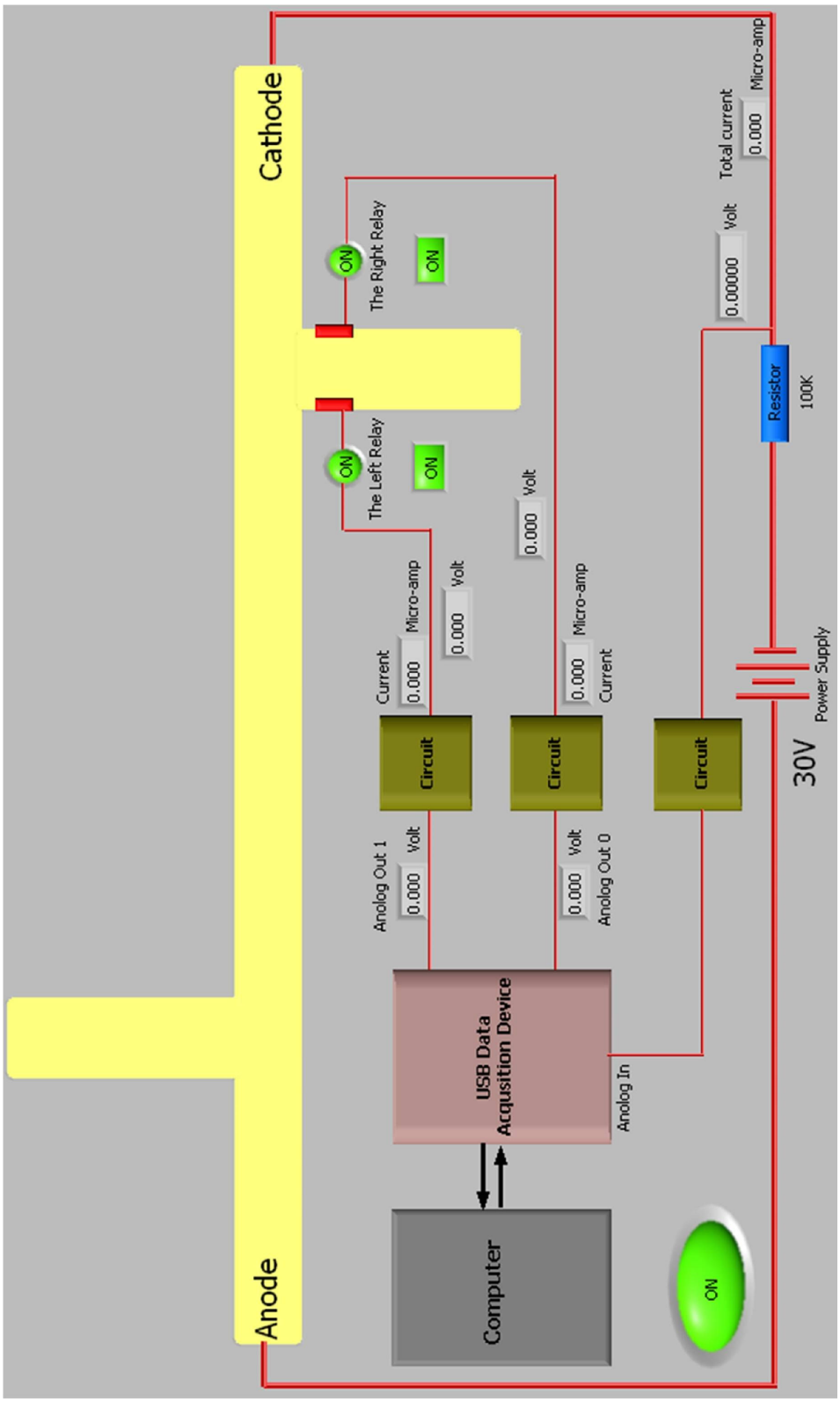

D. The LabVIEW application for the automated electric valve control system

Part 1

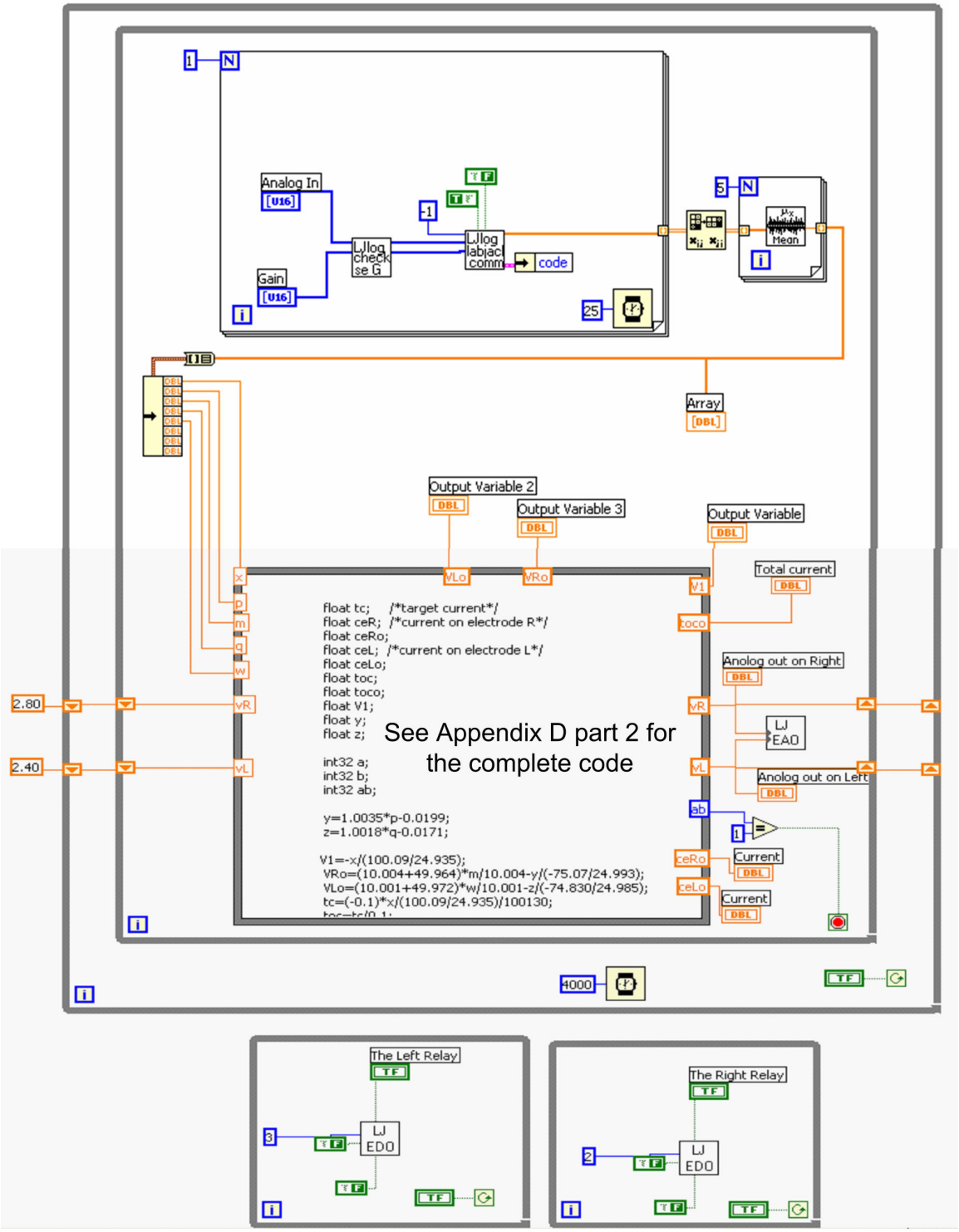

Part 2

```
  float tc;     /*target current*/
  float ceR;  /*current on electrode R*/
  float ceRo;
  float ceL;  /*current on electrode L*/
  float ceLo;
  float toc;
  float toco;
  float V1;
  float y;
  float z;

  int32 a;
  int32 b;
  int32 ab;

  y=1.0035*p-0.0199;
  z=1.0018*q-0.0171;

 V1=-x/(100.09/24.935);
  VRo=(10.004+49.964)*m/10.004-y/(-75.07/24.993);
  VLo=(10.001+49.972)*w/10.001-z/(-74.830/24.985);
  tc=(-0.1)*x/(100.09/24.935)/100130;
  toc=tc/0.1;
  ceR=y/(-75.07/24.993)/10070000;
  ceL=z/(-74.830/24.985)/10207000;

   toco=toc*1000000;
   ceRo=ceR*1000000;
   ceLo=ceL*1000000;

if(ceL<1.7*tc && ceL>1.5*tc)
 {
     a=1;
 }
 else
 {a=0;
  if(ceL>=1.7*tc)
    {vL=1.001*vL;}
    else
      {vL=0.999*vL;} }

if(ceR>-1.3*tc && ceR<-1.1*tc)
 {  b=1;}
  else
  {b=0;
   if(ceR>=-1.1*tc)
      {vR=1.001*vR;}
   else
   { vR=0.999*vR;}}

   ab=a*b;
```